Comparison of Perovskite PV technology with other PV technologies under indoor illumination

Sakshi Thote

Delft University of Technology

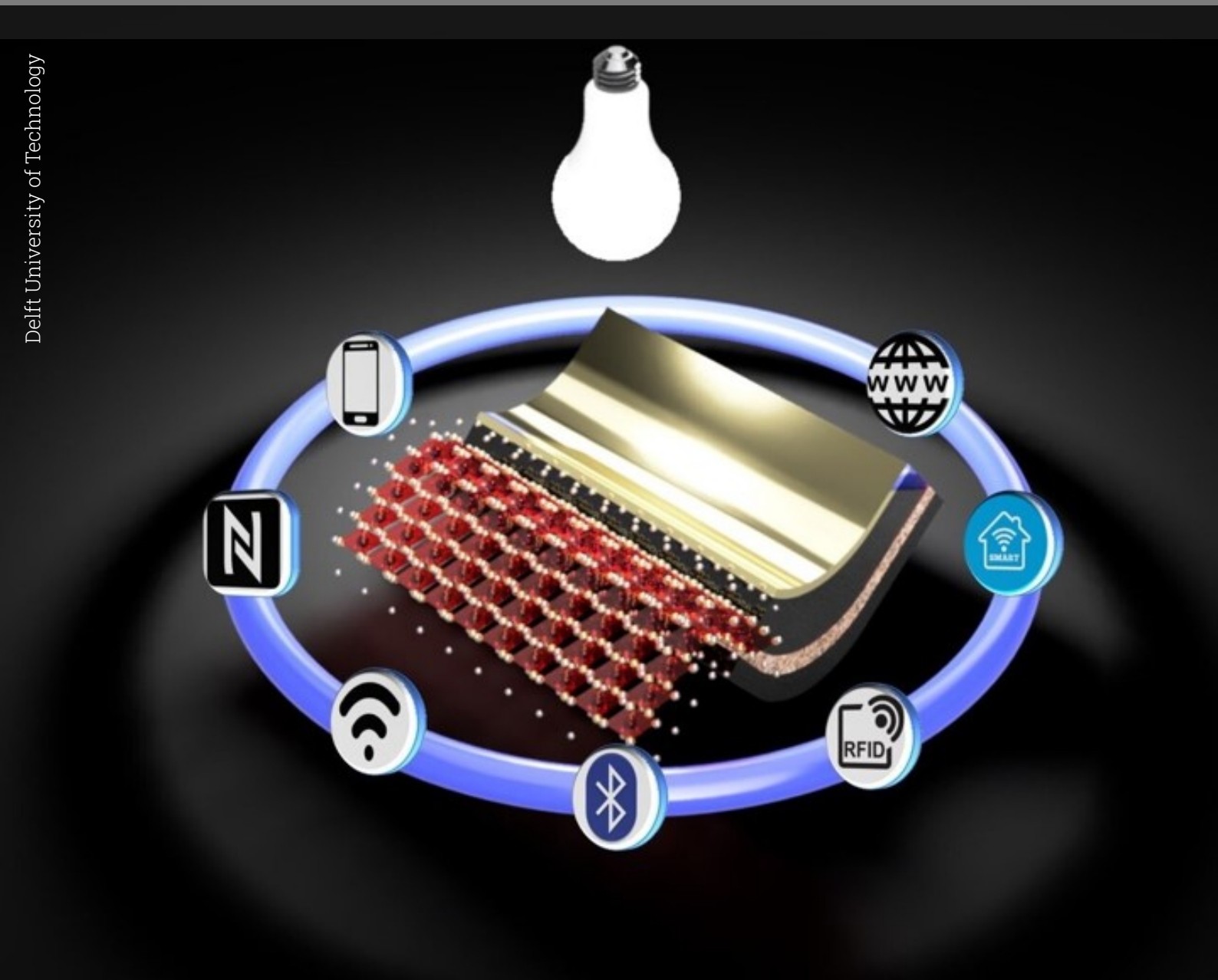

Comparison of Perovskite PV technology with other PV technologies under indoor illumination

by

Sakshi Thote

to obtain the degree of Master of Science in Sustainable Energy Technology at the Delft University of Technology, to be defended publicly on November 25, 2024.

Student number:	5828600	
Project duration	Jan 2024 - Nov 2024	
Supervisor	Prof. Dr. Ivan Gordon	TU Delft
Daily Supervisors	Dr. Aranzazu Aguirre	imec
	Dr. Anurag Krishna	imec
Thesis committee:	Prof. Dr. Ivan Gordon	
	Dr. Aranzazu Aguirre	
	Asst. Prof. Dr. Hesan Ziar	
	Asst. Prof. Dr. Wenli Shi	
Faculty	Electrical Engineering, Mathematics and Computer Science	

TU Delft

Abstract

Solar energy is predominantly harvested under the AM 1.5G spectrum. However, with the expanding integration of PV into Internet of Things (IoT) devices, such as sensors, actuators, Radio Frequency identification (RFID) tags and Bluetooth beacons, has sparked a growing research interest in indoor photovoltaic (IPV) technologies. As the IPV market expands and IoT devices become more affordable, there is significant potential for energy harvesting from indoor environments. Among the IPV technologies, Perovskite solar cells are leading due to their tunable bandgap, high absorption coefficients, defect tolerance and low fabrication costs. This thesis investigates the performance of Perovskite solar cells under indoor lighting conditions, characterized by low-intensity, narrow-spectrum light sources such as LEDs, compact fluorescent lamps (CFLs), and incandescent lamps.

The primary objective of this research is to compare the indoor performance of Perovskite technology with other photovoltaic technologies, namely Silicon, Organic photovoltaic (OPV), and CIGS, available in the EnergyVille2 lab at imec, Belgium. The study was conducted using an experimental setup designed to replicate controlled indoor lighting conditions, with adjustable illumination levels and controlled distances between the PV devices and light sources.

The study also involved analyzing the spectral profiles of typical artificial light sources, including LEDs, CFLs, and incandescent lamps, and determining the correlation between spectral irradiance and illuminance at varying intensities and distances resulting in finding out a linear relation between the spectral irradiance and illuminance of the light source. Subsequently, the performance of Perovskite and other PV technologies was evaluated under different light sources, including warm CFL (2700K), cold LED (4000K), warm LED (3000K), and cold LED (6500K), across illumination ranges from 100 lx to 1000 lx, using experimental setups at imec and CHOSE (Center for Hybrid Organic Solar Energy), Italy.

Results showed that Perovskite technology demonstrated the highest efficiency of 17.52% under warm LED (3000K) at 1000lx illumination, followed closely by OPV (10.9%), which exhibited strong stability. Consequently, Silicon and CIGS showed an indoor performance of 7.05% and 5.97%, respectively at 1000lx under warm LED(3000K). Overall, the findings indicate that perovskite technology demonstrates the highest performance among the tested PV technologies and provide valuable insights into the working of different PV technologies in indoor environments.

Keywords: **Perovskite technology, indoor photovoltaics (IPV), indoor power conversion efficiencies.**

Acknowledgement

This thesis represents the culmination of my nine-month research project within the Photovoltaic Materials and Devices (PVMD) research group at the Technical University of Delft, in collaboration with imec's EnergyVille2 lab in Genk, Belgium. The collaboration provided me the invaluable opportunity to work in a prestigious research environment, where I not only gained extensive hands-on experience but also developed meaningful professional relationships with experts in the field. I am particularly thankful for the chance to travel to Belgium, as it significantly broadened my professional network and contributed to both my personal and career growth.

I would like to extend my deepest gratitude to my supervisor, Prof. Dr. Ivan Gordon, whose insightful feedback and guidance have been instrumental in shaping this project. I am also incredibly thankful to my daily supervisors, Dr. Aranzazu Aguirre and Dr. Anurag Krishna at EnergyVille2 lab, for teaching me the fundamentals of academic research and for their constructive feedback and continuous support throughout the thesis journey.

I am also deeply appreciative of Zeynab Skafi for her unwavering cooperation and patience throughout our collaboration with the Centre for Hybrid Organic Solar Energy (CHOSE) in Italy. This partnership was pivotal in making this thesis possible.

This journey truly tested my resilience, and I am deeply thankful to my friends and family for their unwavering support, especially during the most challenging moments of this master's experience. To the friends I've made along the way, and to those who stood by me despite the time zone differences, I raise a toast—thank you for being there through every high and low. A special mention goes to my mother, Neha Thote, and my sister, Nilaya Thote—the two women who have been my constant pillars of strength, helping me navigate through the ups and downs with their unwavering and constant encouragement and critique. I would like to express my heartfelt gratitude to my father, Niranjan Thote, for his unwavering support and financial assistance throughout this journey.

Lastly, I want to acknowledge myself for being both a friend and a critic during this journey, and for consistently picking myself up when needed.

Contents

List of Figures

List of Tables

Nomenclature

Abbreviations

Abbreviation	Definition
PV	PhotoVoltaic
RFID	Radio Frequency Identification
IoT	Internet of Things
IPV	Indoor PhotoVoltaics
R&D	Research and Development
c-Si	Crystalline Silicon
AM 1.5G	Air Mass 1.5 Global
CFL	Compact Fluorescent Lamps
FL	Fluorescent Lamp
LED	Light Emitting Diodes
RGB	Red, Green and Blue
GaAs	Gallium Arsenide
InP	Indium Phosphate
InGaP	Indium Gallium Phosphate
AlGaAs	Aluminium Gallium Arsenide
TFPV	Thin Film PhotoVoltaics
OLED	organic Light Emitting Diodes
SI	International System of Units
CIE	Commission Internationale de l'Éclairage
Q	Energy
a-Si:H or a-Si	hydrogenated amorphous Silicon Solar Cell
RGB	Red, Green and Blue
OPV	Organic PhotoVoltaic
DSSC	Dye-Sensitized Solar Cell
PVK	Perovskite solar cell
c-Si	Crystalline Silicon
CIGS	Copper Indium Gallium Selenide
CdTe	Cadmium Telluride
CdS	Cadmium Sulphide
LUMO	Lowest unoccupied Molecular Orbital
HOMO	Highest Orbital Molecular Orbital
BHJ	Bulk Heterojunction
PTB7-Th	Poly(3-hexylthiophene- 2,5-diyl)
PC71BM	[6,6]-phenyl-C71-butyric acid methyl ester
NFA	Non-Fullerene Acceptors
FF	Fill Factor
PCE	Power Conversion Efficiency
ITO	Indium Tin Oxide
TCO	Transparent COnducting Oxide
NiO	Nickel Oxide
HTL	Hole Transport Layer
SAMS	Self Assembled Monolayers
ETL	Electron Transport Layer
LiF	Lithium Fluoride
C_{60}	Fullerene

Abbreviation	Definition
mono-Si	monocrystalline Silicon

Symbols

Symbol	Definition	Unit
h	Planck's constant	$[J \cdot s]$
ν	frequency of wave	[Hz]
c	velocity of light	[m/s]
λ	Wavelength	[nm]
V_{OC}	Open Circuit Voltage	[V]
J_{SC}	Short Circuit Current Density	$[A/cm^2]$
I_{SC}	Short Circuit Current	[A]
I	Current through the circuit	[A]
I_0	Saturation current	[A]
q	Charge of an electron	[C]
V	Voltage through the circuit	[V]
n	Ideality factor	[-]
k_B	Boltzmann's constant	[J/K]
T	Absolute temperature	[K]
I_L	Photo-generated current	[A]
V_{MP}	Voltage at maximum power point	[V]
I_{MP}	Current at maximum power point	[A]
R_s	Series resistance	$[\Omega.cm^2]$
R_p	Parallel resistance	$[\Omega.cm^2]$
A	Surface area of the solar cell	$[cm^2]$
J	Current density in circuit	$[A/cm^2]$
J_0	Saturation current density	$[A/cm^2]$
J_L	Photo-generated current density	$[A/cm^2]$
Jsc	Short circuit current density	$[A/cm^2]$
P_{max}	maximum power	[W]
P_{in}	Incident power intensity	[W]
η	Efficiency	[%]
Ω	Solid Angle or Steradian	[sr]
$V(\lambda)$	Spectral luminous efficiency function for photopic vision	[-]
Φ_e	Radiant Flux	[W]
$I_{e,\Omega}$	Radiant Intensity	[W/sr]
E_e	Irradiance	$[W/m^2]$
$L_{e,\Omega}$	Radiance	$[W/sr/m^2]$
Φ_v	Luminous FLux	[lm]
I_v	Luminous Intensity	[cd]
E_v	Illuminance	$[lux = lm/m^2]$
L_v	Luminance	$[cd/m^2]$
P_{in}	Input Power Density	$[\mu W/cm^2]$
P_{max}	Maximum Power Density of solar cell	$[\mu W/cm^2]$
Mo	Molybdenum	
ZnO	Zinc Oxide	
$J_{sc,3000K}$	Short circuit current density at 3000K colour temperature	$[\mu A/cm^2]$
$J_{sc,6500K}$	Short circuit current density at 6000K colour temperature	$[A/cm^2]$

1

Introduction

"Anyone who has never made a mistake has never tried anything new."
— Albert Einstein

1.1. Introduction

The rise in global population and improving living standards are driving a significant increase in energy demand. This is particularly evident in the rapid economic growth of developing countries. As the living conditions improve worldwide, so does our reliance on energy resources. Many global forums and conventions are now focusing on decarbonizing energy systems, as the traditional ways of extracting energy contribute to the rise in greenhouse gas emissions. Advances in research and development have positioned renewable energy sources as the future solution to reduce this dependency on conventional energy production.

Solar, wind, hydro, biomass and thermal energy are at the forefront of efforts to significantly cut greenhouse gas emissions, helping to meet the targets set by the Paris Climate Agreement of 2015 [1]. In particular, solar energy which converts the Sun's radiation into electrical energy via photovoltaic (PV) cells, has emerged as a critical tool in this transition. As the solar industry continues to grow, the PV technology offers a sustainable and scalable solution for reducing global reliance on fossil fuels.

Whenever solar energy is addressed, the mental image of large solar panels often dominates; however, the potential of solar energy extends far beyond these visible installations. It encompasses the conversion of thermal energy into electricity through solar thermal heaters, and the transformation of solar radiation into electrical power using PV panels. Additionally, solar energy powers solar cookers, solar ventilation, solar lighting and more. With the increase in the integration of solar technology with various Internet of Things (IoT), energy can now be harvested in low light conditions such as indoor environments, where light sources are typically artificial light sources or a combination of artificial and natural sunlight.

The illuminations produced by artificial light sources can be utilized by the photovoltaic cells to power Internet of Things (IoT) devices, as demonstrated in Figure 1.1. These IoT systems, composed of interconnected physical objects ("things"), communicate through wireless networks, exchanging data and responding to external stimuli [2].

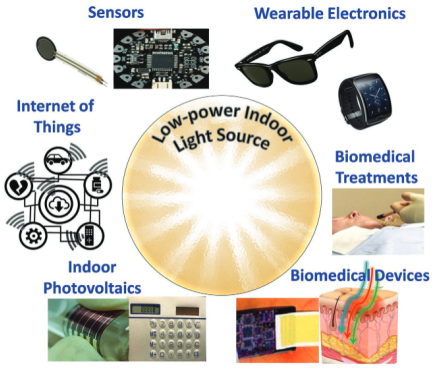

Figure 1.1: Applications of utilization of electrical energy from the low light indoor conditions [3].

Indoor PV applications extend to building-integrated elements and product-integrated devices such as sensors for security and healthcare, electronic shelf labels, wearable electronics and luminaires [4]. Additionally, they are applied in smart grids, smart homes, and wireless sensor networks, forming the backbone of the IoT ecosystem. Common IoT components include wireless sensors, actuators, Radio Frequency Identification tags (RFID) and Bluetooth beacons which are all interconnected and managed by IoT technologies [5].

The earliest memory of seeing applications in indoor PV is that of amorphous silicon (a-Si) solar cells in handheld calculators. This technology gradually expanded into more consumer goods such as watches, IKEA solar lamps and toys [6]. Today, indoor PV plays an essential role in supporting the rapidly growing IoT ecosystems. As shown in Figure 1.2, the x-axis represents the decades from the 1980s to 2020s, and the y-axis depicts the cost of new IPV devices. IPV technology, which began with simple consumer goods in the 1980s, has since evolved into advanced IoT applications like sensors, beacons, and RFID tags, while their costs have decreased, driving widespread adoption. The purple curve in Figure 1.2 illustrates the growing market for IPV devices in IoT, with unit sales potentially reaching 100 million by the 2020s and expected to increase further.

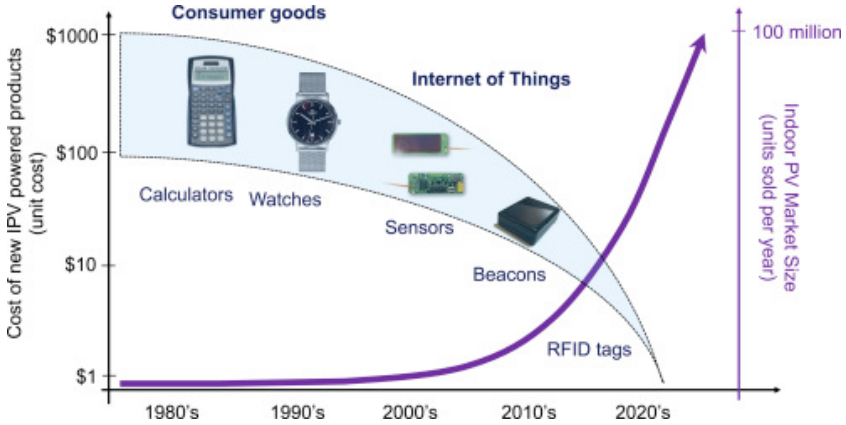

Figure 1.2: Decline in rates of solar-powered IoT applications [7].

While indoor PV initially focused on small-scale applications in consumer electronics, it now plays a crucial role in IoT systems. This move has the potential to lessen reliance on batteries, enabling a pathway to sustainability and self-sufficiency. Batteries are often expensive, environmentally harmful and require periodic replacement, issues that can be mitigated by integrating with solar cells [8]. PV integration also enhances device portability and reliability.

The artificial light sources typically used in indoor environments are the halogen bulbs, the incandescent and fluorescent lamps (FL) and Light Emitting Diodes (LEDs). The IoT devices used indoors usually consume low power, ranging from 1 μW to 1 W as demonstrated in Figure 1.3. For instance,

a sensor typically operates in two modes, active and sleep, which corresponds to a state where the sensor responds to external stimuli by transitioning to a dynamic state and when it is in a stationary state, respectively. This is useful for enhancing energy conservation, as it corresponds to consuming merely 10nW to 1 μW of power [9]. This implies that the low power consumption of IoT devices can be fulfilled by the integration of solar cells. Thus, under ambient light conditions, the light produced by the artificial light sources can be harvested to power these IoT devices.

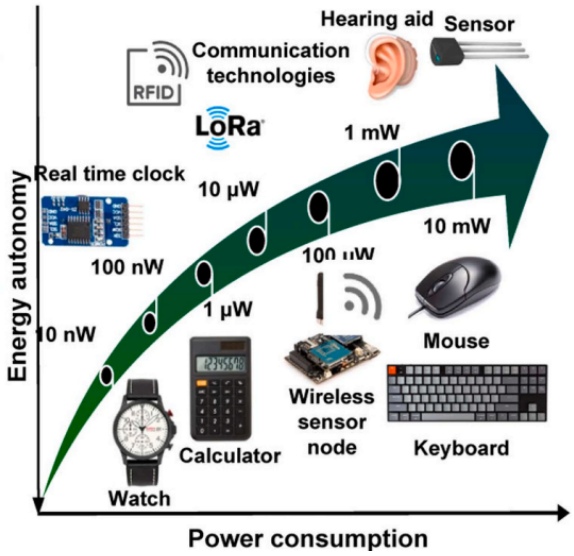

Figure 1.3: Power consumption of various IoT devices [4].

When talking about artificial light sources often the photometric unit termed "Illuminance" is used, which is the amount of light falling on a surface area in a given direction. The detailed explanation about photometric units can be found in Section 2.2.2. The indoor PV devices are set to absorb the light in the 100 to 1000lux range. The efficiency of the PV harvester depends on the type of PV technology used, in addition to the incident light intensity in indoor environments and the varying spectrum of the artificial light sources used [10].

Over the past few years, significant research has been carried out in the field of indoor photovoltaics. This research has focused on improving the power conversion efficiency (PCE) of the solar cells under ambient lighting conditions . This can be achieved by matching the optical properties of the active layer of the solar cell to the spectrum of the indoor light source [11]. This involves exploring new photovoltaic technologies in addition to the already well-established Silicon cell technology. Significant efforts have been directed towards optimizing the active materials in the PV cell, architectures, and manufacturing processes to achieve an optimal matching between the spectral sensitivity of active materials and indoor light spectra. These aim to minimize recombination mechanisms in the junctions and enhance cell architecture [10].

Although crystalline silicon (c-Si) show recorded high efficiencies under 1 Sun illuminations, however, this is reversed under indoor lighting conditions as they suffer from lower PCEs due to decreased open circuit voltages (Voc) [12]. In contrast, amorphous Silicon (a-Si:H) solar cells, with optical bandgaps of approximately 1.7 eV [13], efficiently absorb light in the visible region. This makes them well-suited for generating electricity from indoor light sources, such as LEDs and fluorescent lamps (FL). Moreover, amorphous silicon technology is commercially a mature and well-established technology in the IPV market.

Additionally, Group III-V semiconductors such as GaAs, InP, InGaP, and AlGaAs also appear to be suitable for indoor energy harvesting, having a bandgap tunability of ~1.4eV to 1.9eV [10] matching the spectra of artificial light sources, ensuring minimizing thermalization losses and reduction in below-bandgap losses, thus enabling efficient light harvesting by maintaining higher voltage outputs [14]. However, the cost of these materials may pose a significant barrier to their widespread commercializa-

tion. As an alternative thin film chalcogenide compounds—such as copper indium gallium selenide (CIGS) and cadmium telluride (CdTe), and other mixed compounds—offer similar optoelectronic properties with the potential for large-scale and low-cost production [10].

Within the field of indoor PV research, several emerging PV technologies are gaining siginificant attention due to their adaptability to indoor environments. These technologies, which include Organic photovoltiac (OPV), Dye-Sensitized Solar Cells (DSSCs) and Perovskite (PVK) solar cells, stand out for their high bandgap tunability, high absorption coefficients, solution-processability and low manufacturing costs when compared with conventional PV technologies [10]. Additionally, Quantum Dot Solar Cells (QDSCs) represent a promising technology still in the experimental phase. These emerging PV technologies can also be deposited on flexible, lightweight substrates, making them highly suitable for integration into sensors and other portable indoor PV devices [15].

Among these technologies, Perovskite solar cells are at the forefront of indoor PV development due to their tunable bandgap, superior absorption coefficient and cost-effective production methods. The focus of this thesis is primarily on perovskite technology, investigating its performance under indoor lighting conditions, which are characterized by low-intensity and narrow-spectrum light sources, such as LEDs and fluorescent lamps. By understanding the indoor performance of perovskite technology, the research aims to identify its potential as a leading technology for powering IoT devices and other indoor applications.

The focus of this study is powering IoT devices with solar cells which work on the principle of Photovoltaic effect. Thus, the other techniques of harvesting ambient light are not being discussed in detail. The reason for emphasizing photovoltaic harvesters is that, despite their commercial availability and established presence in the market, research into their application for indoor environments has gained significant research attention.

1.2. Research gap and Motivation

Interest in photovoltaics has grown significantly in recent years, with a notable increase in research focused specifically on indoor photovoltaic (IPV) technologies, particularly since the early 2000s with the advent of IoT. This growing attention is reflected in Figure 1.4, illustrating the number of annual publications from 2001 to September 2024. The growing interest in this area is driven by several factors. Firstly, the widespread replacement of traditional incandescent and halogen lamps with energy-efficient LEDs and fluorescent lamps. Secondly, the rapid expansion of the Internet of Things (IoT) has spurred the integration of IPV devices. Thirdly, advancements in efficient thin-film technologies, such as perovskite and organic photovoltaics, which are lightweight, flexible and well-suited for energy harvesting under indoor lighting conditions due to their tunable bandgaps, have further accelerated this trend.

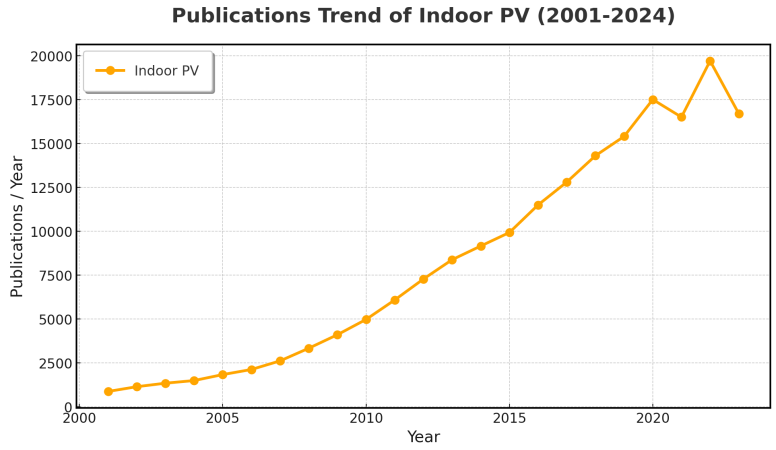

Figure 1.4: Publications trend for indoor PV technologies from 2001 to 2024. Produced from searching 'Indoor Photovoltaic' on research websites.

As noted by Jagadamma et al., no other light-absorbing material has attracted as much research attention for solar energy applications as organometallic halide perovskites, with reported efficiencies exceeding 25.5% under the AM 1.5G spectrum [16] [17]. While significant progress has been made in optimizing PV performance under outdoor conditions, there remains a substantial gap in understanding how perovskites, as well as other PV technologies, perform under various indoor lighting conditions.

This thesis aims to address this gap by evaluating the performance of various PV technologies in indoor environments, with a focus on the leading indoor PV technology which is the Perovskite PV technology. Moreover, no established benchmark currently exists for imec's baseline perovskite technology under indoor conditions. In order to understand indoor performance, the use of an experimental setup simulating a controlled indoor environment is essential. Consequently, this study focuses on evaluating perovskite technology alongside other PV technologies under an experimental setup specifically designed to adjust to different illumination intensities representative of indoor environments. Based on this motivation, we can delve deep into the understanding of indoor photovoltaics, in order to do that it is essential to first formulate critical research questions, which are as follows:

Research Questions

1. **What are the key differences between outdoor and indoor illumination environments?**
   - What are the standard units used to measure illuminations in both outdoor and indoor conditions?
   - What is the correlation between the outdoor and indoor measured units?
   - How does the spectral composition of typical artificial indoor light sources differ from outdoor illuminations (AM 1.5G spectrum)?

2. **How does perovskite photovoltaic technology perform in indoor environments?**
   - What are the typical indoor PV technologies being used extensively for indoor PV? What are the parameters that determine the performance of solar cells in indoor environments?
   - How does perovskite perform compared to other PV technologies used in indoor environments? Is the indoor performance affected by varying illumination intensities?

The experimental setup is designed to simulate a variety of indoor lighting conditions with adjustable illumination levels and distances from the light source to replicate real-world scenarios. Through this experimental approach, measurements will be taken to evaluate the efficiency of these technologies under different lighting conditions. These findings will provide crucial data for comparing the suitability of each PV technology for indoor energy harvesting, ultimately contributing to the advancement of Perovskite and other emerging PV technologies for indoor applications through detailed JV analysis.

1.3. Research Objectives

The following objectives address the core questions explored in this thesis and contribute to a deeper understanding of the challenges and opportunities in indoor photovoltaics (IPV) technologies:

Objective 1 : Investigating the difference between Indoor and Outdoor illuminations.

The first objective is to explore the significant difference between outdoor illuminations, represented by the AM 1.5G spectrum and the artificial lighting conditions commonly found in indoor environments. Understanding this distinction is critical to the overall research. Specifically, this objective aims to:

- Identify and understand the distinct Radiometric and Photometric units used for outdoor and indoor lighting and the ones which are most relevant to the thesis.
- Correlate irradiance (outdoor) and illuminance (indoor), analyzing the relationship between these two unit systems for a better understanding of their impact on indoor PV.

- Analyze the spectral difference between artificial indoor light sources (such as LEDs, CFLs and incandescent or halogen lights) and sunlight (under AM 1.5G spectrum)

Objective 2: Evaluation and comparative analysis of Perovskite with other PV technologies

The second objective aims to evaluate and compare the performance of perovskite and other photovoltaic (PV) technologies in controlled indoor environments. The evaluation is based on both a literature review and experimental analysis conducted at the experimental setup at EnergyVille2 lab, imec, Belgium, and the experimental setup at CHOSE (Centre for Hybrid and Organic Solar Energy) lab, Italy.

The scope of this objective includes:

1. **Literature review on Perovskite and other PV technologies used in indoor environments.** A review of PV technologies relevant to the experimental work, focusing on their material properties and performance characteristics under indoor lighting conditions. The review is limited to PV technologies for which samples were provided at the EnergyVille2 lab, imec, Belgium.This review covers:
   - Silicon technologies
   - Copper Indium Gallium Selenide (CIGS)
   - Organic Photovoltaics (OPV)
   - Perovskite Solar cells (PVK)

   These PV technologies will be compared based on their efficiency under indoor lighting conditions, by analyzing their J-V curve parameters. The review will serve as a foundational understanding of the material properties and performance characteristics of each technology, specifically in the context of the indoor lighting experiments conducted later in the thesis.
2. **Experimental Analysis of perovskite and other PV technologies through J-V curve analysis.** A comparative experimental analysis of the aforementioned PV technologies under different indoor light sources and intensities. The experiments involve:
   - Measuring key J-V curve parameters, such as short-circuit current (Jsc), open-circuit voltage (Voc), fill factor (FF), maximum power output (Pmax) and power conversion efficiency (PCE), under various indoor lighting conditions (e.g., LED and CFL)
   - Evaluating how different light intensities and distances from the light source affect PV performance, simulating real-world indoor scenarios.
   - Comparing the performance of perovskite solar cells with other PV technologies in terms of efficiency and their suitability for low-light indoor energy harvesting applications.

This research will provide valuable insights into the suitability and efficiency of these technologies for indoor energy harvesting. Ultimately, the findings from this study will contribute not only to the optimization of indoor PV systems but also to further advancements in sustainable energy solutions for indoor environments.

1.4. Structure

The structure of the thesis is as follows: Chapter 2 provides the theoretical background and literature review, addressing Objective 1 and Objective 2. This chapter focuses on understanding the difference between indoor and outdoor illumination, as well as reviewing relevant photovoltaic (PV) technologies. Chapter 3 outlines the fabrication process and specifications of the PV samples used in this thesis, followed by a description of the experimental setups employed to analyze their performance under indoor lighting conditions. Chapter 4 presents the results of the experiments, along with a brief discussion of the findings. Chapter 5 draws conclusions from the experimental work and literature review, while Chapter 6 offers recommendations based on the research outcomes, suggesting future directions for improving indoor PV systems.

2

Theoretical Background and Literature Review

2.1. Outdoor vs Indoor Illuminations

There are three primary distinctions between outdoor and indoor illumination. Firstly, the source differs: outdoor illumination is provided by the Sun, whereas indoor illumination comes from artificial light sources such as halogen bulbs, compact fluorescent lamps (CFLs), and light-emitting diodes (LEDs). Consequently, the spectrum of light also varies as it is focused more in the visible region, with indoor light primarily encompassing the spectra of LEDs and CFLs, which are commonly used in daily life.

Secondly, the intensity of indoor light is approximately 10 to 1000 times lower compared to outdoor light, which can be easily understood by analyzing the AM 1.5G spectrum and the light source spectra which are mostly limited to visible region [18]. Unlike the broad spectrum of 1 Sun, artificial light sources emit light within a narrower spectral range as seen in Figure 2.1, contributing to the significant difference in intensity between indoor and outdoor environments.

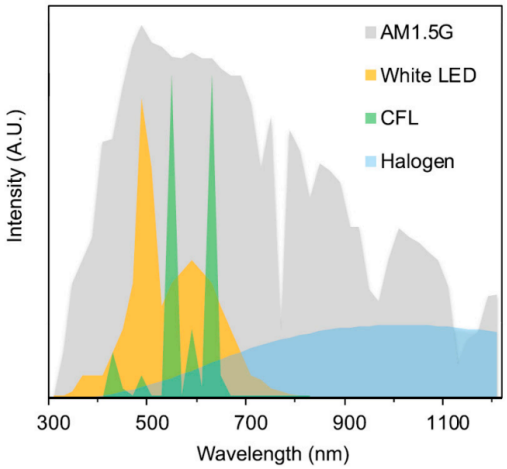

Figure 2.1: Different light spectrum of outdoor and indoor light sources [19].

Thirdly, the difference in the units of measurement: indoor illuminance is measured in lux, while outdoor irradiance is measured in W/m^2 [20]. It is interesting to note that, while measuring solar energy under the AM 1.5 spectrum is well-established, there are no notable standards or protocols for measuring in indoor environments, making it challenging to test, compare, and evaluate the capabilities and

limitations of indoor photovoltaic technologies. This is because indoor lighting conditions are different from outdoor conditions and are typically defined in photometric units weighted by the sensitivity of the human eye when compared with radiometric units, which are used for outdoor conditions.

And lastly, the calculation of power conversion efficiency (PCE) is different in indoor environments. PCE which is the ratio of maximum power output to the input or incident power on the solar cell. However, in an indoor environment, the input power needs to be calculated separately depending on the type of light source being used as it would be different than AM 1.5G's $1000W/m^2$ because the spectrum is different. Recent advancements in materials and device architectures have enabled the development of different photovoltaic technologies that are more suitable for indoor applications, this is discussed in Section 2.4.

2.1.1. Artifical light sources

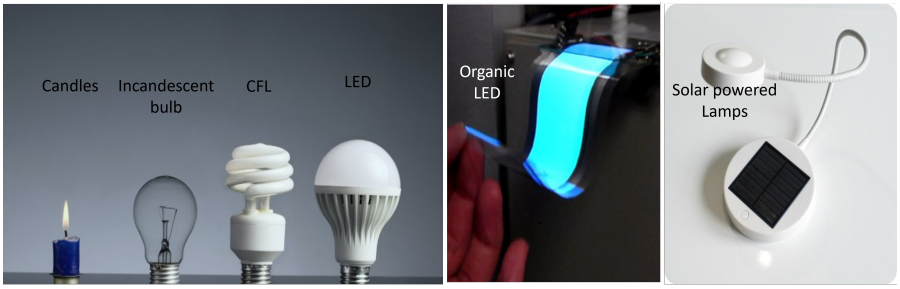

Figure 2.2: Pictorial representation of Evolution of Lighting Technology.
(a) from candles to LED lighting. [21] (b) Organic LED. [22] (c) Solar-powered lamps [23].

The evolution of artificial lighting has progressed from the traditional candles and fire lamps to the electric lighting method of incandescent and halogen light bulbs and then to more energy-efficient technologies such as compact fluorescent lamps (CFLs) and light-emitting diodes (LEDs). These proving to improve the energy efficiency, longevity and light quality.

In the 1960s, LEDs became a milestone, providing greater energy efficiency and longevity compared to incandescent bulbs. More recently, organic LEDs (OLEDs) have gained traction due to their flexibility and low power consumption [24]. These newer lighting technologies are especially relevant for indoor photovoltaic (IPV) applications, as their spectral properties directly impact the performance of IPV devices.

Integration of solar cells has been added to the list of lighting as well. Solar-powered lighting, as the name implies, is driven by energy harvested from solar cells. This form of lighting plays a significant role in promoting sustainable and self-reliable energy solutions, particularly in areas where access to electricity is unreliable. Table 2.1 provides a short synopsis of the evolution of Lighting technologies.

Table 2.1: Evolution of Lighting Technology

Technology	Key Features	Reference
Fire lamps & candles	Inefficient; Prone to hazards	[25]
Incandescent bulbs	Initial electric lighting; Inefficient	[26]
Fluorescent lamps	Energy efficient; Long lifespan	[27]
Halogen bulbs	Brighter than incandescent; Higher efficiency	[28]
LEDs	High energy efficiency; Long lifespan	[29]
OLEDs	Smart lighting; Flexible; Efficient	[24]
Solar-Powered lighting	Sustainable; Self-reliable	[30]

In general indoor illuminations mostly consist of lighting provided by artificial light sources such as Halogen bulbs, CFLs and LEDs depending on the day-to-day necessities.

When it comes to deciding what light source is appropriate for the room setting, the colour temperature of the light source is often taken into consideration. Colour temperature is determined by the spectral distribution of the emitted light, which affects whether the light appears warm or cool. While heat emission can occur with certain light sources, such as incandescent bulbs, it does not define the colour temperature. Instead, colour temperature is characterized by the radiance temperature, also measured in Kelvin, which describes the quality of the light. In this context, the temperature serves as an indicator of how the light is perceived—either warm or cool—while heat emission remains a secondary effect that does not directly influence this perception.

Thus, it is also one of the few specifications that are often mentioned on the box of the light source.

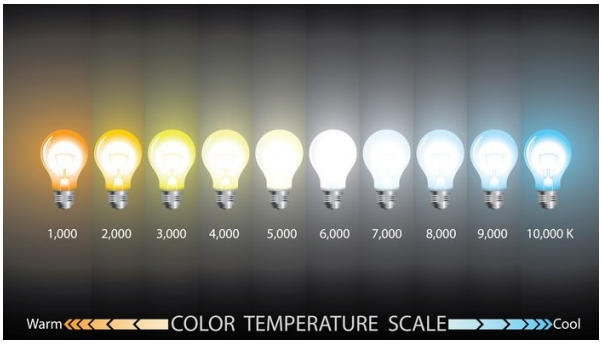

Figure 2.3: Range of colour temperature of light [31].

As can be seen in Figure 2.3, there are a few temperatures of the light sources:

- **2700K - 3500K :** these are the typical 'warm white' light bulbs. These generally have orange or yellow hues to them.
- **4000K - 5000K :** these range of temperatures make up the 'cool white' light bulbs. Often used in commercial settings, as they appear closer to pure white.
- **6000K - 6500K :** The light sources with colour temperatures of this range are designed to replicate the bright, cool light of natural daylight during midday, making them ideal for spaces where bright, natural-like illumination is desired.
- **6500K and above :** colour temperatures beyond 6500K emit a bright bluish light, commonly used in commercial settings. They are ideal for providing strong, focused task lighting.

This characteristic is significant as it influences the intensity of the spectral power densities within the emission spectra of the light sources.

2.2. Radiometry and Photometry

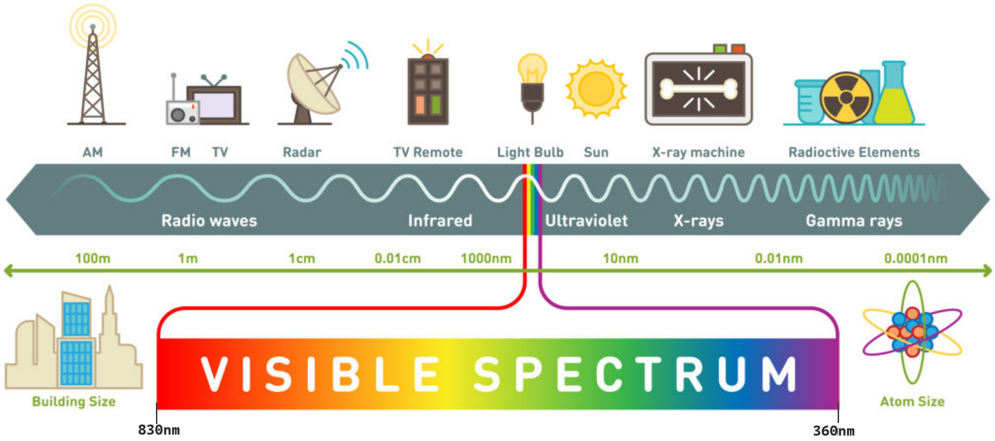

Figure 2.4: Electromagnetic spectrum [32].

Radiometry is the measurement of electromagnetic radiation in the range of 10nm to 1000 μm as can be seen in the Figure 2.4 and includes ultraviolet, visible and infrared regions. Radiometric units focus on the physical properties of electromagnetic radiation based on its wavelength. Additionally, they are often expressed in units including watts, watt per steradian,watt per square meter and watt per square meter per steradian as can be read further in section 2.2.1.

Steradian is a unit of solid-angle measure in the International System of Units (SI)[33]. Since a light source is generally considered as a point source, the solid angle is defined as the ratio of the area of the light source projected onto the surface of a sphere centered at the receiver, to the square of the radius of the conical shape formed by the light. This concept is illustrated in Figure 2.5. Here, Ω represents the Solid angle and the unit is in steradian(sr).

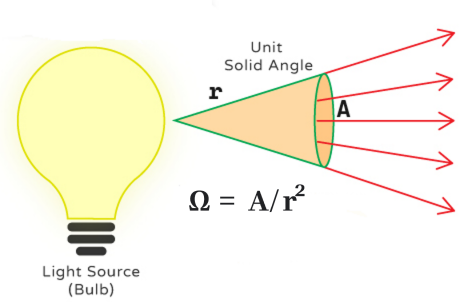

Figure 2.5: Depiction of a steradian [34].

Photometry is the measurement of light that is visible to the human eye, covering the spectrum from 360 nm to 830 nm, as seen in the Figure 2.4 as well. All quantities in photometry are weighted according to the spectral response of a human eye. The basis of photometry is the measurement of visible optical radiation in such a way that it correlates to the visual sensation to a normal human eye when exposed to such a radiation. The relative responsivity of the human eye was first defined by CIE (Commission Internationale de l'Éclairage) in 1924, which was redefined as a part of colourimetric standard observers in 1931 [35]. This function is known as the *spectral luminous efficiency function for photopic*

vision, or the V(λ) function. It is defined over the domain from 360 to 830nm wavelength range and is normalized to a value of one at its peak wavelength of 555 nm as seen in Figure 2.6.

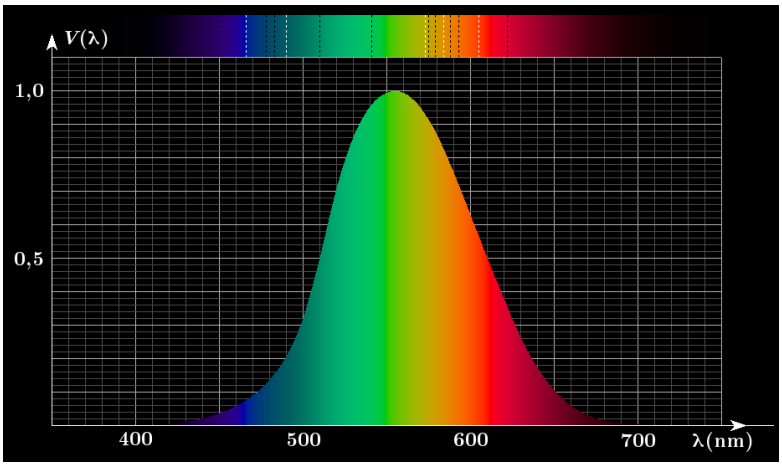

Figure 2.6: Photopic vision better known as the V(λ) function is most of the times taken from 380-780nm wavelength range because it is adequate for minimal errors [36].

In most cases, the wavelength range from 380 nm to 780 nm is taken because it is adequate for calculations with minimal errors, as the value of the V(λ) function drops below 1 x 10^{-4} outside this interval. Therefore, a photodetector with spectral responsivity aligned to the V(λ) function can effectively substitute for the human eye in photometric measurements [35].

2.2.1. Radiometric units

Radiometric units focus on the physical properties of the electromagnetic radiation. In this study, only four relevant radiometric units will be discussed and with the help of Figure 2.7, the relevant four quantities are as follows:

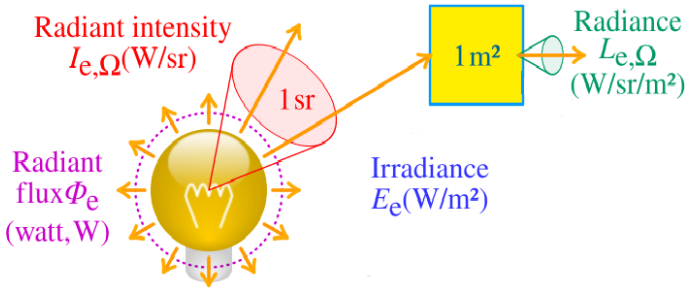

Figure 2.7: Schematic of Radiometric units [37].

1. **Radiant flux (Φ_e):** The total amount of electromagnetic radiation emitted, transferred or received is measured in watts. Mathematically, radiant flux is the energy Q radiated by a source per unit of time.

$$\Phi_e = \frac{dQ}{dt} \tag{2.1}$$

2. **Radiant Intensity ($I_{e,\Omega}$):** is the radiant flux emitted by a source per unit solid angle, measured in watts per steradian, in a given direction. It is defined by the following formula:

$$I_{e,\Omega} = \frac{d\Phi_e}{d\Omega} \tag{2.2}$$

3. **Irradiance (E_e):** The radiant flux received by a surface, measured in watts per square meter. Basically, it is the density of the incident radiant flux at a point on a surface. Irradiance can be

measured by the Equation 2.3:

$$E_e = \frac{d\Phi_e}{dA} \tag{2.3}$$

where $d\Phi_e$ is the amount of radiant flux incident on the element dA of the surface area containing the point.

4. **Radiance ($L_{e,\Omega}$):** It is the radiant flux emitted, reflected, transmitted or received by a surface, per unit solid angle of per unit projected area. It is measured in watts per square meter per steradian. It combines the concepts of radiant flux and the geometry of the radiation, providing a comprehensive description of how much light is travelling in a specific direction from a surface. Radiance can be better understood by Equation 2.4.

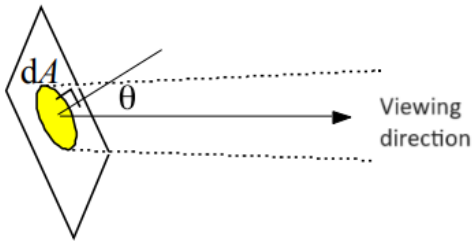

(a) Radiance and also similar to Luminance [35].

$$L_{e,\Omega} = \frac{\mathrm{d}^2\Phi_e}{\mathrm{d}\Omega \cdot \mathrm{d}A \cdot \cos\theta} \tag{2.4}$$

Figure 2.8: Radiance schematic and equation.

where:
$\mathrm{d}^2\Phi_e$ represents the double differential of radiant flux,
$d\Omega$ denotes the differential of the solid angle,
dA refers to the element of surface area,
θ is the angle between the direction of incident light and the normal to the surface.

Figure 2.9: A radiometer. [38]

In addition to that these Radiometric quantities can be measured with the help of Radiometers as seen in Figure 2.9. They are used to measure the amount of electromagnetic energy present within a specific wavelength range. The measurement is expressed in Watts (W) which is a unit of measurement for power. The speciality of this equipment is that it is used also to measure outside the visible region, meaning measuring UltraViolet (UV) and Infra-red regions.

2.2.2. Photometric units

As mentioned before, these units are essential to measure the amount of brightness and intensities of the light source. They have their own specific quantities, but some general terms that are essential to understand are lumen (lm) and candela (cd). A lumen measures the total brightness of the light source

whereas, a candela is the measurement of how bright the light source appears in a specific direction. In addition to that Figure 2.10a helps to understand these quantities better.

(a) Schematic of Photometric units [39].

(b) Photometric units specified on the box of the light source.

Figure 2.10: Photometric units and thier products in market.

1. **Luminous Flux (Φ_v):** The total amount of visible light emitted by a source, measured in lumens (lm). In simple terms, the total brightness provided by the light source. It is often mentioned at the back of the light source box when going to purchase them, also seen in Figure 2.10b. If to be defined mathematically, it is the integral product of the spectral radiant flux ($\Phi_{e,\lambda}$) and the spectral luminous efficiency function ($V(\lambda)$) over all wavelengths, thus converting the radiometric quantity (spectral radiant flux) into a photometric quantity (luminous flux).

$$\Phi_v = K_m \int \Phi_{e,\lambda} V(\lambda) \, \mathrm{d}\lambda \tag{2.5}$$

where:
Φ_v is the luminous flux (in lumens, lm),
K_m is the maximum spectral luminous efficacy for photopic vision (approximately 683 lm/W),
$\Phi_{e,\lambda}$ is the spectral radiant flux (in W/nm),
$V(\lambda)$ is the spectral luminous efficiency function for photopic vision, and
λ is the wavelength (nm).

2. **Luminous Intensity (I_v):** The intensity of light emitted in a particular direction, measured in candelas (cd). It is defined similarly to that of radiant intensity, but the difference is the ratio between the differential of luminous flux and the differential of solid angle as expressed in Equation 2.6.

$$I_v = \frac{d\Phi_v}{d\Omega} \tag{2.6}$$

3. **Illuminance (E_v):** The amount of light falling on a surface in a specific direction, measured in lux or lumens per square meter. In technical terms, it is the amount of luminous flux falling on a surface of element dA in a given direction. This term is of importance in context for analyzing the performance of solar cells and can be calculated by Equation 2.7.

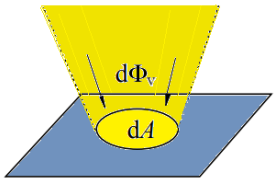

(a) Incident luminous flux from a light source on an element dA of area A [35].

$$E_v = \frac{\mathrm{d}\Phi_v}{\mathrm{d}A} \tag{2.7}$$

Figure 2.11: Illuminance and its formula.

4. **Luminance ($L_{v,\Omega}$):** The amount of light emitted from a surface, measured in candelas per square meter. In simple terms it is the photometric measure of the Luminous Intesity per unit of area of light travelling in a given direction [40]. As seen in Figure 2.8a for radiance, lumiance is very similar to that, the difference lies with lumonius flux.

$$L_{v,\Omega} = \frac{\mathrm{d}^2\Phi_v}{\mathrm{d}\Omega \cdot \mathrm{d}A \cdot \cos\theta} \tag{2.8}$$

Here, Φ_v is the luminous flux, Ω is the solid angle in steradian, A is the area and θ is the angle between the normal to the surface and the direction of light as also seen in Figure 2.8a.

(a) Luxmeter, majorly used in photography [41].

(b) A handheld Photometer.[42]

Figure 2.12: Various types of photometric devices.

Typical equipments used to measure photometric quantities are photometers and luxmeters. Figure 2.12a shows a luxmeter or light meter, a device used to measure the illumination level in lux (lux), which quantifies the amount of visible light present in a given area. A typical luxmeter has a sensor head that detects light and a digital display to read the measured value.

Figure 2.12b shows more advanced handheld photometer, it measures photometric quantities such as illuminance, luminance, and light color properties. They provide comprehensive analysis of light properties, aiding in precise light measurement and evaluation for various applications.

Table 2.2 categorizes all the photometric and radiometric units that are relevant to this study.

Table 2.2: Photometric and Radiometric units and Quantities [35].

Photometric Quantity	Units	Relation with lm	Radiometric Quantity	Units
Luminous FLux	lm		Radiant Flux	W = (J/s)
Luminous Intensity	cd	lm/sr	Radiant intensity	W/sr
Illuminance	lux	lm/m^2	Irradiance	W/m^2
Luminance	cd/m^2	lm/sr/m^2	Radiance	W/sr/m^2
Colour Temperature	K (Kelvin)		Radiance Temperature	K (Kelvin)

2.2.3. Conversion of Illuminance to Power

As human eyes can see indoor light, therefore the brightness of the light sources is quantified in the photometric unit of Illuminance (lux). Thus converting this photometric unit to radiometric unit becomes of utmost importance for the calculation of PCE for IPV devices as it requires knowledge of the incident power intensity in W/m^2.

The incident power intensity can be found for a monochromatic light, if the illuminance is known, as the relationship between illuminance and incident power intensity can be calculated by using Equation 2.9.

$$L(\lambda) = K_m \cdot P_{in} \cdot V(\lambda) \tag{2.9}$$

where,
$L(\lambda)$ is the illuminance measured by a photometer or a calibrated luxmeter,
K_m is the maximum spectral luminous efficacy for photopic vision (approximately 683 lm/W),
$V(\lambda)$ is the CIE 1988 2° spectral luminous efficiency function for human photopic vision,
P_{in} is the incident power intensity of the light source.

The emission spectra needs to be normalized by its total emission intensity, so that the area under each spectral power distribution is 1, the following can be used to get normalized S_{norm} :

$$S_{norm} = \frac{S(\lambda)}{\int_{\text{visible}} S(\lambda)\,\mathrm{d}\lambda} \tag{2.10}$$

Due to the spectral sensitivity of human eyes, the effective brightness, namely, illuminance needs to be weighed by $V(\lambda)$, which accounts for the visual sensitivity. [43] For more than one light sources, the total illuminance (L) involves the integral of the emision spectrum of photopic vision, $S(\lambda) \cdot V(\lambda)$ over the visible region which can be understood by Equation 2.11 [43].

$$L = K_m \cdot P_{in} \cdot \int_{\text{visible}} S_{norm} \cdot V(\lambda)\,\mathrm{d}\lambda = K_m \cdot P_{in} \cdot \frac{\int_{\text{visible}} S(\lambda) \cdot V(\lambda)\,\mathrm{d}\lambda}{\int_{\text{visible}} S(\lambda)\mathrm{d}\lambda} \tag{2.11}$$

The integral is the visible region which is from 360nm to 830nm. And $S(\lambda)$ is the spectral power distribution of the emission spectra of the light source measured by the photometer. Thus, using Equation 2.11, the input or incident power intensity can be calculated, albiet if the illuminance L, is known. The product of normalized $S(\lambda) \cdot V(\lambda)$ is different for different light sources.

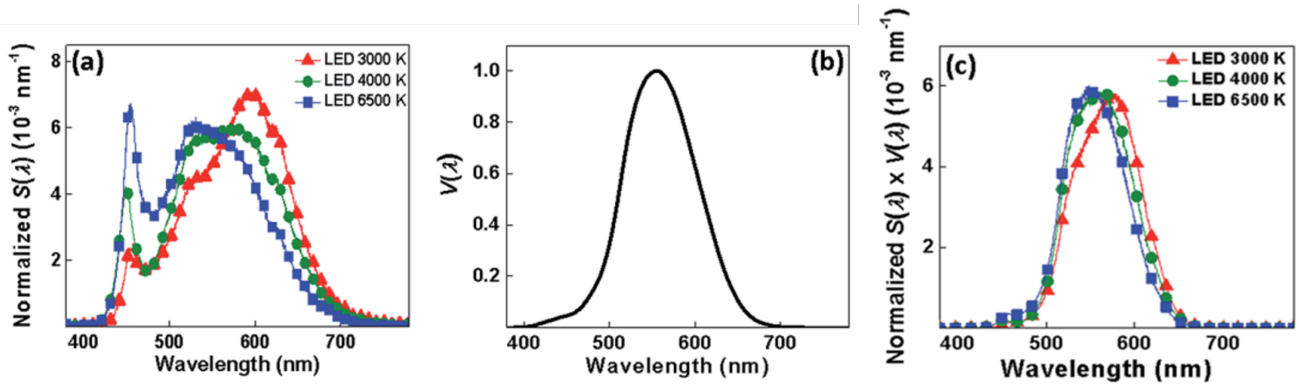

Figure 2.13: (a) Normalized $S(\lambda)$, (b) V(λ) function, (c) Normalized $S(\lambda) \cdot V(\lambda)$. Figures are taken from [43].

2.2.4. Typical Illumination levels

One thing to understand when talking about ambient light is that it is diffused lighting. Additionally, scattering and reflections of light indoors also contribute to the effect of light diffusion. To elaborate

further, when measuring illumination levels within a residential setup, the recorded lux values will vary depending on the specific location of measurement within the space. Similarly, this can be seen in Figure 2.14. As one moves from room to room and between different light sources, it becomes evident that illumination levels fluctuate.

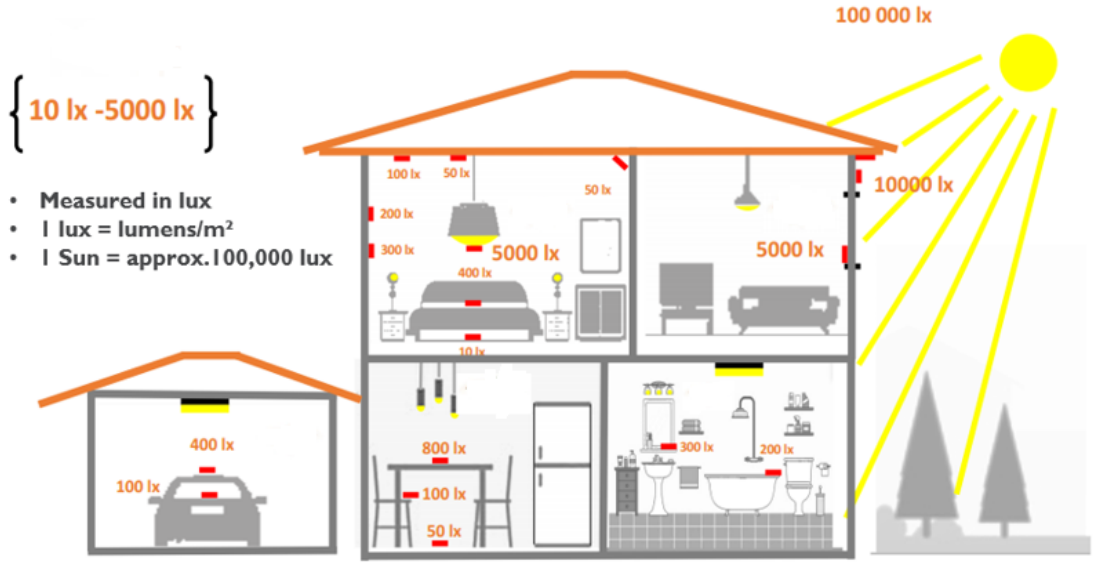

Figure 2.14: Typical illumination levels inside a Residential setup. (Courtesy of Dracula Technologies)

The typical illuminance levels for various environments can be categorized based on their corresponding power intensities. For instance, 1 lux is equivalent to 0.0079 W/m^2 for a solar light spectrum [44]. In an office setting, the typical illumination range is 100 to 1000lx which translates into 0.79 to 7.9 W/m^2 of power intensity. From this, it becomes clear that higher illumination levels do not necessarily indicate higher power intensities, particularly under artificial light sources that emit narrower spectral bands compared to 1 Sun illuminations.

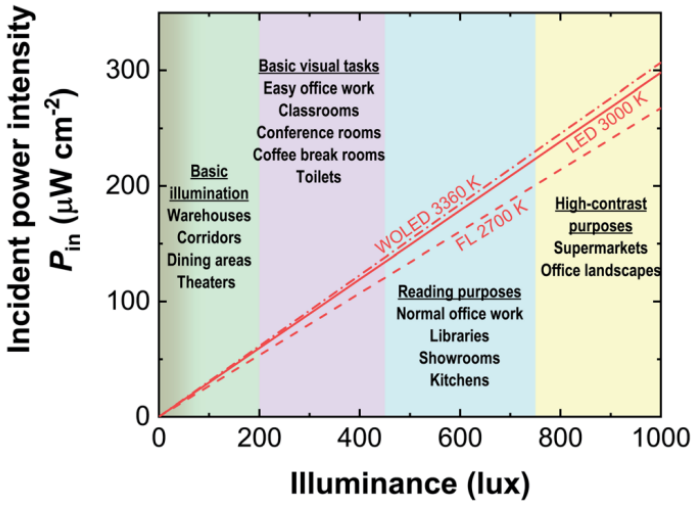

Figure 2.15: Typical illumination levels in indoor environments as a function of incident power intensity(P_{in}) as reported by Johnny Ka Wai Ho and colleagues. [45]

As seen in Figure 2.15, the typical range of illumination levels from 100lx to 1000lx as a function of incident power intensity (P_{in}) is illustrated for selected light sources [45]. Typical illumination levels

for indoor environments such as offices, libraries and classrooms generally range from 200lx to 800lx, with 1000lx being the upper limit commonly used in specialized settings like supermarkets, open office areas and hospital operation theatres. Therefore, when evaluating the indoor performance of solar cells, it is crucial to focus on these specific illumination levels for an accurate and relevant analysis.

2.3. Photovoltaic Effect

A solar cell uses the principle of the 'Photovoltaic effect' to convert the Sun's solar radiation into electricity. Photovoltaic effect refers to the generation of voltage and electric current in a material when exposed to light. The photovoltaic effect is closely related to the Photoelectric effect, where the electrons are emitted from a material that has absorbed light with a frequency above a material-dependent threshold frequency [46]. Figure 2.16 illustrates the working of a solar cell, which works on the Photovoltaic effect. This effect can be broken down into three main steps as the following:

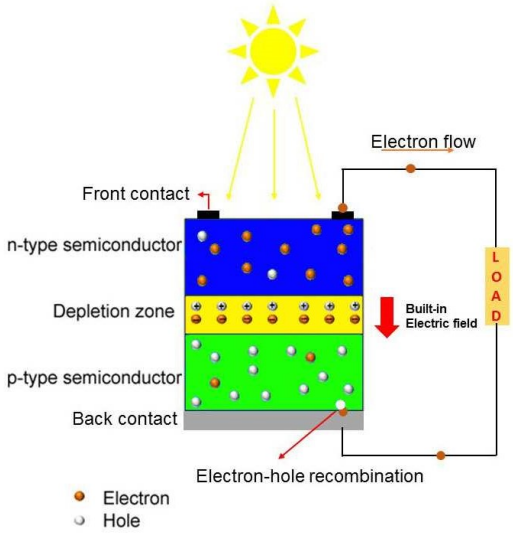

Figure 2.16: Working of a solar cell [47].

1. **Absorption** of light by the absorber layer in the solar cell, followed by generation of electron-hole pairs.
2. **Separation** of these photogenerated carriers to prevent their recombination. Oppositely charged carriers need to be collected at different parts of the solar cell so they do not recombine.
3. **Collection** of the separated carriers towards the metal electrodes which provides the source of electricity to the external circuit.

Absorption of light

When light or electromagnetic radiation falls on solar cells, it consists of photons. These photons consist of energy that is proportional to their frequency and inversely proportional to their wavelength. This energy can be expressed by the well-defined formula derived by Albert Einstein:

$$E = h\nu = \frac{h \cdot c}{\lambda} \tag{2.12}$$

where, E is the energy of the photon,
h is Planck's constant,
ν is the frequency of the electromagnetic radiation,
c is the speed of light in a vacuum, and
λ is the wavelength of the electromagnetic radiation.

The energy provided by the photons contributes to electron excitation. Thus, when the electrons are excited they move from the lower state of energy to a higher state of energy i.e. from the valence band to conduction band. The energy difference between the valence and conduction band is known as the 'Bandgap' of the solar cell. This movement leads to the generation of electron-hole pairs. It is to be noted that these photons need to have energy higher or equal to the semiconductor's bandgap energy. Photons with energy less than the bandgap cannot be absorbed, leading to no generation of electricity. Thus, this requirement needs to be fulfilled for electron-hole pair generation.

Separation of charge carriers

After the first step, the electron-hole pair needs to be separated to not be recombined in the cell itself. A p-n junction is present in the solar cell, where the p-type region consists mainly of holes and the n-type consists of electrons. The region near the interface of the p-type and n-type regions is known as the 'depletion region'. This depletion region generates an internal electric field which helps in separating the opposite charge carriers. Consequently, the generated electron-hole pair gets separated: the hole moves to the p-type region, and the electron moves to the n-type region of the solar cell. These separated charge carriers are then collected by metal electrodes.

Collection of the separated carriers

A solar cell consists of metal electrodes, one at the top and the other at the bottom. These metal contacts help in the collection of charge carriers. The generated hole is collected by the electrode at the p-type region and the electron gets collected by the n-type region electrode. The electrons are then pushed forward to the external circuit. After passing through the circuit the electron recombines with the hole at the p-type side, completing the circuit. When these three steps are fulfilled, the photovoltaic effect is achieved, and electricity is produced.

2.3.1. Solar cell performance parameters

The performance of a solar cell is typically evaluated under standard test conditions (STC), where spectrum AM 1.5G is the primary source of illumination. A Solar Simulator is a device that provides illumination approximating natural sunlight in the AM 1.5G spectrum, the purpose of this device is to provide a controllable indoor testing facility under laboratory conditions [48]. Figure 2.17 illustrates a solar simulator used in a lab mainly to measure the performance of a solar cell or solar module.

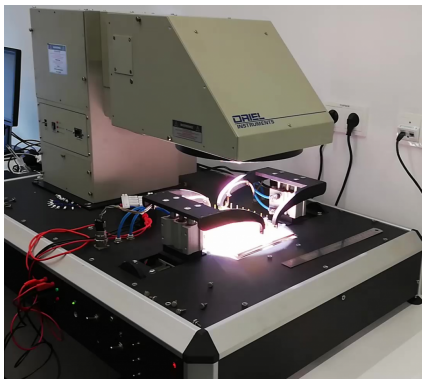

Figure 2.17: Solar Simulator. [49]

The performance of a solar cell is analyzed by four main factors:

1. **Open Circuit Voltage** (V_{OC})
2. **Short Circuit Current Density** (J_{SC})
3. **Fill Factor** (FF)
4. **Power Conversion Efficiency** (PCE)

All of these factors are derived from the current-voltage (I-V) curve to examine the relationship between current and voltage produced by the solar cell.

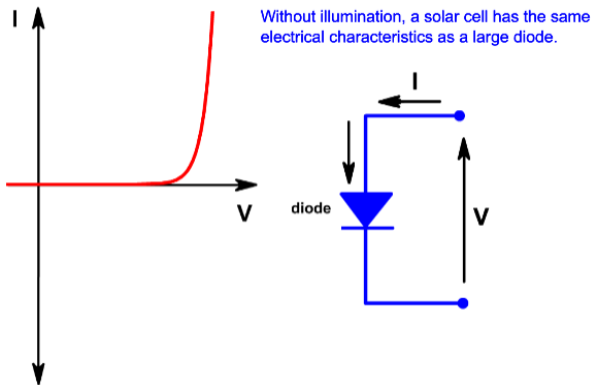

Figure 2.18: The IV curve of the solar cell in the dark, showing behavior similar to a large diode [50].

Figure 2.18 illustrates the behaviour of the IV curve when the solar cell is in the dark, predominantly in the first quadrant. Without illumination, a solar cell has the same electrical characteristics as a large diode. Equation 2.13 represents the ideal diode equation, which behaves as a large diode when in the dark.

$$I = I_0 \left[\exp\left(\frac{qV}{nk_BT} \right) - 1 \right] \tag{2.13}$$

where:
I is the current through the solar cell,
I_0 is the saturation current or the current produced in the dark,
q is the charge of an electron (approximately 1.602×10^{-19} coulombs),
V is the voltage across the solar cell,
n is the ideality factor,
k_B is Boltzmann's constant (approximately 1.381×10^{-23} J/K),
T is the absolute temperature in Kelvin.

When a solar cell is illuminated, it generates a photo-generated current. The performance of the solar cell is typically assessed by analyzing its IV curve, which represents the superposition of the IV curve of the solar cell in the dark with the light-generated current [50]. In simple terms, when the light illuminates the cell, it adds to the dark current, shifting the IV curve into the fourth quadrant where power can be extracted. This can also be seen in Equation 2.14.

$$I = I_0 \left[\exp\left(\frac{qV}{nk_BT} \right) - 1 \right] - I_L \tag{2.14}$$

When the sign convention is changed by multiplying by -1 to Equation 2.14, we get Equation 2.15.

$$I = I_L - I_0 \left[\exp\left(\frac{qV}{nk_BT} \right) - 1 \right] \tag{2.15}$$

where I_L is the photo-generated current by the solar cell.

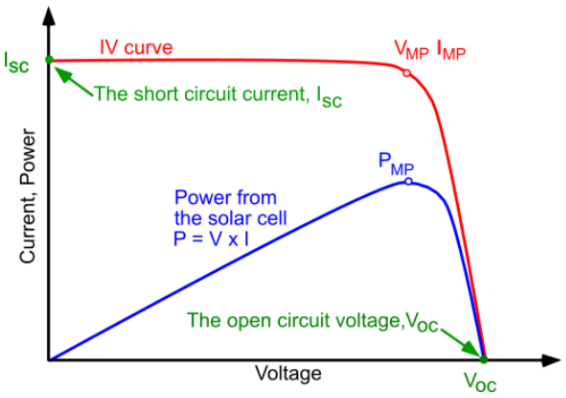

Figure 2.19: IV curve parameters to analyze the performance of a solar cell [50].

1. Open Circuit Voltage (Voc)

The open circuit voltage V_{OC}, is the maximum voltage generated by a solar cell when there is no external load connected, this means that the circuit is open, as a result no current is flowing. This voltage is the result of forward bias caused by the photo-generated current across the solar cell junction. On the graph (see Figure 2.19), the open circuit voltage is when the current is zero, thus indicating the maximum potential difference created by the light induced charge carriers. The open circuit voltage can be calculated by the Equation 2.16.

$$V_{OC} = \frac{nk_BT}{q} \ln\left(\frac{I_L}{I_0} + 1\right) \tag{2.16}$$

As seen in Equation 2.16, the open circuit voltage has a logarithmic dependence on the photo-generated current. This means that as the photo-generated current increases, the open-circuit voltage increases logarithmically. Consequently, a large increase in I_L results in a smaller relative increase in V_{OC}.

$$V_{OC} = \frac{nk_BT}{q} \ln\left(\frac{I_L}{I_0} + 1\right) \tag{2.17}$$

The derivation of open circuit voltage is derived by the Equation 2.15, in this condition, the net current passing through the circuit is zero. Hence, the following would happen :

$$0 = I_L - I_0\left[\exp\left(\frac{qV_{OC}}{nk_BT}\right) - 1\right] \tag{2.18}$$

$$I_L = I_0\left[\exp\left(\frac{qV_{OC}}{nk_BT}\right) - 1\right] \tag{2.19}$$

$$\frac{I_L}{I_0} + 1 = \exp\left(\frac{qV_{OC}}{nk_BT}\right) \tag{2.20}$$

$$V_{OC} = \frac{nk_BT}{q} \ln\left(\frac{I_L}{I_0} + 1\right) \tag{2.21}$$

Rearranging Equation 2.20 and solving it for V_{OC} results in Equation 2.21. If the value of ideality factor is close to 1, then there will be fewer recombination chances [51] [4]. The reduction in I_L value and increase in n results in extra Energy loss (E_{loss}) of 0.15eV to 2.0eV in the case of organic solar cells [51].

Experiments are often conducted using solar simulators under different illumination conditions, quantified relative to the standard AM 1.5G spectrum, where 1 unit represents standard solar irradiance.

As described by Equation 2.22, the open-circuit voltage (V_{OC}) exhibits a logarithmic dependence on the illumination intensity, increasing as the illumination is intensified and decreasing as it is reduced.

$$V'_{OC} = \frac{nkT}{q} \ln\left(\frac{XI_L}{I_0}\right) = \frac{nkT}{q}\left[\ln\left(\frac{I_L}{I_0}\right) + \ln X\right] = V_{OC} + \frac{nk_BT}{q} \ln X \tag{2.22}$$

where, X represents the relative illumination level, and V'_{OC}, is the open-circuit voltage under X intensity.

Under typical indoor lighting conditions, the illumination ranges between 200 and 1000 lux, which corresponds to approximately 0.0002 to 0.01 Suns, given that 1 Sun is equivalent to 100,000 lux [52]. As light intensity decreases, the factor X in Equation 2.22 also decreases, resulting in a logarithmic reduction in the open-circuit voltage (V_{OC}). Consequently, under indoor conditions, the open circuit voltage is lower compared to outdoor conditions.

This reduction in V_{OC} is due to the extra loss in energy because of the shifting of quasi-Fermi levels which can also be seen in Figure 2.20, where E_{Fn} and E_{Fp} corresponds to the electron and hole quasi fermi levels, respectively. Under low illumination, the E_{Fn} shifts down and the E_{Fp} shifts up, which is the reason for the reduction in V_{OC} of the cells with relatively thicker active layer [51].

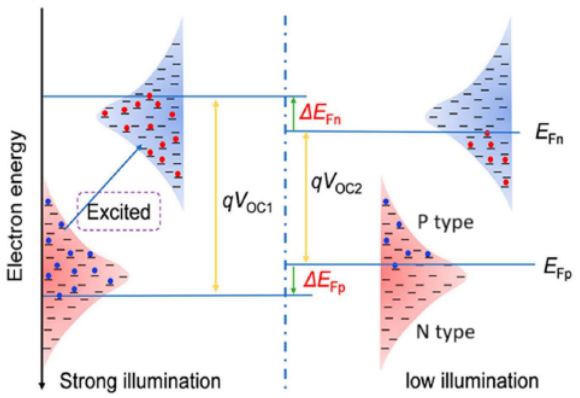

Figure 2.20: Schematic of the density of states under strong and low illumination, indicating that at lower illumination [4], the quasi-Fermi levels shift, leading to Energy loss (E_{loss}) and loss in V_{OC} [51].

2. Short Circuit Current Density (Jsc)

The short-circuit current (I_{SC}) is the maximum current generated by a solar cell when the voltage across the cell is zero—this occurs when the electrodes are short-circuited, meaning there is zero external resistance [46]. On the IV curve (see Figure 2.19), I_{SC} corresponds to the current value when the voltage is zero. The short-circuit current density (J_{sc}) is derived from I_{SC} using Equation 2.23, where A is the surface area of the solar cell. I_{SC} is directly proportional to the surface area of the solar cell and the incident spectral irradiance [53].

$$J_{sc} = \frac{I_{sc}}{A} \tag{2.23}$$

The photo-generated current (I_L), which represents the current generated within a solar cell when exposed to light, is typically equal to the short circuit current (I_{SC}) at short circuit conditions. For simplicity, I_L and I_{SC} are often used interchangeably in the analysis of solar cell performance, although it is important to note that in cases of high series resistance, I_{SC} may be less than I_L [54].

The factors affecting short circuit current density under indoor ambient conditions are as follows:

1. **Incident Light Intensity:**
   There is a linear relationship between short circuit current density and the incident light intensity.

Under typical indoor low light conditions, the short circuit current density is significantly lower compared to that under 1 Sun illumination. Variations in incident light intensity influence all key solar cell parameters, including the open circuit voltage (V_{OC}), the FF and PCE. Among these, the FF is particularly sensitive to changes in light intensity, as further elaborated in Section 2.3.1.

2. **Charge Carrier Generation:**
   The properties of the active material within the solar cell are crucial in determining the efficiency of electron-hole pair generation. This efficiency directly impacts the short circuit density. The effectiveness of the active material in facilitating the extraction of electrons from the absorber layer to the external circuit is vital for maximizing the photo-generated current [55]. Given the inherently low incident light intensity in indoor environments, the ability of the active material to generate sufficient electron-hole pairs becomes a critical factor in maintaining a higher current output. As a result, absorber materials in emerging photovoltaic technologies are being actively researched for indoor PV applications. This is being discussed in Section 2.4

3. **Surface Recombination:**
   Surface recombination is one of the factors that affect short-circuit current density, especially in low-light indoor conditions. With limited photon flux indoors, the generation of electron-hole pairs is minimal, making recombination processes driven by thermal energy more pronounced [56]. As the solar cell typically reaches thermal equilibrium with its surroundings in an indoor setting, surface recombination becomes a more significant contributor to the overall recombination current [46]. Although the absolute recombination current may be low, its impact on the total current is more pronounced due to the diminished photo-generated current.

3. Fill Factor

The Fill Factor is the ratio between the maximum power generated by the solar cell to the product of V_{OC} x J_{SC}. The maximum power generated is estimated at the maximum power point (MPP) of the solar cell which can be seen in the IV curve as well (Figure 2.19).

$$FF = \frac{V_{MP} \cdot I_{MP}}{V_{OC} \cdot I_{SC}} = \frac{AreaA}{AreaB} \tag{2.24}$$

As seen in Figure 2.21, the Fill Factor is the ratio of Area A to Area B.

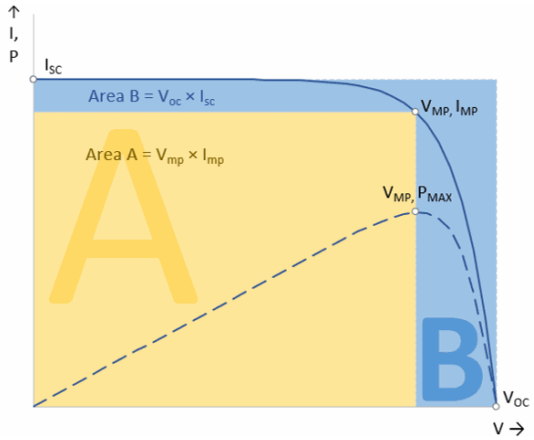

Figure 2.21: Fill Factor [57].

In practice, the Fill Factor is affected by the following factors:

1. **Series Resistance** (R_s)
2. **Parallel Resistance** (R_p)

The impact of these factors on the J-V characteristics of the solar cell can be analyzed through the equivalent circuit depicted in the following figure.

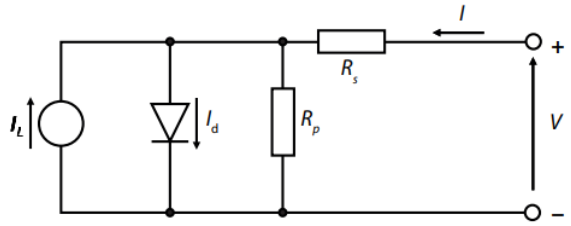

Figure 2.22: Equivalent circuit with series (R_s)and parallel resistance (R_p) [46].

The J-V characteristics of the Equivalent circuit as seen in Figure 2.22, the

$$J = J_0 \left\{ \exp\left[\frac{q\,(V - AJR_s)}{k_B T} \right] - 1 \right\} + \frac{V - AJR_s}{R_p} - J_L \tag{2.25}$$

where,
J is the current density in the external circuit,
J_0 is the saturation current density equivalent to an ideal diode current density,
A is the surface area of the solar cell,
R_s is the series resistance,
R_p is the parallel resistance, since it is connected in parallel to the diode,
V is the voltage in the circuit, and
J_L is the photo-generated current density.

Figure 2.23, depicts the behaviour of FF under 1 Sun, 1 Sun approximates the standard illumination of AM 1.5G. As shown in Figure 2.23a, with increasing series resistance R_s and a constant parallel resistance R_p of 100 kΩ·cm^2, the Fill Factor (FF) begins to deteriorate under an incident power intensity of 1 Sun [46]. Conversely, as illustrated in Figure 2.23b, increasing R_p while keeping R_s constant leads to an improvement in the FF. This suggests that under 1 Sun (AM 1.5) conditions, maintaining a low R_s and a high R_p is beneficial for optimizing the FF of the solar cell.

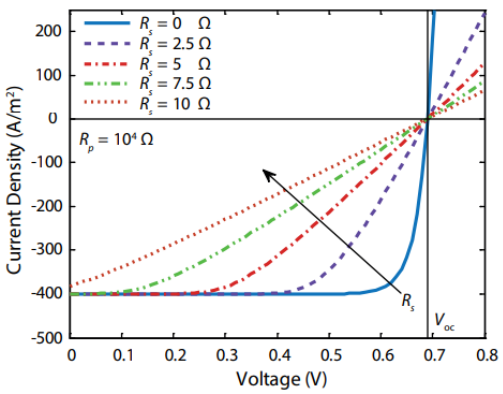

(a) Effect on FF by changing R_s under 1 Sun [46].

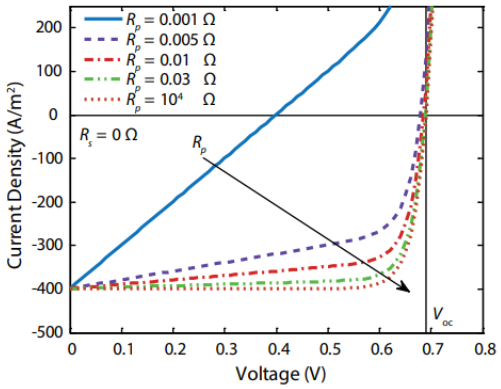

(b) Effect on FF by changing R_p under 1 Sun [46].

Figure 2.23: Effects on FF by changing R_s and R_p under 1 Sun.

Under indoor or low light conditions, the behaviour FF is influenced by the lower intensity of light from artificial sources such as LEDs, CFLs and halogen bulbs, compared to the AM1.5G spectrum. Due to the significantly reduced light intensity indoors, the magnitude of photogenerated carriers is much lower than under 1 Sun illuminations. This reduction in carrier generation affects the recombination processes within the cell, particularly the recombination of independent electron-hole pairs. Specifically, bimolecular recombination - where an electron and hole recombine directly without the involvement of any defects or impurities- may be reduced in these conditions, potentially contributing to higher FF values under indoor illumination [51].

This behaviour is illustrated in Figure 2.24, where increasing the shunt resistance R_p while keeping the series resistance R_s constant, under the intensity of 0.05 Sun, leads to an improvement in the FF. In indoor conditions, where the light intensity is often lower than 0.05 Sun and the spectrum shifts to that of artificial light sources, the R_p tends to be higher. This increase in R_p explains the improvement in FF under low-light conditions. Conversely, changes in R_s have a negligible effect on the FF under these low-light conditions.

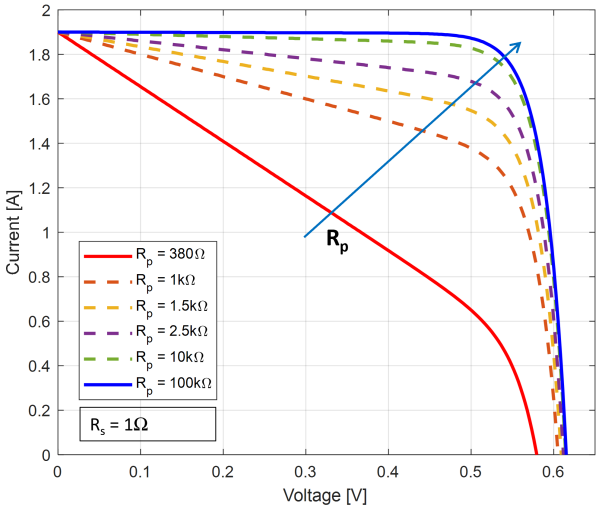

Figure 2.24: Effect on FF by increasing the R_p, under low light intensity of 0.05 Sun. Reproduced from [58].

Various experimental reports and simulations on indoor Organic PV devices have highlighted the importance of high parallel resistance, which should be sufficiently high to reduce leakage currents [59]. Leakage currents are unintended currents that flow through the circuit. In solar cells, leakage currents often occur due to imperfections in the material such as defects or impurities, or through pathways such as parallel resistance. It can degrade the performance of electronic components, leading to inefficiencies and potential damage over time. High R_p are thus desirable in low light intensities because they indicate fewer leakage paths, meaning that more of the generated current is collected and not lost to these unwanted paths.

As a rule of thumb, the minimum parallel resistance (R_p) should be larger than the ratio of open circuit voltage (V_{OC}) and short circuit current density (J_{SC}), i.e. $R_p^{\min} > V_{OC}/J_{SC}$ [60]. Typically, an IPV device operates at low light indoor intensities approximating a few hundred lux, these devices need to have a parallel resistance in the range of $M\Omega.cm^2$ range [11]. Achieving that can be challenging for a few PV technologies due to a very thin photoactive layer ($<1\mu m$), it is a common issue that the absorber layer does not fully cover the substrate [11]. Different device designs (p-i-n or n-i-p) can be utilized for the optimization of parallel resistance for the absorber material.

4. Power Conversion Efficiency

The Power Conversion Efficiency (PCE) is calculated as the ratio between the maximum power generated and the incident power [61]. Several factors influence the PCE of a solar cell, including the material properties and physical structure of the cell, its sensitivity to various wavelengths within the solar spectrum, the intensity of incident light, the operating (local) temperature, the efficiency of electron-hole pair generation, and the cell's ability to extract charge carriers with minimal losses [62]. More recently, the presence or absence of anti-reflecting coatings and surface texturing have also become important considerations [62]. The maximum power can be calculated by Equation 2.26.

$$P_{max} = V_{OC} I_{SC} FF \tag{2.26}$$

$$\eta = \frac{V_{OC} I_{SC} FF}{P_{in}} = \frac{P_{max}}{P_{in}} \tag{2.27}$$

In Equation 2.27, the P_{in} is the incident power. In cases of outdoor illuminations or analyzing the efficiency under a solar simulator, the incident power is taken as $1000W/m^2$ according to the AM 1.5G spectrum. In the case of indoor illuminations, where the light source is mainly artificial light sources such as LED, CFL and Halogen bulbs, the spectrum varies from the type of light source. Hence, under an artificial light source or more than one light source, the P_{in} values need to be calculated separately.

PCEs under indoor low light intensities are higher compared to the standard AM 1.5G solar spectrum. This can be understood by analyzing the spectral composition of indoor artificial light sources, such as LEDs, Halogen lamps and Fluorescent lamps, which emit light in narrow spectral bands (refer Figure 2.1). Unlike the broad spectrum of AM 1.5G, these artificial light sources predominantly emit within the visible region (380-830nm wavelength range). Consequently, the narrower and more concentrated spectral output of indoor lighting aligns more closely with the absorption characteristics of the absorber material of the solar cells, leading to enhanced efficiency in converting light to electricity under these conditions.

2.4. Indoor PhotoVoltaics

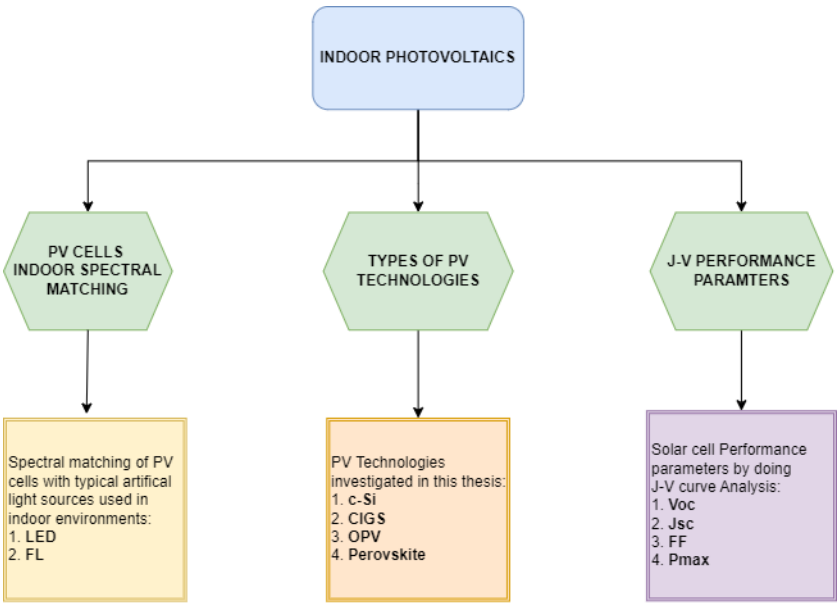

Figure 2.25: Overview on the literature review on Indoor PhotoVoltaics in this thesis.

Figure 2.25 presents a comprehensive overview of the literature review on indoor photovoltaics (PV) conducted in this thesis. The review is designed to provide clarity on the spectral characteristics of common artificial light sources used in indoor environments, such as LEDs and fluorescent lamps, and their interaction with photovoltaic cells. A crucial focus is placed on how well these light sources match the absorption spectrum of the PV cells and the strategies employed to maximize energy harvesting in low-intensity ambient conditions. By analyzing this spectral matching, the review seeks to explore how PV technologies can be optimized to perform efficiently under the specific constraints posed by indoor lighting, where light intensity is significantly lower than under standard test conditions (1 Sun).

Following this, the review delves into various PV technologies that are relevant to the experimental work presented in this thesis. These technologies include crystalline silicon (c-Si), organic photovoltaics (OPV), thin-film chalcogenides (CIGS and CdTe), and perovskite solar cells (PSC). For each technology, the discussion includes an examination of the material composition, working principles, and the specific design parameters that make them suitable for indoor light harvesting. The key focus is on understanding the physical and chemical properties of the materials used, their charge transport mechanisms, and the innovations that have been applied to enhance their performance under low-light conditions.

While the detailed explanation of the J-V curve parameters has already been provided in Section 2.3.1, this section focuses on the reported values from the literature and their direct impact on the power conversion efficiency (PCE) of the respective PV technologies. The tables included summarize the J-V curve parameters—such as open-circuit voltage (Voc), short-circuit current density (Jsc), fill factor (FF), and maximum power output (Pmax) for respective illuminations or lux levels—as reported for various indoor PV cells. These values offer valuable insights into the performance of PV cells under indoor illumination, emphasizing how these parameters contribute to the overall PCE, which is critical for optimizing energy conversion in practical indoor applications.

2.4.1. PV Cells Indoor Spectral Matching

The irradiance spectra of commonly used indoor light sources such as LEDs, Halogen and FLs have high energy photons and have a narrow spectrum (300nm-1000nm) as discussed in Section 2.1. Thus, indoor light sources are comprised of only the ultraviolet and visible region photons. Therefore, for the solar cells to avoid unexpected energy losses due to thermalization and non-absorption of light, the absorber layer of the solar cells used in IPV devices should have narrow absorption bands [63]. The spectral range of indoor lighting is confined to the visible region, resulting in a higher optimal bandgap for indoor photovoltaics compared to the optimal bandgap associated with the 1 Sun illumination spectrum [14].

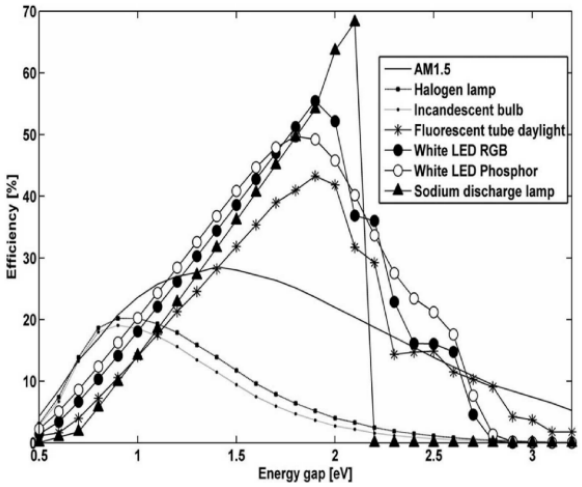

Figure 2.26: Maximum Power Conversion Efficiencies with respect to bandgap energy (eV) of an ideal PV converter under numerous light sources. Illustrating the ideal band gap energy near 1.9eV to 2.0eV for energy harvesting in ambient light conditions [60].

Additionally, Figure 2.26 illustrates the bandgap energies associated with various light sources, including the AM 1.5 spectrum, a fluorescent bulb, a 3-colour (RGB) LED, a Halogen lamp, an incandescent lamp and a phosphor LED bulb. Under the commonly used LED lighting, the maximum achievable conversion efficiency can reach up to 58.4% and under fluorescent tube (FT) illumination, the maximum predicted efficiency can attain 46%. Based on calculations by Freunek et al., the optimal bandgap energy for photovoltaic materials under artificial light sources is approximately 1.9 eV to 2.0 eV, which is ideal for fabricating highly efficient indoor solar cells [60]. In comparison, the optimized energy bandgap for photovoltaic materials under 1 Sun illumination is approximately 1.35 eV [14]. Therefore, crystalline silicon technology, with a bandgap of 1.12 eV, can efficiently perform better under 1 Sun illumination.

2.4.2. Types of PhotoVoltaic Technologies

The current photovoltaic (PV) market is predominantly dominated by silicon (Si) technology, with Si-based wafer PV technology accounting for approximately 97% of global production as of 2023, according to the Fraunhofer Institute for Solar Energy Systems [64]. This widespread adoption stems from crystalline silicon (c-Si) technology's proven efficiency in converting sunlight into electrical energy.

Under standard test conditions (1 Sun illumination), c-Si cells demonstrate high power conversion efficiencies. However, their efficiency drastically diminishes under indoor low-light environments due to a reduction in open-circuit voltage, which is essential for generating significant electrical output under such conditions [12].

While significant research has explored the use of c-Si for indoor light harvesting, the performance of these cells, particularly in polycrystalline form, remains suboptimal. In contrast, amorphous silicon (a-Si) has shown more promise, demonstrating the ability to achieve higher power conversion efficiencies under indoor lighting. This is largely due to a-Si's narrow absorption spectrum, which is better suited to the visible light spectrum typical of indoor lighting. Although a-Si is known to experience light-induced degradation due to the Staebler-Wronski effect, it has still found commercial success in indoor PV applications. Its ability to be deposited on glass substrates and its relatively good initial performance under low-light conditions make it advantageous for device fabrication [10]. Despite the lower outdoor performance of a-Si compared to c-Si, its characteristics make it more suitable for indoor energy harvesting.

In addition to c-Si and a-Si technologies, thin-film photovoltaic technologies (TFPV), have emerged as promising candidates for indoor light applications. The PV technologies which are currently being researched for the application under low light intensities are namely:

- amorphous - Silicon (a-Si:H)
- Thin film chalcogenide (CdTe, CIGS,etc)
- Organic Solar Cells (OSC)
- Perovskite Solar Cells (PVSC)
- Dye-Sensitized Solar Cells (DSSC)

Although TFPV has not been as extensively studied as silicon-based technologies, their ability to achieve high power conversion efficiencies under low-light artificial conditions has generated significant interest. Similarly, newer PV technologies, such as Dye-Sensitized Solar Cells (DSSCs), Organic Solar Cells (OSCs), Perovskite Solar Cells (PVSCs) have been the focus of recent research due to their flexibility, lightweight structures, and compatibility with indoor lighting conditions. These technologies hold considerable promise for the future of indoor energy harvesting, where efficiency under low-light conditions is paramount [65] [66].

The growing attention on perovskite, organic and dye-sensitized solar cells for research into emerging PV technologies highlights their potential for achieving high power conversion efficiencies in artificial low-light environments. Only photovoltaic technologies relevant to the experimental work of this thesis will be explored further in the literature review.

2.4.3. Silicon technology

Crystalline silicon (c-Si) solar cells are nearing the Shockley-Queisser (SQ) limit, with a theoretical maximum efficiency of about 33% [62]. Monocrystalline silicon (mono-Si) has reached a peak laboratory cell efficiency of 27.3% [67], benefiting from low defect density and efficient light absorption in the 400 to 1100nm range. In comparison, multi-crystalline silicon (multi-Si) achieved 23.3% power conversion efficiency (PCE) for its cost-effective production despite slightly lower performance [68].

However, these performance advantages under outdoor conditions of c-Si solar cells, including both mono-Si and multi-Si, significantly diminish under indoor illumination conditions. The lower bandgap of c-Si, which works well for sunlight, results in higher thermalization losses and suboptimal light absorption in the visible range, where indoor lighting primarily resides [10]. With a spectral response of 0.5 to 0.7 A/W around 950nm, c-Si is less effective at harnessing indoor light, leading to lower overall efficiencies [69].

In contrast, thin-film amorphous silicon (a-Si) has a wider bandgap (~1.7eV) and is better suited for indoor environments. Its spectral response, ranging from 350 to 800nm with a peak absorption of 0.3 to 0.4A/W around 500-600nm, matches well with indoor light spectra [70].

Table 2.3: Crystalline and amorphous silicon technologies under indoor illumination conditions, as reported in the literature. The data includes the light source, illumination intensity, and cell details, followed by the J-V parameters under indoor illumination, and the power conversion efficiency (PCE) under 1 Sun conditions. The abbreviations "S" and "M" indicate whether the device is a single cell or a module, respectively.

	Specification			Lamp	Incident light	J-V parameters under indoor illumination					1 Sun	
Active layer	Substrate	Area [cm²]	Cell type	Light source	Illumination [lux]	Voc [V]	Jsc [μA/cm²]	FF [%]	[a]Pmax [μW/cm²]	PCE [%]	PCE [%]	Ref.
Crystalline Silicon												
c-Si	Rigid	1	S	LED	186	0.37	22	63	5.99	6.92	13.49	[12]
c-Si	Rigid	1	S	LED	890	0.43	120	71	35.1	9.65	13.49	[12]
c-Si	Rigid	1.93	S	LED	200	0.22	20.16	-	2.09	-	-	[72]
c-Si	Rigid	1.93	S	LED	1000	0.33	102.29	-	17.89	-	-	[72]
c-Si	Rigid	4	S	LED	1000	0.43	126	67	36.6	12.5	-	[73]
c-Si	Rigid	48	M	LED	1000	1.18	41.73	59	29.92	9.3	-	[74]
c-Si	Rigid	4	S	LED	1000	0.519	119.2	71.3	44.1	15.5	25.7	[19]
c-Si	Rigid	36	S	LED	1000	0.55	1500	44	-	3.55	-	[75]
Amorphous Silicon												
a-Si	Rigid	7.65	S	LED	1000	0.71	89.4	73.1	46.4	16.3	7.9	[19]
a-Si semitransparent	Rigid	0.25	S	LED	900	0.73	160	49.5	57.5	5.75	6.05	[13]
a-Si	Rigid	1.04	S	LED	200	0.63	21.8	68	9.4	12.2	-	[76]
a-Si semitransparent	Rigid	0.25	S	LED	1000	-	-	-	-	29.9	-	[19]
a-Si	Rigid	31.8	M	CFL	200	-	-	-	-	8.1	6.8	[77]
a-Si	Rigid	31.8	M	CFL	1000	0.73	83	-	46.5	-	6.8	[77]
a-Si	Rigid	31.8	M	LED	200	-	-	-	-	9.4	6.8	[77]
a-Si	Rigid	31.8	M	LED	1000	-	-	-	-	46.4	6.8	[77]
a-Si	Flexible	30	M	CFL	300	8	1.5	67	8	8.7	-	[78]
a-Si	Flexible	38	M	LED	200	0.69	9.36	32.2	0.70	1.05	-	[79]
a-Si	Rigid	6.63	M	LED	200	2.44	13.7	64.8	4.32	6.55	-	[79]

[a] **Pmax**: Maximum power density is the highest power output per unit area (μW/cm²) that the solar cell can deliver under specific illumination conditions.

The lower mobilities and high resistivity of a-Si do not notably impact performance under indoor lighting. Additionally, its low production cost, compatibility with low-temperature fabrication and longer operational lifetime make a-Si a commercially viable choice for indoor PV applications [71]. However, from a stability point of view, amorphous silicon and crystalline-based cells have a much longer operational lifetime and can be effectively implemented under low-light conditions.

Table 2.3 presents J-V parameters from various studies on crystalline and amorphous silicon technologies under indoor lighting conditions. This table offers a quick overview of how these technologies perform under different light sources and intensities, highlighting key metrics such as Voc, Jsc, FF and PCE under indoor conditions and under 1 Sun respectively.

In a recent study, Sin et al. developed a 3D-shaped c-Si device to enhance direct and indirect light absorption. Compared to the conventional flat c-Si solar cell of $1.73cm^2$, the tetrahedron cell (with three connected cells covering 97.43 cmcm^2) showed significantly higher output power under 1469lx LED illumination, despite occupying the same floor area [80], [10]. A larger module of tetrahedron c-Si cells further outperformed emerging indoor PV technologies like OPV and perovskite, demonstrating the potential of c-Si for indoor applications despite its bandgap limitations.

Additionally, Kim et al. achieved 36% PCE at 3000lx and a power density of 0.92 mW/cm^2 with an a-Si /$\mu c-Si$ tandem device featuring an advanced architecture for stability and efficiency under indoor conditions [76].

In summary, the research into both crystalline silicon and a-Si highlights their unique strengths in indoor applications. With innovative configurations such as the tetrahedron shape, c-Si demonstrates adaptability and potential for enhanced light absorption. Further exploration of these materials could lead to even more efficient and tailored solutions for indoor energy harvesting.

2.4.4. Thin film chalcogenide cells

Thin-film chalcogenides, specifically Copper Indium Gallium Selenide (CIGS) and Cadmium Telluride (CdTe), represent a prominent class of thin-film solar cell technologies due to their optoelectronic properties and cost-effective production potential. CIGS and CdTe have achieved record efficiencies of 23.6% and 22.1%[81] [68], respectively under AM1.5G spectrum.

The working principle of these thin-film chalcogenide solar cells follows a similar structure to conventional photovoltaic devices. Figure 2.27 highlights a typical CIGS solar cell structure and the band alignment in a typical CIGS solar cell. The structure of the cells consists of a glass substrate, a molybdenum (Mo) back contact and a p-doped CIGS absorber. This is followed by an n-doped CdS buffer layer and a transparent conducting oxide (TCO), typically ZnO, forming a p-n junction where the electric field separates photogenerated electron-hole pairs.

Light enters through the TCO and photons absorbed in the CIGS layer excite electrons from the valence band to the conduction band. Electrons are collected at the ZnO front contact, while holes move to the Mo back contact, generating current. The conduction band alignment between ZnO, CdS and CIGS ensures efficient electron transport while minimizing recombination losses.

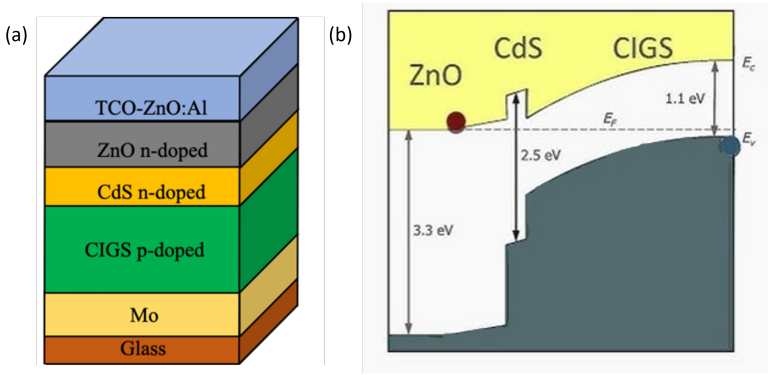

Figure 2.27: (a) Typical CIGS solar cell structure and (b)The band alignment in CIGS solar cells [82].

Table 2.4 presents studies on thin-film chalcogenide cells under indoor conditions, detailing key J-V parameters such as Voc, Jsc, FF, and PCE. It is clear from the table that relatively few studies have focused on indoor conditions compared to the extensive research conducted under 1 Sun illumination.

Table 2.4: Thin film chalcogenides (CIGS, CdTe,etc) technologies under indoor illumination conditions, as reported in the literature. The data includes the light source, illumination intensity, and cell details, followed by the J-V parameters under indoor illumination, and the power conversion efficiency (PCE) under 1 Sun conditions. The abbreviations "S" and "M" indicate whether the device is a single cell or a module, respectively.

	Specification			Lamp	Incident light	J-V parameters under indoor illumination					1 Sun	
Active layer	Substrate	Area [cm^2]	Cell type	Light source	Illumination [lux]	Voc [V]	Jsc [$\mu A/cm^2$]	FF [%]	[a]Pmax [$\mu W/cm^2$]	PCE [%]	PCE [%]	Ref.
CIGS	Rigid	0.5	S	LED	100	0.36	11.5	33.8	1.4	4.5	17	[19]
	Rigid	0.5	S	LED	1000	0.51	114.3	65.5	38.6	12.5	17	[19]
CdTe	Rigid	0.25	S	LED	100	0.51	12.7	68	4.5	15.7	15.8	[19]
	Rigid	0.25	S	LED	1000	0.58	113.4	77.1	50.9	18	15.8	[19]
CdSeTe/CdTe	Rigid	0.65	S	LED	350	-	-	-	-	17.1	-	[83]
CdTe	Rigid	3.49	M	FL	1000	2.2	17.5	-	14.1	1.41	-	[84]
CIGS	Flexible	450	M	FL	1000	2	1.8	23	0.83	0.17	-	[85]
CIGS	Flexible	211	M	LED	200	0.14	21	26	0.9	-	5.6	[86]

[a] **Pmax**: Maximum power density is the highest power output per unit area ($\mu W/cm^2$) that the solar cell can deliver under specific illumination conditions.

Despite their success in outdoor applications, thin-film chalcogenides have seen limited research in low-light conditions like indoor artificial lighting. Addressing this gap could enable their integration into indoor PV (IPV) systems. Yang et al. conducted a comparative study of c-Si and CIGS cells under

various indoor light sources, with higher short circuit current under fluorescent lighting (FL) [87]. In contrast, CIGS cells exhibited greater variation in both Voc and Isc based on light type, with slightly lower values under FL compared to c-Si cells.

In conclusion, this study suggests that while CIGS cells perform well under outdoor conditions, their efficiency in indoor environments is limited. Research on CIGS for indoor applications is still scarce, as these cells are inherently better suited for outdoor use.

2.4.5. Organic Solar cells

Organic photovoltaics (OPVs), employ organic materials as the active layer in solar cells. They have attracted attention in the field of research due to their low-cost processing, suitability for both rigid and flexible substrates, potential for large-area applications, and the wide variety of organic molecules available with diverse optoelectronic properties [88]. Fabrication methods for OPVs include vacuum evaporation, spin-coating, inkjet printing, blade coating, drop-casting, screen printing, and roll-to-roll (R2R) printing [88] [14].

OPVs function by converting light into electrical energy using a blend of two organic semiconductors: a donor (p-type) and an acceptor (n-type). The active layer of these cells consists of a blend of these materials, where light absorption, charge generation and separation take place.

Figure 2.28illustrates the working principle of an organic solar cell. Upon illumination, the **(1)** incident photons are absorbed, generating excitons (electron-hole pairs). Due to the short exciton diffusion length ($\approx 10nm$) in organic semiconductors [89], these excitons **(2)** diffuse to the donor-acceptor interface, where they **(3)** dissociate into free charge carriers. The electron moves from the lower energy, the highest occupied molecular orbital (HOMO) of the donor to the higher energy, the lowest unoccupied molecular orbital (LUMO) of the acceptor. This charge separation is energetically favourable when the energy difference between the donor's HOMO and the acceptor's LUMO exceeds the exciton binding energy, which typically ranges between 0.3 - 1 eV [88]. Once separate, the **(4)** free electrons travel through the acceptor to the cathode, while holes move through the donor to the anode, generating a current extracted at the electrodes.

To improve exciton dissociation and charge separation, OPV cells commonly employ a bulk heterojunction (BHJ) architecture, where the donor and acceptor materials are blended at the nanoscale as seen in Figure 2.28, creating an extensive interface for excitons to dissociate, thereby improving efficiency. Proper energy alignment between the donor HOMO and acceptor LUMO is essential for effective exciton dissociation and charge transfer.

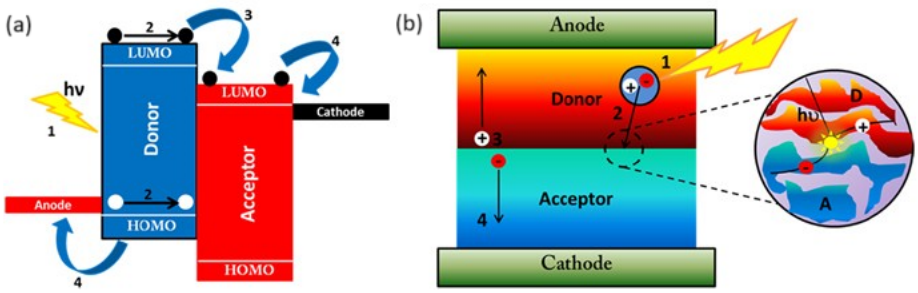

Figure 2.28: (a)Working principle of an Organic solar cell illustrating (1) Light absorption and exciton (electron-hole pair) generation, (2) Diffusion of exciton to interface, (3) Dissociation into free electrons and holes at the donor-acceptor interface and (4) Charge transport of electrons and holes to the respective electrodes, (b)Schematic of charge separation at the donor-acceptor interface [88].

A significant amount of research is being conducted on OPV to study their performance under indoor lighting conditions. Table 2.5 presents a selection of reported J-V parameters from these studies

Compared to inorganic and hybrid systems, OPVs exhibit lower efficiency under standard test conditions (AM 1.5G) primarily due to significant recombination losses associated with their active layer material [95]. The current record for OPV power conversion efficiency (PCE) is 19.2% under AM 1.5G

Table 2.5: Organic photovoltaic technologies (OPV) under indoor illumination conditions, as reported in the literature. The data includes the light source, illumination intensity, and cell details, followed by the J-V parameters under indoor illumination, and the power conversion efficiency (PCE) under 1 Sun conditions. The abbreviations "S" and "M" indicate whether the device is a single cell or a module, respectively.

	Specification			Lamp	Incident light	J-V paramters under indoor illumination					1 Sun	
Active layer	Substrate	Area [cm2]	Cell type	Light source	Illumination [lux]	Voc [V]	Jsc [μA/cm²]	FF [%]	[a]Pmax [μW/cm²]	PCE [%]	PCE [%]	Ref.
PTB7-Th PC70BM	Rigid	1	S	LED	186	0.56	19	72	7.63	10.55	8.43	[12]
	Rigid	1	S	LED	890	0.74	92	74	42.3	11.63	8.43	[12]
P3HT:ICBA	Rigid	-	S	FL	500	0.73	50	62	22.57	13.76	4.90	[90]
	Rigid	-	S	LED	500	0.73	50	63	22.97	13.05	4.90	[90]
P3HT:P60CBM	Rigid	-	S	FL	500	0.43	62	59	15.77	9.5	3.68	[90]
	Rigid	-	S	LED	500	0.43	62	59	15.67	8.90	3.68	[90]
PBDTTT-EFT:PC70BM	Rigid	-	S	FL	500	0.58	63	59	21.56	13.14	6.95	[90]
	Rigid	-	S	LED	500	0.59	66	58	23.23	13.20	6.95	[90]
P3HT:ICBA	Rigid	100	M	LED	1000	0.56	104.7	60	35	14.6	0.3	[91]
PBDB-TF:IO-4Cl	Rigid	1	M	LED	200	1.03	18.2	71.5	13400	22.2	9.8	[51]
	Rigid	1	M	LED	500	1.07	45.1	76.8	37100	24.6	9.8	[51]
	Rigid	1	M	LED	1000	1.10	90.6	79.1	79	26.1	9.8	[51]
P3HT:PC60BM	Rigid	100	M	FL	300	0.41	20.6	56.6	4.8	5.8	2.4	[92]
PCDTBT:PC71BM	Rigid	100	M	FL	300	0.72	27.7	69.3	13.9	16.6	6	[92]
PTB7:PC71BM	Rigid	100	M	FL	300	0.61	28.6	69.5	12.2	14.6	6.8	[92]
PTB7:PC71BM:EP-PDI	Rigid	0.15	S	LED	500	0.65	57.8	68.5		15.68	8.53	[93]
PBDB-TS:IT-4F	Rigid	-	S	FL	500	0.36	66.8	30.9	7.5	5.3	8.7	[94]
	Rigid	-	S	FL	1000	0.48	125.5	36.2	22	7	8.7	[94]
PBDB-TS-3Cl:IT-4F	Rigid	-	S	FL	500	0.64	62.8	72.2	29.2	20.4	12.6	[94]
	Rigid	-	S	FL	1000	0.66	123.8	72.8	60.2	19.4	12.6	[94]
	Rigid	-	S	FL	1000	0.66	123.8	72.8	60.2	19.4	12.6	[94]

[a] **Pmax**: Maximum power density is the highest power output per unit area (μW/cm²) that the solar cell can deliver under specific illumination conditions.

conditions [68]. However, the OPVs exhibit superior performance under indoor or low-light intensity compared to crystalline silicon solar cells.

Mori et al. conducted a comparative study on the performance of OPVs based on Poly(3-hexylthiophene-2,5-diyl) (PTB7-Th) and [6,6]-phenyl-C71-butyric acid methyl ester (PC71BM) versus c-Si solar cells [12]. Their findings revealed that under 1 Sun illumination, the c-Si solar cells exhibited a higher PCE of 13.49% compared to the OPV (PTB7-Th) which achieved a PCE of 8.43%. However, under an LED illumination intensity of 890 lux, the PCE of the c-Si solar cells decreased to 9.65%, while the OPV achieved a higher PCE of 11.63%. Notably, when the illumination intensity was further reduced to 186lux, the OPVs maintained a PCE of 10.55%, whereas the PCE of the c-Si solar cells dropped to 6.93%. This can be seen in Figure 2.29. The lower recombination losses and effective spectral utilization by OPVs significantly contribute to their enhanced relative performance compared to c-Si cells in indoor environments.

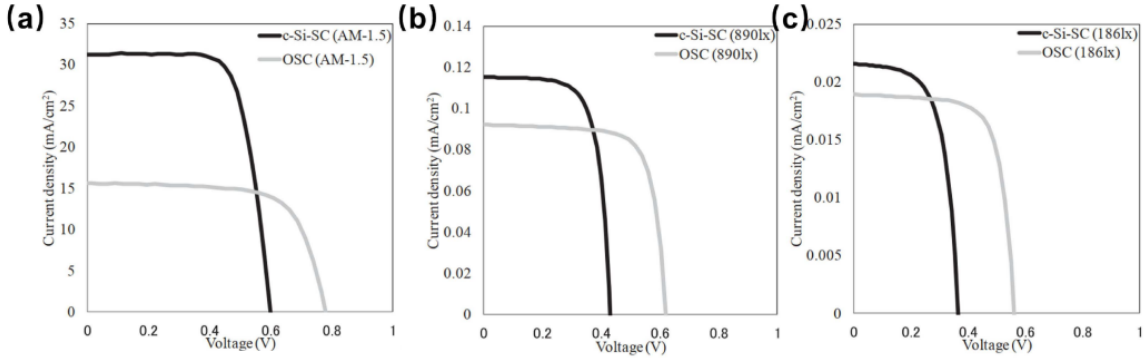

Figure 2.29: The J-V curves of crystalline silicon and organic solar cells, which is denoted as c-Si-SC and OSC, respectively, (a) Under AM1.5G spectrum, (b) under 890lux and (c) 186lux of an LED light source [12].

Fullerene acceptors have been extensively utilized in indoor OPV due to their strong absorption in the near UV region and large bandgap [96]. The Voc in OPV is directly related to the energy difference between the HOMO of the donor material and the LUMO of the acceptor material. Typically, OPVs with higher Voc are more suitable for indoor applications. To achieve high Fill Factors (FF), trap-assisted recombination must be minimized through effective passivation [97].

Furthermore, recent developments in OPV technology, including non-fullerene acceptors (NFAs), have led to improved spectral compatibility and further reductions in recombination losses, resulting in PCE improvements of up to 20% under low-light conditions [98].

In summary, recent advancements in OPV have highlighted their strong potential for indoor energy harvesting, particularly under artificial light sources such as LED and Fluorescent lamps. While c-Si solar cells perform efficiently under standard conditions, OPVs have demonstrated superior performance in indoor environments due to their better spectral compatibility with indoor lighting. The development of non-fullerene acceptor (NFA) materials has further enhanced the performance of OPVs, making them a promising option for indoor applications.

2.4.6. Perovskite Solar cells

Perovskite material is an organometal halide with a chemical structure of ABX_3, where (A) and (B) are both cations and (X) is the halogen which generally consists of Cl^-, Br^- and I^- as seen in Figure 2.30b which depicts a cubic perovskite lattice which also happens to be the most common crystal structure for perovskite materials. In the perovskite crystal structure, the A-site is predominantly occupied by methylammonium ($CH_3NH_3^+$) cations, while the B-site is occupied by lead (Pb^{2+}) cations.

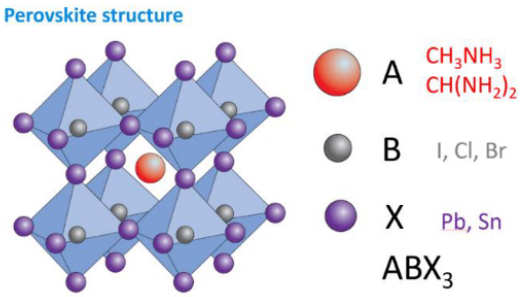

(a) A cubic perovskite lattice, one of the most common crystal structures for perovskite materials. The lattice is made up of corner-sharing octahedra, where each octahedron is composed of a metal cation (B) surrounded by six halide anions (X) [99].

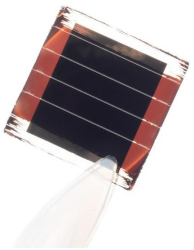

(b) Perovskite solar cell [100].

Figure 2.30: Perovskite Solar Cell

The first perovskite material-based solar cell, developed by Kojima et al. in 2009, demonstrated an initial PCE of 3.8% [101]. Since then, perovskite (PVK) solar cells have improved significantly with the highest reported efficiency under outdoor conditions reaching approximately 25.5% [17]. Under indoor lighting conditions, PVKs have also exhibited remarkable efficiencies, with the highest recorded value reaching 40.1% at an illumination intensity of 824 lux from an LED lamp (2700K) for a single cell [102].

The high efficiency of perovskite solar cells under indoor illumination can be attributed to a combination of their material properties and adaptability to low-light conditions. These characteristics make them highly effective in harvesting energy from typical artificial light sources.

The key advantages of perovskite in indoor low-light environments are as follows:

1. **Long charge carrier diffusion length:** Enables efficient charge collection boosting PCE.
2. **Tunable bandgap:** The bandgap of perovskites can be adjusted by varying the composition of halogens, organic ions, and metals. This tunability allows for optimization for specific indoor light sources.

3. **Low fabrication costs:** Solution-based, low-temperature fabrication processes make PVK affordable for large-scale applications.
4. **High Absorption Coefficient:** PVK absorb light efficiently at low intensities, making them well-suited for indoor applications.
5. **Scalability:** Devices designed for indoor use are significantly smaller in size compared to outdoor applications, making them highly scalable and more cost-effective for IPV applications.
6. **Low process temperature:** allows production of flexible, lightweight cells ideal for indoor use.
7. **Defect tolerance:** Perovskites exhibit good tolerance to defects, maintaining high performance even with structural imperfections, crucial for low light environnments.

Moreover, perovskite modules can be fabricated on flexible substrates, thus being suitable for applications where conformability, low weight, and portability are required [103].

Similar to OPV, substantial research has been conducted on the indoor performance of perovskite solar cells. Table 2.6 presents some of the reported J-V parameters from these studies.

Table 2.6: Perovskite technologies under indoor illumination conditions, as reported in the literature. The data includes the light source, illumination intensity, and cell details, followed by the J-V parameters under indoor illumination, and the power conversion efficiency (PCE) under 1 Sun conditions. The abbreviations "S" and "M" indicate whether the device is a single cell or a module, respectively.

	Specification			Lamp	Incident light	J-V parameters under indoor illumination					1 Sun	
Active layer	Substrate	Area [cm2]	Cell type	Light source	Illumination [lux]	Voc [V]	Jsc [μA/cm2]	FF [%]	[a]Pmax [μW/cm²]	PCE [%]	PCE [%]	Ref.
$CH_3NH_3PbI_{3-x}Cl_x$	Rigid	5.44	S	FL	100	0.75	13.57	65	6.61	20.90	-	[104]
	Rigid	5.44	S	FL	600	0.83	79.55	74	48.85	25.10	-	[104]
	Rigid	5.44	S	FL	1000	0.84	132.26	75	83.32	26.30	-	[104]
$MAPBI_3$	Rigid	0.15	S	CFL	200	0.41	31	60	13.4	20.8	11.1	[105]
	Rigid	0.15	S	CFL	400	-	-	-	24.9	-	-	[105]
	Rigid	0.15	S	LED	200	-	-	-	11.6	17.4	-	[105]
	Rigid	0.15	S	LED	400	-	-	-	24.9	18.9	-	[105]
$Cs_{0.17}FA_{0.83}Pb(I_{0.7}Br_{0.3})_3$	Flexible	0.68	S	CLED	500	0.792	49.4	74	28.95	20.5	-	[19]
$CH_3NH_3PbI_{3-x}Cl_x$	Flexible	2.5	M	LED	200	0.64	15.8	75.2	7.2	10.80	9.2	[103]
	Flexible	2.5	M	LED	400	0.66	33.7	77.3	16	12.10	9.2	[103]
$CH_3NH_3PbI_3$	Rigid	-	S	LED	200	0.72	33.49	47	12.36	-	15.27	[8]
	Rigid	-	S	LED	400	0.73	63.29	55	28.03	-	15.27	[8]
	Rigid	-	S	LED	800	0.77	126.34	62	63.79	-	15.27	[8]
	Rigid	-	S	LED	1600	0.78	261.17	64	147.74	-	15.27	[8]
$MAPBI_3$	Flexible	-	M	LED	200	0.80	23.68	49.59	9.77	12.85	14.8	[106]
	Flexible	-	M	LED	400	0.84	40.26	52.57	19.2	13.32	14.8	[106]
$MA_{0.85}Cs_{0.15}Pb(I_{0.75}Br_{0.15})_3$	Rigid	0.1	S	LED	200	0.83	25.48	75	16	22.9	-	[107]
	Rigid	0.1	S	LED	1000	0.89	124.02	80	88.3	25.1	-	[107]
$FA_0.75MA_0.25SnI_2Br$	Rigid	0.07	S	LED	1000	0.54	133	63	45.39	13.57	-	[108]
BiOI	Rigid	-	-	LED	1000	0.60	56	38	12.77	4	-	[109]
$CH_3NH_3PbI_{3-x}Cl_x$	Rigid	5.44	M	FL T5	200	0.70	23.96	74	12.41	19.2	-	[104]
	Rigid	5.44	M	FL T5	1000	0.75	118.49	71	63.09	20.1	-	[104]
$MAPbI_{2-x}BrCl_x$	Rigid	2.25	M	FL	1000	0.96	130	-	84.27	30.6	-	[110]

[a] **Pmax**: Maximum power density is the highest power output per unit area (μW/cm²) that the solar cell can deliver

Although most studies focus on PVK solar cells under AM 1.5G spectrum, research on indoor performance remains limited. Existing studies indicate that PVK cells perform well under indoor light due to bandgap tunability through halide substitution [10] [14]. For instance, $MAPbI_3$ perovskites (bandgap of 1.6eV) can be tuned by partially substituting iodine with bromine, increasing the bandgap to 1.79eV ($MAPbI_2Br$) [110]. This adjustment improves efficiency under indoor lighting, with open-circuit voltages (Voc) exceeding 0.9V, as wider bandgaps align better with the indoor light spectrum [110].

However, trap-induced recombination, cause by poor morphology or ion migration, remains a challenge for PVK cells. Various strategies are being implemented to overcome these limitations and enhance performance [10]. Trap-induced recombination is more prominent under indoor lighting due to

fewer photocarriers compared to AM 1.5G conditions. Reducing trap density via interface modification is crucial for enhancing indoor performance and reducing hysteresis [14].

Xu et al. demostrated that doping triple-cation lead halide perovskite with $EuCl_3$ improved film morphology, reduced defects and increased photoluminescence lifetime from 229 ns to 345.2 ns [97].These improvements not only enhanced performance, increasing PCE from 22.8% to 25% at 200lx and from 27.4% to 30% at 1000lx, but also minimized hysteresis under indoor conditions.

The quality of PVK films, influenced by deposition techniques, also plays a key role in efficiency. Spin-coating though commonly used, often results in defects like pinholes or small grains. Optimizing morphology through methods such as anti-solvent treatment and thermal annealing reduces these defects, lowering recombination and hysteresis which significantly boosts performance [10].

Morphological and compositional optimizations have enabled PVK to achieve near ideal bandgaps for artificial light. Sun et al. optimized a mixed-cation perovskite $Cs_{0.05}MA_{0.95}PbBr_xI_{3-x}$ with Nb-doped TiO_2 as electron transporting layer (ETL), achieveing PCEs of 36.3% under warm LED, 33.2% under cool fluorescent and 19.5% under solar light [111].

The presence of toxic lead as a key component in the absorber layer of high-efficiency perovskite solar cells has raised concerns regarding their use in indoor environments [112]. As a result, considerable research is focused on developing lead-free perovskite materials that can maintain high performance and offer improved stability for PSCs [113] [114].

In summary, recent advancements in optimizing perovskite solar cells for indoor applications through bandgap engineering, interface modifications and improved deposition techniques. Strategies such as doping and optimizing both the absorber and electron transport layer have been shown to significantly enhance PCEs under indoor lighting.

3

Experimental and Methodology

This chapter discusses the experimental setup that has been used to measure the performance of IPV devices under artificial light sources, especially CFL and LED lamps in a controlled environment setting. Section 3.1 describes the samples that are used for the experiments while Section 3.2 provides insights on the experimental setups used in this study.

3.1. Samples

This research focuses on the comparison of different PV technologies based on small minimodules, except for the silicon sample, which is a single cell of monocrystalline silicon. The rationale for comparing minimodules is that Indoor Photovoltaic (IPV) devices are typically small in size and often have limited surface area. Minimodules are well-suited for these applications because they can be incorporated into the available space while still generating sufficient power output depending on the power requirement of the IPV device even under limited light availability which is often encountered in indoor environments. Here, is a description of the samples that are being used for the comparative study.

Overview of the samples

Figure 3.1 shows the samples that are being used for the analysis under indoor light in the experimental setup as illustrated in Figure 3.5 and discussed in Section 3.2.1. Table 3.1 categorizes the specific dimensions of the samples and their power conversion efficiency (PCE) under Air Mass (AM) 1.5G. These samples are then used for analyzing the performance of different PV technologies under indoor conditions, in a controlled indoor experimental setup, which is further discussed in Section 3.2.

Table 3.1: Sample Dimensions

PV Technology	Type	Active Area [cm2]	Bandgap [eV]	Cells in Series	1 Sun PCE*	Rigidity
Monocrystalline silicon (mono-Si)	Single cell	4	1.11	1	12.29	Rigid
CIGS	Minimodule	165	1.12	6	11.97	Flexible
OPV	Minimodule	22	not specified (commercial)	6	0.69	Flexible
PVK	Minimodule	4	1.6	7	15.55	Rigid

***Indicates the 1 Sun PCE measured under a solar simulator at EnergyVille2, imec, Belgium.**

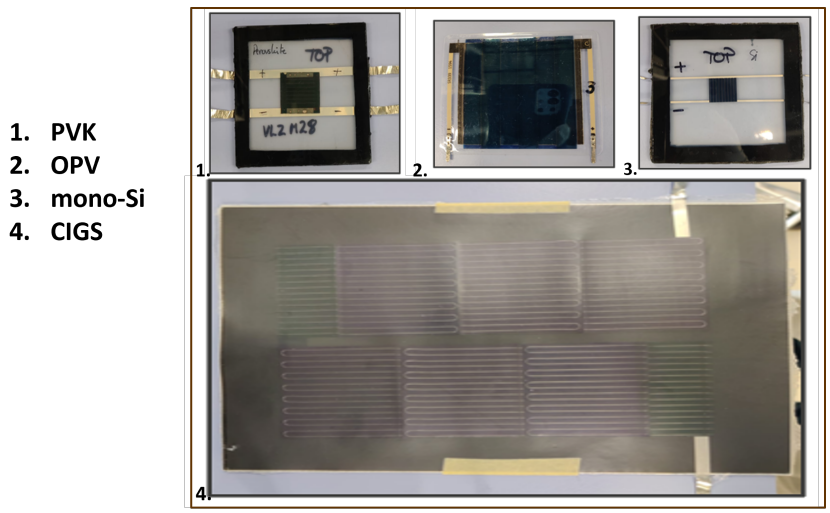

Figure 3.1: Pictures of the samples used for indoor testing.

As observed in Table 3.1, the sample dimensions are not uniform, particularly for the CIGS sample, which is notably larger than the other samples. This size disparity raises concerns about the sample's suitability for comparative analysis, especially in an IPV application. However, the focus is on the overall performance within the indoor experimental setup, the larger surface area affects the results, particularly about uniform illumination. Therefore, it is crucial to ensure that the samples used in the experimental setup are consistent in size and receive homogeneous illumination. This issue is further discussed in Section 3.3.

3.1.1. Perovskite minimodule

It is a minimodule consisting of 7 subcells connected in series, with an active area of 4 cm^2 and a bandgap of 1.6eV as discussed in Table 3.1. The perovskite minimodule was fabricated at the EnergyVille2 lab, imec, in Genk, Belgium. Figure 3.2a illustrates the structure of the semi-transparent PVK and Figure 3.2b after the monolithic interconnection of cells in series. The device begins with a glass substrate to provide structural support. On top of the glass, an Indium Tin Oxide (ITO) layer is deposited serving as the transparent conducting oxide (TCO) with a striped pattern. P1 laser scribing is then employed to define the cell boundaries within the TCO layer, ensuring electrical isolation between individual cells.

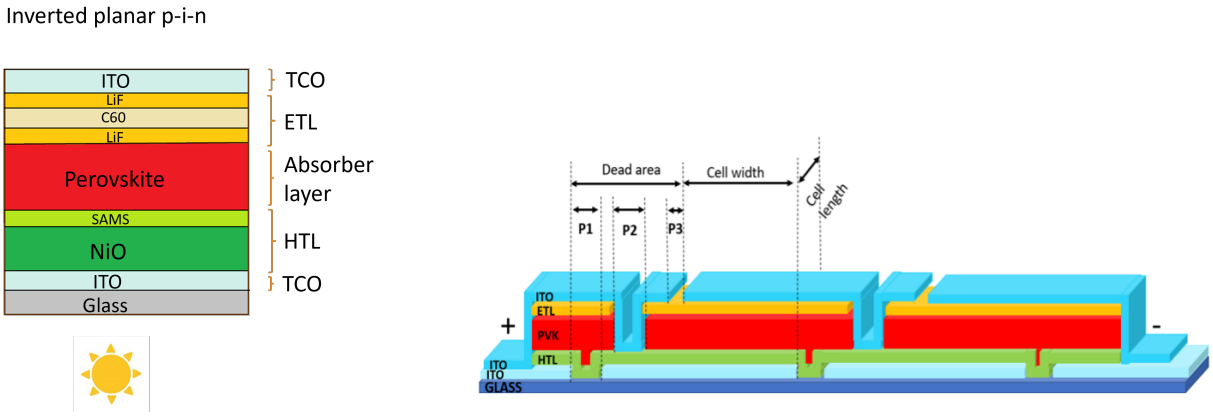

(a) Inverted p-i-n composition of the semi-transparent PVK. **(b)** P1, P2, and P3 laser scribes.

Figure 3.2: (a) Inverted p-i-n composition of the semi-transparent PVK. (b) Monolithically interconnection with the help of P1, P2 and P3 laser scribes.

Next, a layer of NiO (Nickel Oxide) is applied via sputtering, NiO serves as the HTL (Hole Transport

Layer), helping to move holes from the perovskite layer to the electrode. On top of the NiO, SAMS (Self-Assembled Monolayers) are applied to fine-tune the surface properties and enhance energy level alignment with the perovskite layer.

After that, the perovskite layer is deposited. This deposition can be done with various methods such as thermal evaporation, slot die coating, blade coating and spray coating. But for this sample, the deposition method of the absorber layer is done by the blade coating method. This is a crucial layer for absorbing light and generating charge carriers i.e. the electrons and holes. Above the perovskite layer, the electron transport layer, which consists of several sublayers, is formed. A LiF (Lithium Fluoride) layer is first deposited to enhance the interface properties and for passivation. This is followed by a layer of C_{60}, a fullerene derivative which acts as the primary electron transport material. Another layer of LIF is deposited on top of C_{60} to further aid in electron extraction and to reduce recombination losses. The device is completed with the deposition of another ITO layer, thus this layer makes it a semi-transparent PVK minimodule.

To ensure efficient electrical connections and proper integration, we use P2 and P3 laser scribing steps. The P2 scribe establishes the connection between the back of one cell and the front of the adjacent cell. P3 laser scribing, on the other hand, defines the cell width and length i.e. the active area of the cell. Thus, completes the necessary electrical connections. P2 and P3 steps are crucial for connecting the cells in series, increasing the module's voltage while keeping the current constant in series. The series connection, done monolithically through laser scribing, guarantees precise and clean cuts, reducing losses and maximizing efficiency.

3.1.2. Organic minimodule

The organic minimodule has an active area of 22 cm^2 and consists of 6 subcells connected in series. The bandgap of the sample is unknown, as it is a commercial product from Epishine, a Swedish company renowned for its innovation in printed organic indoor solar cell technology [115]. As it is a commercial product, the exact composition and polymers are proprietary and not disclosed. However, it features a PET (Polyethylene Terephthalate) substrate for support and flexibility, combined with an indium tin oxide (ITO) transparent electrode to ensure effective light harvesting under low-light conditions. The overall structure is designed for easy integration into indoor environments, making it ideal for powering low-energy devices like sensors in commercial and residential settings [115]. Thus, its performance under 1 Sun is also low as it is specifically designed for artificial light source spectrum.

3.1.3. Monocrystalline-Si

The monocrystalline Si sample used in this study is a single cell, with an active area of 4 cm^2. It is a heterojunction Si solar cell manufactured by the company Meyer Burger, with a general architecture presented in Figure 3.3.

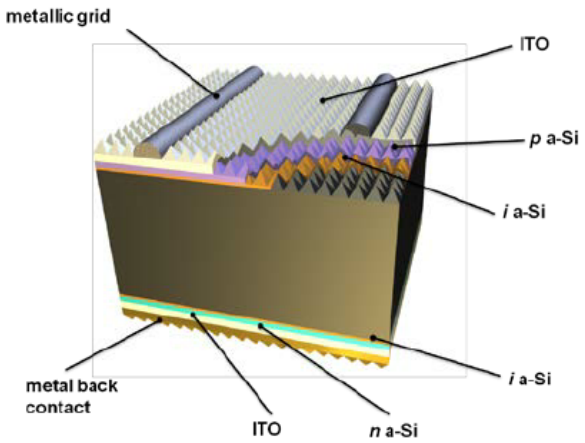

Figure 3.3: General architecture of a heterojunction Si solar cell. The main absorber layer is the n-type monocrystalline Silicon wafer [116].

The specific details of the layer stack for these cells are not disclosed by Meyer Burger, as they are part of their proprietary technology. The full wafer was laser-cut into 2 cm x 2 cm pieces, likely causing damage to the cells and contributing to lower performance under 1 Sun conditions. The low performance of the monocrystalline silicon cell can be attributed to the further losses that may have occurred during the soldering of tabs and the preparation for lamination, due to the difficulty of handling such small cell dimensions. For this analysis, cell dimensions similar to the perovskite module (4 cm^2) were chosen to ensure uniform illumination of the full sample, even when the sample-to-light source distance was only a few centimetres. The performance losses of the Si cell were accepted in exchange for dimensional convenience.

3.1.4. CIGS

The next sample is the CIGS (Copper Indium Gallium Selenide) minimodule manufactured by the company MiaSolé based in the US and then encapsulated in the EnergyVille2 lab in Genk. The minimodule has 6 cells connected in series and an active area of 165cm^2, with a bandgap of 1.12eV as can mentioned in Table 3.1.

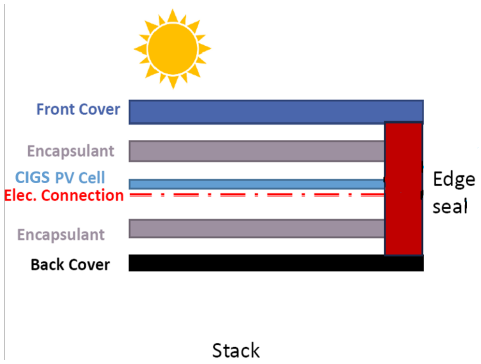

Figure 3.4: CIGS minimodule layup for encapsulation done at EnergyVille2 lab.

In Figure 3.4, the schematic cross-section showcases the layered structure of the module. Starting at the top, the front cover acts as a protective barrier. Beneath this is the Encapsulant, a plastic layer made by the polymer company Yparex, consisting primarily of an extrudable adhesive resin [117]. This resin binds the front and back covers to the PV cell. Its purpose is to safeguard the PV module from moisture and dust while providing structural stability. An Edge Seal encircles the cell, protecting it from moisture and mechanical damage. The configuration is completed with a Back Cover, which adds further protection and functionality.

3.2. The Experimental setups

For the analysis of the indoor performance of the samples outlined in Section 3.1, two experimental setups were employed. The first setup was located at the EnergyVille2 lab, imec, in Genk, Belgium, where the initial results were obtained. The second setup was at the Centre for Hybrid and Organic Solar Energy (CHOSE) laboratory in Italy, where the next set of experiments were carried out due to an equipment malfunction at the earlier lab. Collaboration with the CHOSE lab was necessary to verify the malfunction and ensure the completion of the experiments. As a result, the experiments were successfully conducted at the CHOSE laboratory, ensuring the collection of reliable and conclusive results.

Section 3.2.1 details the setup employed in Belgium, while Section 3.2.2 provides an overview of the experimental setup utilized in Italy. Both experimental setups played a critical role in enabling the comprehensive analysis and evaluation of the samples' performance under indoor conditions.

3.2.1. Experimental Setup at imec, Belgium

The experimental setup at the EnergyVille2 lab consists mainly of three parts, namely the:

1. **Light source** ranging from CFL, LED and Halogen bulbs and tubelights of different watts of

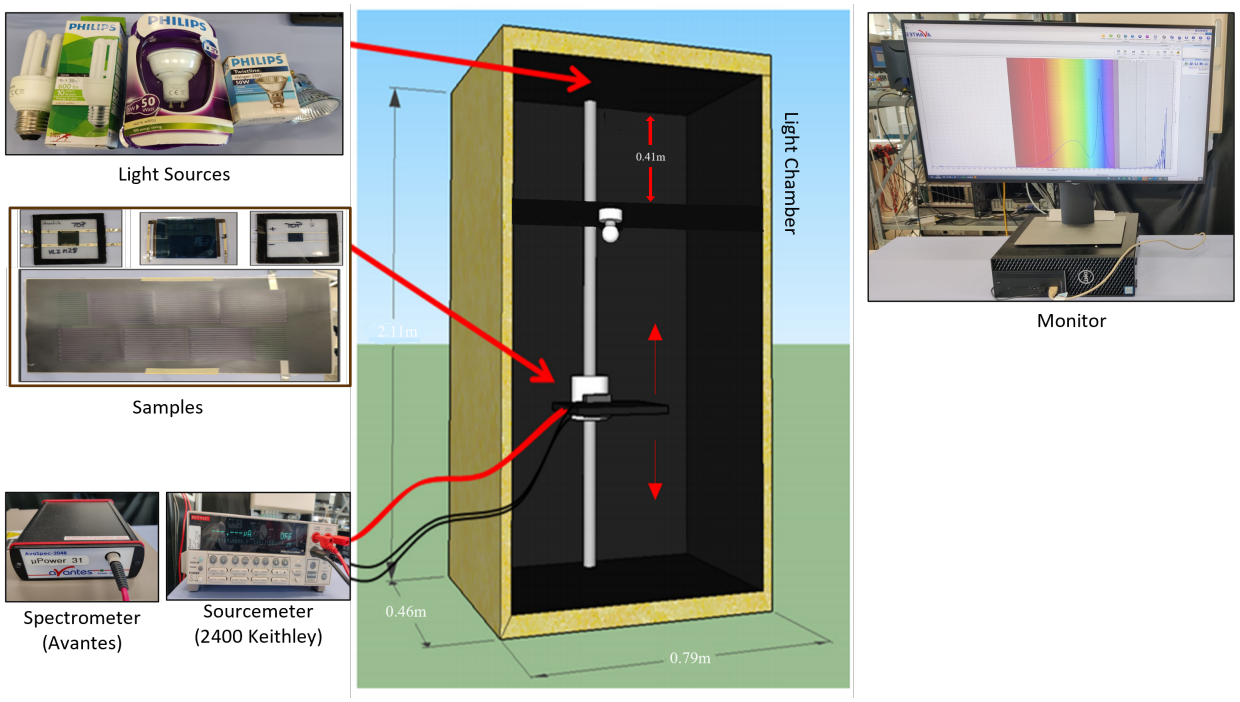

Figure 3.5: Controlled indoor environment experimental setup at the EnergyVille2 lab, imec in Genk, Belgium.

power.

2. **Light chamber**
   - Dimensions : 0.79m x 0.46m x 2.11m in length, width and height.
   - At about 0.41m away from the top the provision to fix the light source is present. Here, the light source can be changed from LED to CFL to Halogen and even a Fluorescent Tubelight.
   - The insides of the light chamber are coloured in black. The intention to choose this colour is to absorb the diffused indoor light and to minimize any scattering and reflections of the light source inside the light chamber. This means to limit the creation of too much diffused light [4].
   - It also consists of a panel, which can be moved up and down to adjust the light intensity by changing the distance between the samples and the light source. This is also the place where the solar samples are placed to measure the indoor performance through JV curve analysis.
3. **Equipments**
   - Sourcemeter (Keithley 2400) : measures currents at different voltages to the solar cell, essential for measuring the JV scans.
   - Spectrometer (Avantes) : equipment used to measure the illuminance[lux] falling directly on the solar cells.Also used to convert Illuminance into input Power density[$\mu W/cm^2$].
   - Monitor is used to analyze the JV scans of the solar cells and to measure the irradiance spectra of the light source by using the spectrometer software called 'AvaSoft8'.

In summary, the experimental setup consists of the light source, light chamber and different equipment. The setup includes a light chamber designed to minimize reflections, and precision equipment like a spectrometer and sourcemeter to measure illuminance and electrical characteristics. This setup provides a comprehensive framework for testing PV performance under indoor lighting conditions as it allows for accurate and controlled evaluation, which is crucial for understanding the efficiency and behaviour of solar cells in varied indoor environments. This is further discussed in Section 3.3.

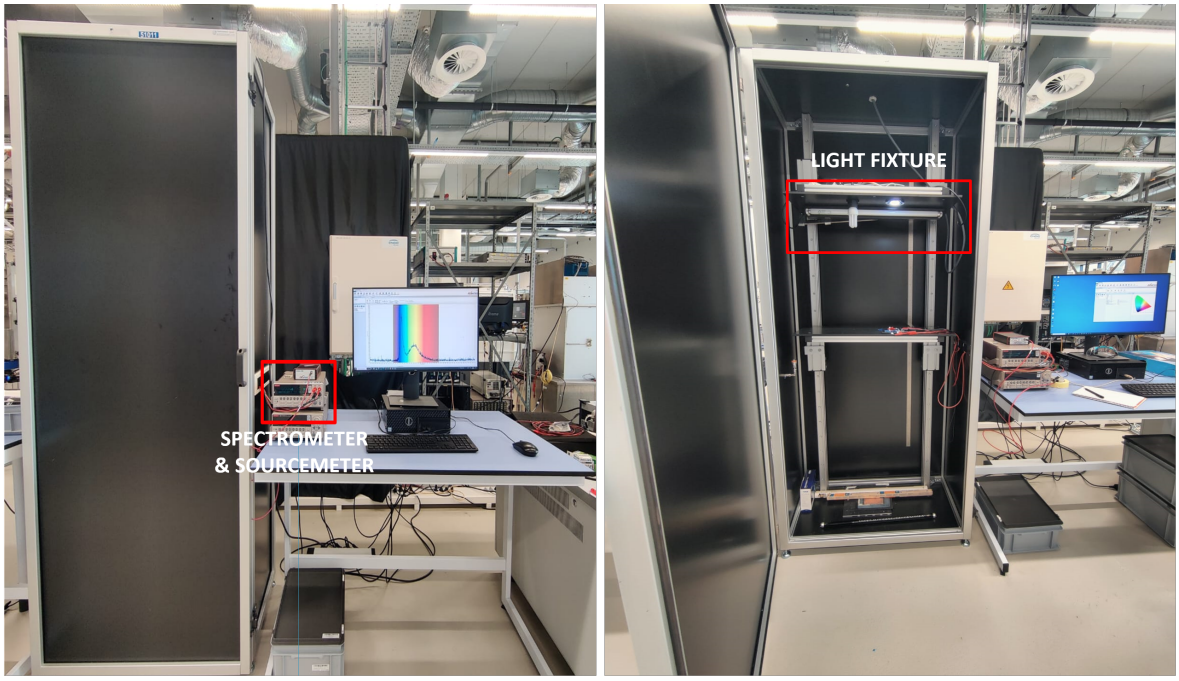

Figure 3.6: Left picture shows when the experiment is taking place and the right picture shows how the light chamber looks when the light source is switched 'on'.

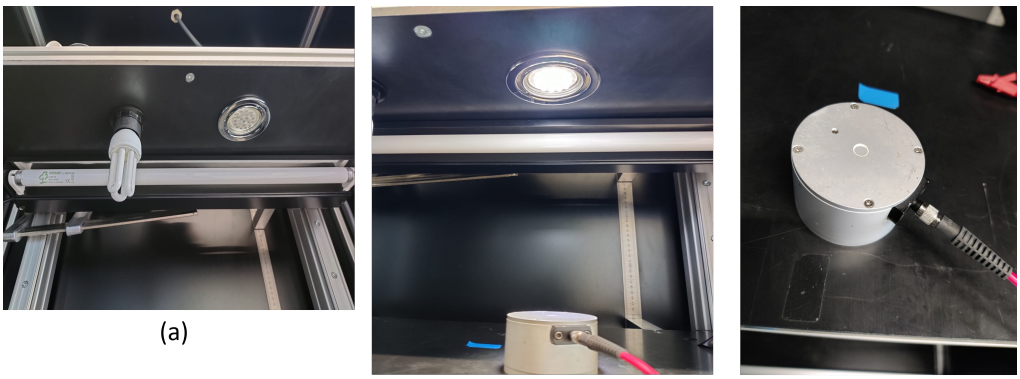

Figure 3.7: (a)Detailed view of the light fixture, (b)Irradiance spectra measurement under an LED lamp by the use of sensor and (c)Spectrometer sensor.

3.2.2. Experimental Setup at CHOSE, Italy

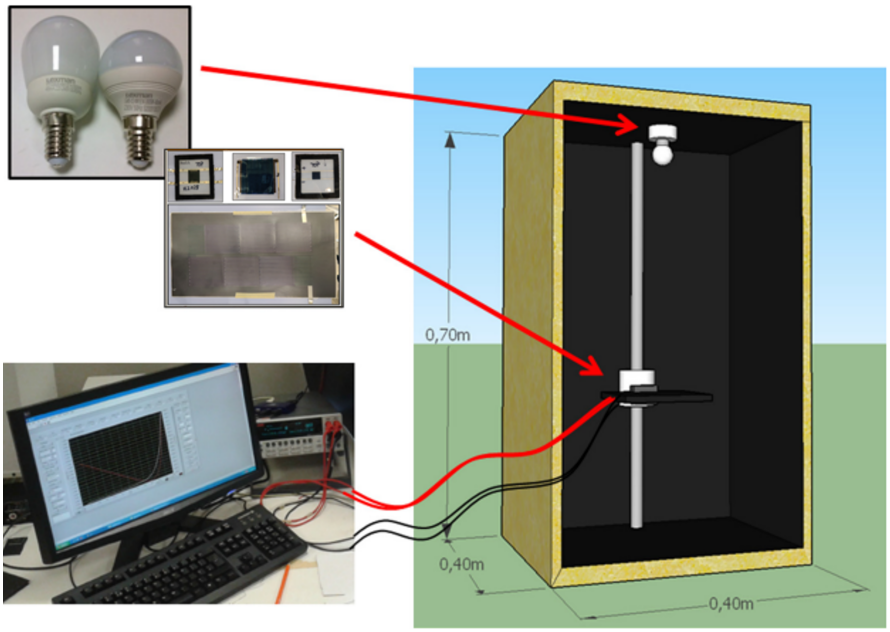

Figure 3.8: Experimental setup at Centre for Hybrid and Organic Solar Energy (CHOSE), Italy [79].

This experimental setup is closely aligned with the one utilized at imec, with both based on similar measurement principles, though differing in their specific configurations. For characterization under typical artificial lighting conditions, only LED light sources were used, specifically warm LED and cold LED lamps, to simulate lighting in typical office environments. The spectral emissions of the light sources are measured with the help of a fibre optic spectrometer (Black-comet C-SR, Stellarnet INC.) with the help of the Spectra Wiz software which sets a ±5% accuracy [118]. A spectrometer is used to measure the irradiance falling on the solar cells, now the irradiance of the light sources is measured in the photometric unit of 'Illuminance'. Thus, a luxmeter is used to measure the illuminance of the light sources. The luxmeter is from the Lafayette company, specifically the LM-1 model with a 0.1 lux resolution, overall providing an accuracy of ±5% [119].

As with the utilization of a Light chamber with the imec setup, this experimental setup also is conducted within a wooden box with dimensions of 0.4m x 0.4m x 0.7m in length, breadth and height, featuring black coloured walls and a light fixture incorporated into the top, the opening of the wooden box is covered with a black curtain during the measurements. The black walls are designed to minimize light losses by reducing reflections and scattering, thereby ensuring more accurate measurement results. The setup includes a support plane on which the solar cells are positioned, allowing light from the artificial sources inside the box to illuminate the cells. This configuration facilitates the measurement of the indoor performance of the solar cells through current-voltage (I-V) curve analysis.

To measure the current and voltage performance of the cells, a Keithley source meter is employed, delivering precise current and voltage with an accuracy of ±0.0012% [79]. The I-V curve analysis is conducted at varying illumination levels, achieved by adjusting the distance between the light source and the supporting plate. This setup allows for the systematic evaluation of the solar cells' response under controlled indoor lighting conditions.

3.3. Methodology

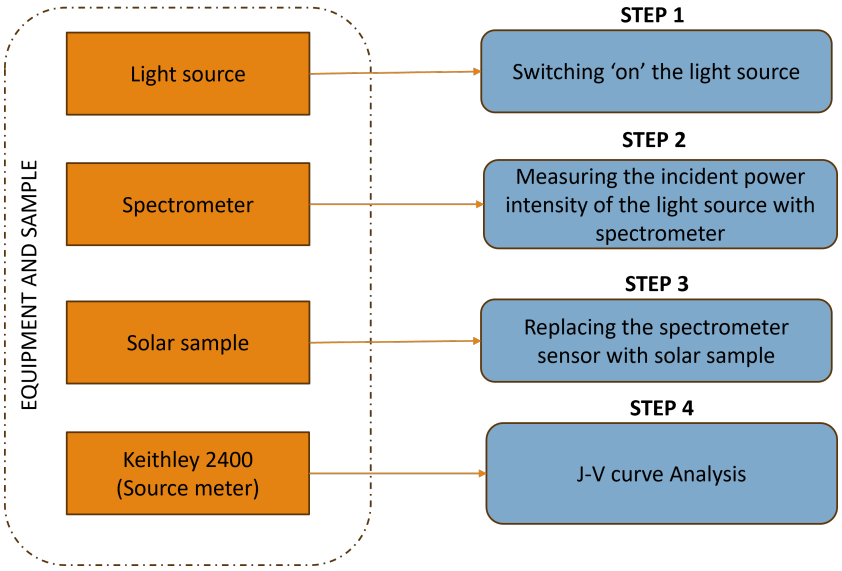

Figure 3.9: Methodology behind the measurements in the controlled indoor environment experimental setup.

The primary objective of these experimental setups is to analyze and evaluate the performance of different photovoltaic (PV) technologies in a controlled indoor environment and to compare their respective efficiencies. Although two distinct experimental setups are utilized for this analysis, the measurement methodology remains consistent across both. By adjusting the distance between the light source and the solar sample, the light intensity incident on the sample can be modulated using a supporting panel. The experiment focuses on specific illumination levels ranging from 100 lx to 1000 lx, simulating typical indoor lighting conditions found in office spaces, parking lots, residential areas, and other similar environments.

To quantify the incident power intensity on the solar samples, a spectrometer is employed to measure the emission spectrum of the light source. Given that the intensity of artificial indoor light sources is significantly lower than standard 1 Sun illumination, the power intensities in this experiments are measured in units of $\mu W/cm^2$ for easier understanding.

Once the light source is activated, the spectrometer is used to measure the illuminance. After this measurement, the solar samples are positioned in place of the spectrometer sensor. The solar samples are then connected to a Keithley 2400 source meter, which measures current at different voltages. The Keithley 2400 series is commonly used for performing J-V (current density-voltage) scans, which allow for precise characterization of the electrical performance of the samples.

J-V scans are conducted under various illumination levels, ranging from low to high intensity, to evaluate the performance of each PV technology. This comparative study aims to identify the most efficient photovoltaic technology and to understand the factors contributing to its superior performance. The J-V curve analysis provides detailed insights into the electrical characteristics, including parameters such as open-circuit voltage, short-circuit current density, fill factor, and overall efficiency, enabling a comprehensive analysis of the samples under different indoor lighting conditions.

As previously discussed, the sensor is replaced by the solar sample at the measurement spot, the size of the spectrometer sensor can be seen in Figure 3.7. It is evident that the sensor size is considerably smaller than the sample. By calculating the ratio of the sensor area to the sample area, it becomes clear that this ratio is always less than 1 due to the relatively small sensor size. As a result, the sensor captures the incident power intensity only at a localized point on the sample, rather than across the entire surface. However, it is important to note that indoor lighting is diffused light in nature, which means that the light will not be concentrated but rather homogeneously scattered.

In the experimental setup, the effect of light distribution on the solar cell is influenced by the distance between the sample and the light source. As the distance between the sample and the light source increases, the light in the chamber becomes more diffused and evenly distributed across the sample. This means that when the sample is further from the light source, the intensity of light across the sample is more uniform, reducing the impact of the sensor size relative to the sample size.

For the perovskite minimodule and Si cell, the potential for non-uniform lighting is minimal due to their smaller areas (4 cm^2). In contrast, achieving uniform illumination is challenging for the larger organic (22 cm^2) and CIGS minimodules (165 cm^2), especially when positioned closer to the light source (e.g., at 1000 lx). At such close distances, the light becomes more concentrated and directional, resulting in non-uniform illumination across the sample surface. This issue is particularly evident in the CIGS sample, where variations in illumination were observed, though it was less pronounced in the OPV sample. In these cases, the relative size of the sensor to the sample becomes more critical, as different parts of the sample may receive varying light intensities, potentially affecting the accuracy of the measurements.

To ensure uniform illumination for the CIGS sample, the incident intensity was measured at all sides of the sample, yielding a relative uniformity of 79.7% at 1000 lx, indicating that the illumination on the sample is although not fully but is fairly uniform. Since the distance between the light source and the sample was sufficiently large at lower intensities (500-100 lx), the need for a uniform illumination check was not deemed necessary, as the light distribution was uniform across the sample.

The experiments were performed under CFL and LED light sources, reflecting the current trend where these types of lighting are predominantly used in indoor environments, while traditional incandescent and halogen bulbs have become less common. Due to the higher energy efficiency and widespread adoption of LED lighting, experiments to compare the performance of the solar cells under both warm and cool LED conditions were carried out further.

4

Results and Discussion

This chapter presents the results of the experimental analysis conducted to evaluate the performance of Perovskite solar cells, alongside other photovoltaic technologies outlined in Section 3.1, i.e., Organic, CIGS minimodules, and monocrystalline silicon single cell. The primary goal is to assess the performance of these technologies through JV curve analysis, performed under controlled conditions at the EnergyVille2 lab at imec in Genk, Belgium, and the CHOSE (Centre for Hybrid and Organic Solar Energy) laboratory in Italy.

4.1. Result from the Experimental Setup at imec

The experiments focused on characterizing the spectral composition of typical artificial light sources commonly used in indoor environments. Subsequently, measurements were taken to determine the relationship between the spectral irradiance and illuminance of these light sources at varying distances, utilizing the experimental setup outlined in Section 3.2.1. First the outdoor performance is analyzed and then the indoor performance of the samples is analyzed. Additionally, performance tests of the selected PV technologies were carried out under different illumination intensities, first using a warm CFL bulb (2700K) and then a cool LED bulb (4000K).

4.1.1. Spectral Irradiance Profiles of Common Indoor light sources

To characterize the nature of light in indoor environments, it is essential to analyze the spectral irradiance profiles of the typically used indoor light sources. In this study, three distinct types of light sources were employed: an LED bulb, a Compact Fluorescent Lamp and an Incandescent lamp. Table 4.1 provides a detailed summary of the specifications for each light source utillized in the experiment.

Table 4.1: Specifications of the light sources used in the experiment.

Light source	Power [W]	Colour temperature [K]	Nature of source	Brand
LED bulb	5	6500	Cool white	Phillips
Incandescent lamp	50	2700	Warm	Phillips Twistline
CFL bulb	11	2700	Warm white	Philips

The spectral irradiance of the light sources was measured using a spectrometer, whose sensor was positioned 0.5m away directly beneath each light source. Figure 4.1 illustrates the captured spectral profiles during these measurements. The spectral irradiance or the power intensity of the light sources expressed in $\mu W/cm^2$, is plotted on the y-axis, while the wavelength measured in nm is shown on the x-axis. This comparison illustrates the differences in spectral distribution and intensity emitted by each light source.

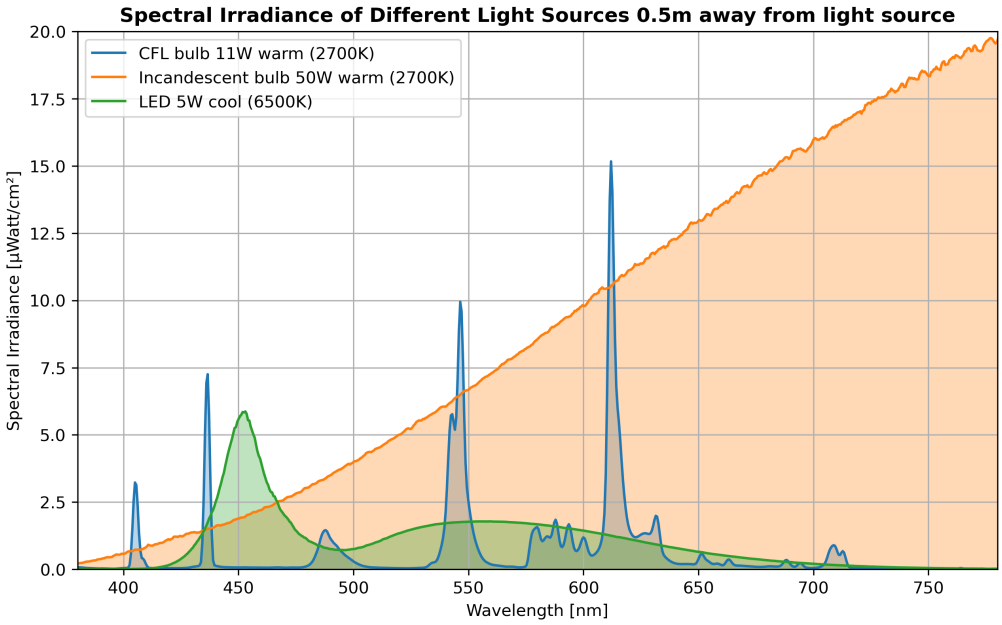

Figure 4.1: Irradiance spectrum of different light sources 0.5m away from the light sources recorded in the visible region.

The CFL bulb displays a spectral distribution with several distinct sharp peaks at specific wavelengths, notably around 450nm, 550nm and 620nm. These peaks indicate that the CFL emits light predominantly in narrow bands, with relatively low overall intensity across the visible spectrum. Similarly, the LED bulb exhibits a spectral distribution with a sharp peak at around 450nm and a broader peak distribution centered around 500 to 800 nm. However, its overall irradiance is higher than that of the CFL.

In contrast, the Incandescent lamps demonstrate a continuous and smooth increase in spectral irradiance with increasing wavelength. Unlike the CFL and LED, the incandescent lamp does not show sharp peaks, but instead, it presents a broad spectral output characteristic of a black body radiator. The spectral profile of the incandescent lamp exhibits a higher intensity in the longer wavelengths, particularly in the red and infrared regions, while emitting significantly less in the blue and green (shorter wavelengths) regions of the spectrum. Additionally, this helps in understanding that the overall intensity of indoor light sources is indeed of lower magnitude compared to the AM 1.5G spectrum

4.1.2. Correlation Between Spectral Irradiance and Illuminance of Light Sources at Incremental Distances

To investigate the correlation between spectral irradiance and illuminance, the spectral profiles of the light sources were measured at incremental distances from the source. From the literature review and previous experiment, it is clear that indoor light sources have significantly lower intensities compared to outdoor conditions.However, the exact relationship between irradiance and illuminance, and by what factor they vary, has yet to be determined. This experiment aims to analyze the relationship between irradiance and illuminance at different intensities for the specified light sources, as outlined in Table 4.1.

1. CFL spectrum at incremental distances from the light source

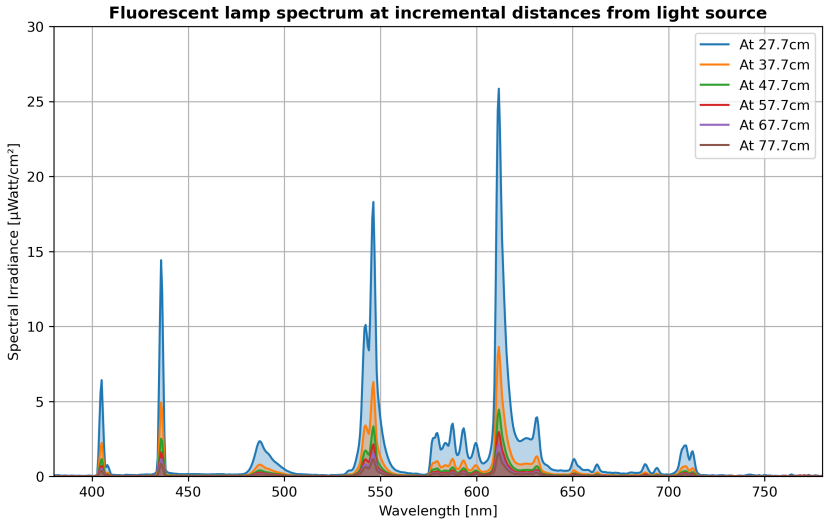

Figure 4.2: CFL in the visible region

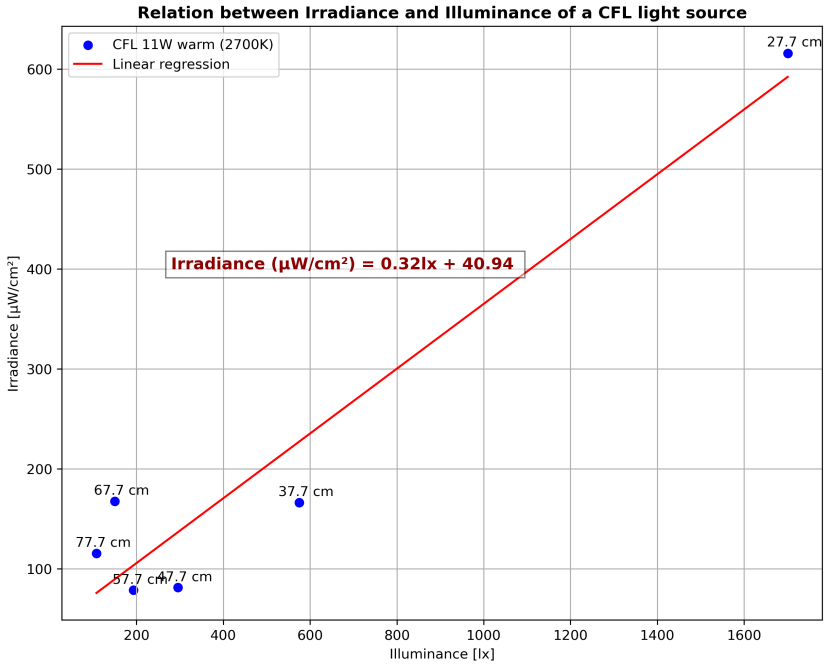

Figure 4.3: Linear regression of CFL

Figure 4.2 shows the spectral profile of the CFL at various distances. The first measurement was taken at 27.7cm from the light sources. This distance was selected because, as observed from the setup at the EnergyVille2 lab, imec, the light fixture is positioned 0.41m below the top of the experimental setup, making 27.7cm an appropriate starting distance. Subsequent measurements were taken at 10 cm increments to assess the correlation. These measurements revealed a decrease in intensity compared to the initial measurement at 27.7cm to 77.7cm and the corresponding illumination levels were recorded.

The experimental results demonstrate a clear linear relationship between irradiance measured in $\mu W/cm^2$ and illuminance measured in lux for the CFL light source which can be seen in Figure 4.3. A linear regression analysis was performed to quantify the correlation, yielding the Equation 4.1.

$$Irradiance(\mu W/cm^2) = 0.32 \cdot Illuminance(lx) + 40.94 \tag{4.1}$$

Equation 4.1 indicates that at every 1 lux increase in illuminance, irradiance increases by 0.32 $\mu W/cm^2$. It is evident that there is a linear relation between irradiance and illuminance. This relationship is consistent with the inverse square law, which states that the illumination of a surface is inversely proportional to the square of the distance between the light source and the illuminated surface, provided the light source can be considered a point source [120]. As the distance increases, the illumination (or irradiance) decreases following this inverse square law relationship and as observed as well.

The results captured a range of illuminance values from approximately 200 lux to 1600 lux, corresponding to irradiance values between 50 $\mu W/cm^2$ and 600 $\mu W/cm^2$. This range confirms the expected decline in both irradiance and illuminance as the distance from the light source increases. Overall, these findings highlight a predictable linear relationship between irradiance and illuminance for the CFL light source under the tested conditions.

2. Incandescent spectrum at incremental distances from the light source

Following the same procedure as the CFL bulb, measurements were taken for the incandescent bulb at incremental distances, starting at 27.7cm from the light source. The spectral profile, shown in Figure 4.4, exhibited the characteristic smooth and continuous spectral distribution of a black body radiator at 3000K colour temperature.

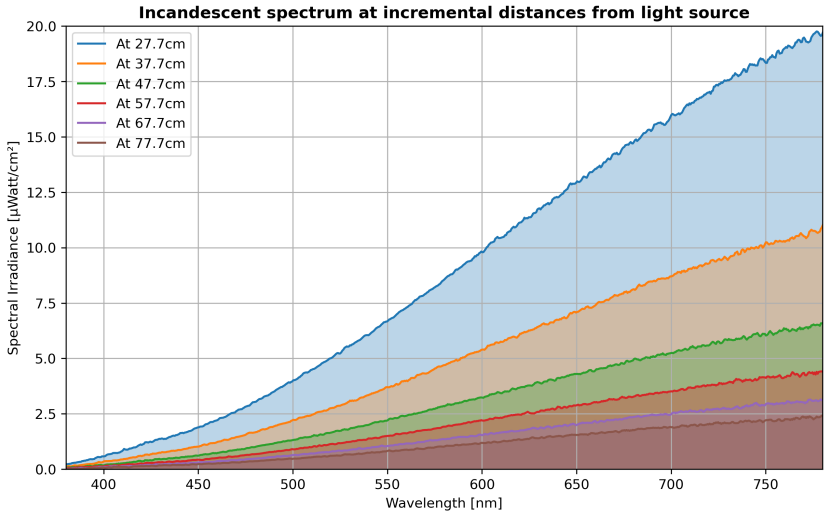

Figure 4.4: Incandescent in the visible region

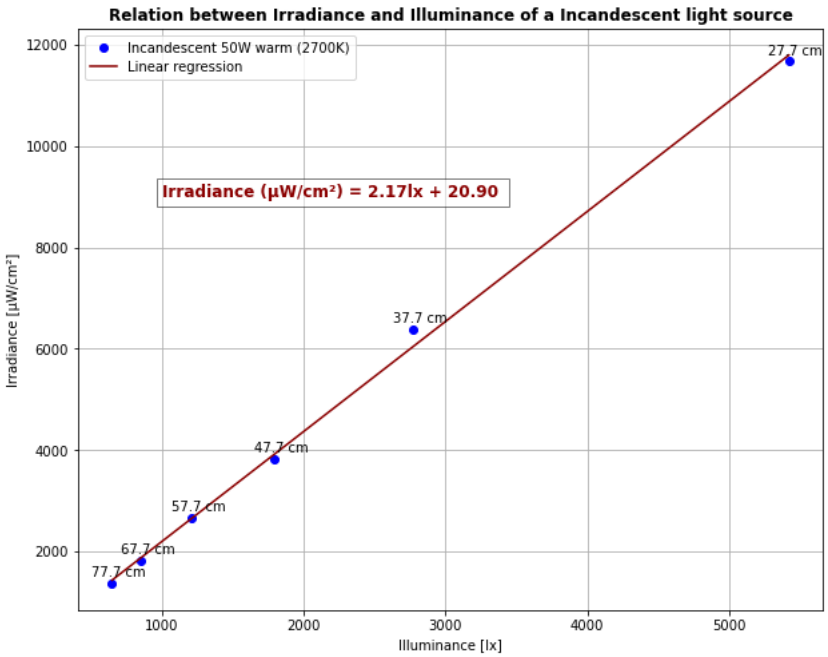

Figure 4.5: Linear regression of Incandescent

As the distance increased, both irradiance and illuminance decreased, consistent with the inverse square law. The relationship between irradiance and illuminance was quantified using linear regression, resulting in Equation 4.2. For every unit increase in illuminance, there is a 2.17 $\mu W/cm^2$ increase in irradiance.

$$Irradiance(\mu W/cm^2) = 2.17 \cdot Illuminance(lx) + 20.90 \tag{4.2}$$

This result confirms a linear relationship between illuminance and irradiance for the incandescent bulb. The data points closely adhere to the regression line, indicating a strong correlation between these variables across tested distances.

3. LED spectrum at incremental distances from the light source

For the LED bulb, measurements were performed following the same methodology as the CFL and incandescent lamps, starting at 27.7cm and increasing in 10 cm increments. The spectral profile of the LED, presented in Figure 4.6, showed a sharp peak centered around 450 nm, typical of a cold LED light source.

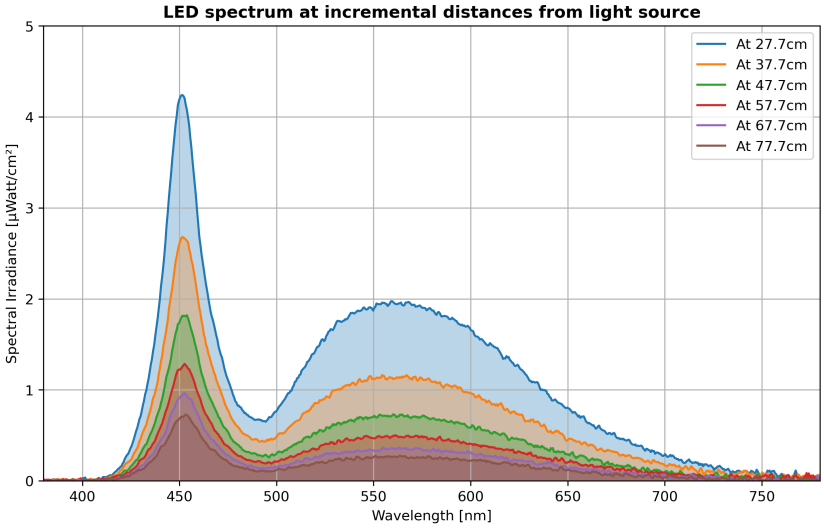

Figure 4.6: LED in the visible region

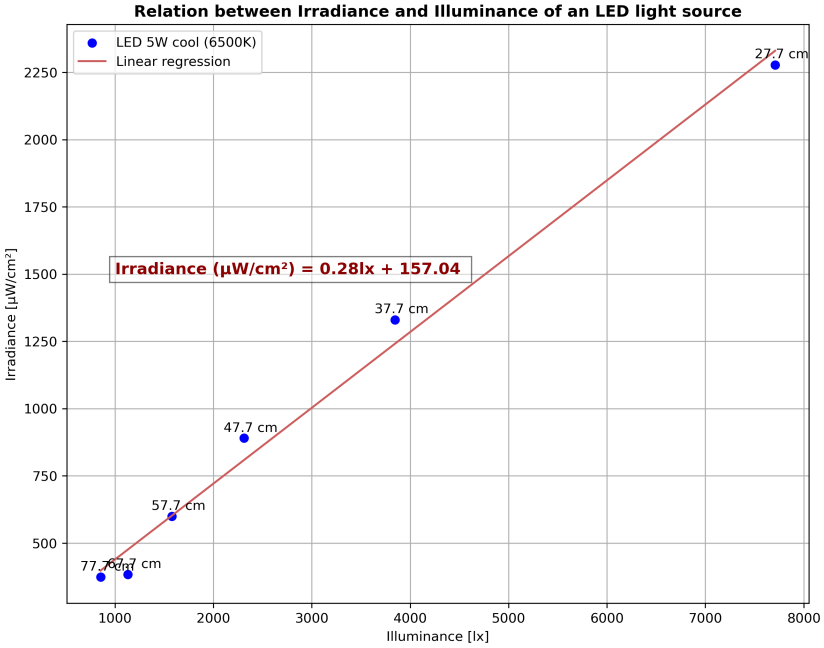

Figure 4.7: Linear regression of LED

Similar, to other light sources, the irradiance and illuminance decreased with increasing distance from the light source. Linear regression analysis was performed, resulting in Equation 4.3. For every unit change of lux, there is an increase of 0.28 $\mu W/cm^2$ in the irradiance.

$$Irradiance(\mu W/cm^2) = 0.28 \cdot Illuminance(lx) + 157.04 \tag{4.3}$$

The intercept appears to be higher compared to CFL and incandescent bulbs, likely due to the spectrometer picking up background noise or a possible calibration issue. However, it is still sufficient to assess the relationship between irradiance and illuminance. Equation 4.3 confirms a consistent linear relationship, in line with the results observed for the CFL and incandescent bulbs. The strong alignment of the data points with the regression line further supports the validity of this correlation for the

LED light source.

Figure 4.8, illustrates the linear regression lines of all the light sources: CFL, Halogen and LED, depicting the difference in their linear relation between irradiance and illuminance on the x-axis and y-axis, respectively.

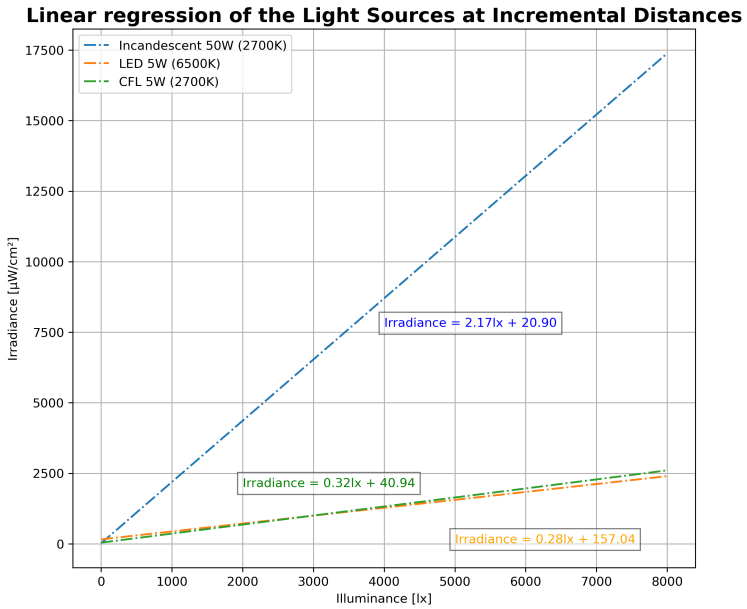

Figure 4.8: Linear regression between the Irradiance and Illuminance of all light sources at an incremental distance from the light source.

The incandescent light source used in this experiment shows a steep increase in irradiance with each unit increase in illuminance. This is mainly because of the continuous spectrum of the incandescent bulb compared to the spectrum of LED and CFL. As a result, even small increases in illuminance lead to a large rise in irradiance.

In contrast, LED and CFL light sources exhibit a gradual increase in irradiance for the same increase in illuminance. LEDs are particularly known for their ability to achieve higher illuminance with smaller increases in irradiance as seen in Figure 4.8. LEDs are more directional in nature, they focus light more effectively in a specific direction, which means to provide more illuminance. CFLs, while more efficient than incandescent bulbs, also show a relatively closer linear relation similar to LED, producing light output with a slower rate of irradiance increase.

Overall, the results demonstrate that the relationship between irradiance and illuminance varies across different light sources, primarily due to differences in wattage and colour temperature. While each light source exhibited a linear correlation between irradiance and illuminance, the rate of change in irradiance for a given change in illuminance (lux) was distinct for each. This variation can be attributed to the inherent characteristics of the light sources, such as their spectral output and power consumption. Notably, the rate of change in irradiance for both the LED and CFL bulbs is consistently lower compared to the incandescent bulb.

4.1.3. Performance under Standard Conditions (1 Sun, AM 1.5G)

To accurately evaluate the indoor performance of the samples, it is essential to first determine their performance under standard conditions using the AM 1.5G spectrum. This baseline measurement provides critical insights into the differences in power conversion efficiency (PCE) between outdoor and indoor environments. Table 4.2 presents the J-V curve parameters of the samples, as outlined in Section 3.1, obtained under a solar simulator at the EnergyVille2 lab, imec, Belgium.

Table 4.2: J-V curve parameters under the solar simulator at EnergyVille2 lab.

PV Technology	Type	Cells in series	Bandgap [eV]	Active area [cm^2]	J-V parameters under 1 Sun				
					Voc [V]	Voc per cell [V]	Jsc [mA/cm^2]	FF [%]	PCE [%]
Monocrystalline silicon	Single cell	1	1.11	4	0.50	0.50	36.40	67.46	12.29
CIGS	Minimodule	6	1.12	165	4.09	0.68	26.94	64.94	11.97
OPV	Minimodule	6	not specified (commercial)	22	4.86	0.81	3.36	25.44	0.69
PVK	Minimodule	7	1.6	4	6.83	0.97	26.17	60.90	15.55

Since the main motive of this research is the comparative analysis of various PV technologies, it is appropriate to compare the performance of open circuit voltage (Voc) on a per-cell basis, as the Si sample consists of a single cell, while the other technologies are minimodules with varying active areas and number of cells in series as illustrated in Table 4.2.

Monocrystalline silicon demonstrated a Voc of 0.50 V and a Jsc of 36.40 mA/cm^2. The cell exhibited a fill factor (FF) of 67.46% and a power conversion efficiency (PCE) of 12.29%. As discussed in Section 3.1.3, the efficiency loss under 1 Sun is likely due to the sample being laser-cut into smaller dimensions, as well as the impact of soldering and lamination while handling the small dimensions of the cell. This was necessary to obtain a sample of comparable size to the perovskite minimodule and to ensure uniform illumination.

The CIGS minimodule under the AM 1.5G spectrum achieves a PCE of 11.97%, comparable to monocrystalline silicon. It has a higher Voc per cell of 0.68 V, Jsc of 26.94 mA/cm^2 and a FF of 64.94% with a bandgap of 1.12 eV. Although the silicon performs better under AM 1.5G, the primary goal is to assess the performance of CIGS under indoor conditions.

The OPV minimodule with an active area of 22 cm^2 extracts a relatively low Jsc of 3.38 mA/cm^2 compared to Silicon and CIGS, alongside a high Voc per cell of 0.56 V and a low FF of 25.44%, contributing to a PCE of 0.69%. The low Jsc under AM 1.5G indicate that the cell is not able to extract large currents, likely contributing to reduced FF and PCE under AM 1.5G, this might be because it is a commercial product specifically designed for low light conditions, likely using thinner layers, which may not be as efficient in transporting charges if the number of generated charges are too high under 1 Sun illumination.

The low PCE can also be attributed to the thin OPV layers, where increased resistance under AM 1.5G may cause heat generation, reducing Jsc, FF, and potentially inducing permanent damage. Although studying the module under varying light intensities (1 Sun, 0.5 Sun, 0.2 Sun, 0.1 Sun) and temperature conditions could provide further insights, these tests were not performed, as the main focus was on indoor performance. Additionally, temperature could also play a role as the temperatures in the solar simulator at the EnergyVille2 lab can reach up to as high as 60°C, potentially impacting results. While the bandgap is unspecified, it is assumed to be optimized for indoor light, which will be further evaluated during indoor testing.

The perovskite (PVK) minimodule demonstrates the highest power conversion efficiency (PCE) of 15.55%, indicating superior performance among the evaluated photovoltaic technologies. Its high open-circuit voltage (Voc) per cell of 0.97 V, combined with a short-circuit current density (Jsc) of 26.17 mA/cm^2, significantly contributes to this high PCE. These results indicate promising performance under standard conditions. Further indoor testing will be conducted to evaluate its performance under indoor lighting, leveraging its tunable bandgap and proven high efficiency under AM 1.5G conditions.

Overall, the perovskite minimodule exhibits a high PCE compared to other samples under standard AM 1.5G conditions. In contrast, the OPV sample, which is a commercial product specifically optimized for indoor environments, demonstrates lower performance under 1 Sun, likely due to its design focus on low-light applications. On the other hand, the Silicon and CIGS samples also show lower efficiencies under 1 Sun, but they were included in this study as the primary objective is to evaluate their performance under indoor illumination.

4.1.4. Indoor Performance of samples

The experiments were conducted under a warm CFL bulb (2700K) and a cool LED bulb (4000K). J-V curve analyses were performed at three different illumination levels: 100lx, 500lx and 1000lx. These specific illumination levels were chosen as 100lx represents typical basic indoor lighting, 500lx corresponds to lighting for standard visual tasks and 1000lx is used for high-contrast conditions, as recommended by Johnny Ka Wai Ho et al. [45].

Indoor performance under Warm CFL (2700K) bulb

Table 4.3 presents the results of the J-V curve parameters at the specified illumination levels under warm CFL (2700K) bulb.

Table 4.3: Indoor performance of samples under warm CFL (2700K), in the EnergyVille2, imec, Belgium experimental setup.

Device	Light source	Illuminance	JV curve parameters				
		lux	Voc	Voc per cell	Jsc	FF	Pmax
		lx	[V]	[V]	$[\mu A/cm^2]$	[%]	$[\mu W/cm^2]$
monocrystalline Si cell		100	0.23	0.23	20.96	49.58	2.49
(Rigid, opaque),	Warm CFL (2700K)	500	0.29	0.29	72.07	51.79	11.19
single cell		1000	0.32	0.32	115.78	55.72	20.71
CIGS minimodule		100	1.33	0.22	17.82	35.81	1.42
(Flexible, opaque),	Warm CFL (2700K)	500	2.24	0.37	59.52	42.01	9.36
6 cells connected in series		1000	2.57	0.42	97.26	47.84	19.94
Organic minimodule		100	3.57	0.59	14.86	72.62	6.45
(Flexible, semi-transparent),	Warm CFL (2700K)	500	3.78	0.63	47.41	72.44	21.73
6 cells connected in series		1000	3.85	0.64	82.24	72.44	38.38
Perovskite minimodule		100	4.22	0.60	24.4	68.68	10.63
(Rigid, semi-transparent),	Warm CFL (2700K)	500	4.64	0.66	63.86	65.58	29.20
7 cells connected in series		1000	4.71	0.67	102.33	65.48	47.42

The summary of the results presented in Table 4.3 is visually depicted in Figure 4.9. The J-V curve parameters namely, the Voc, Jsc, FF and the power output (Pmax) of the samples, are shown for illumination levels ranging from 100lx to 1000lx. The following observations can be made from the data:

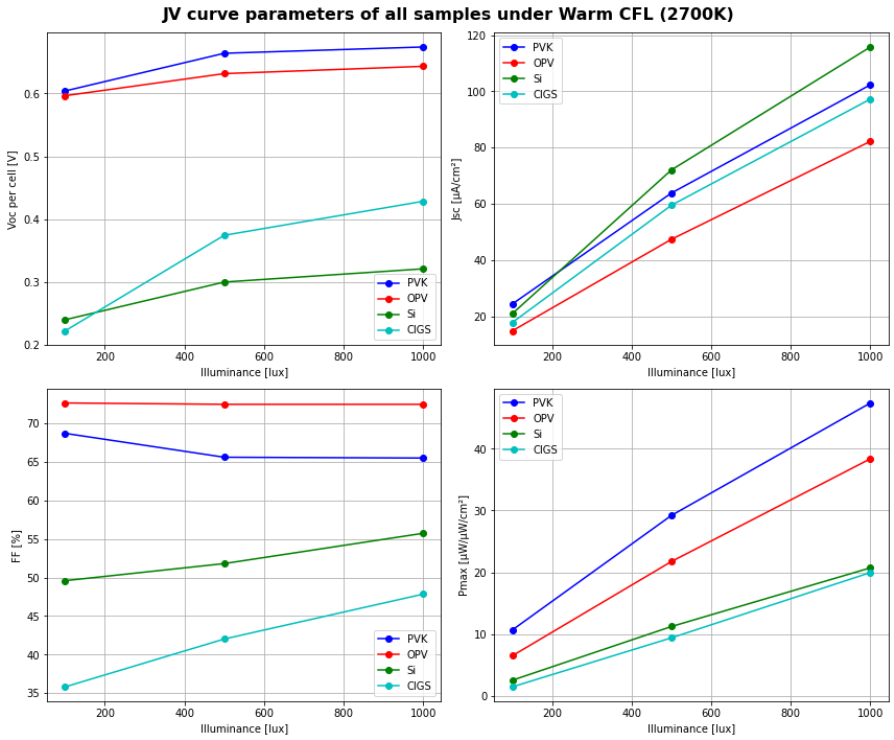

Figure 4.9: Overview of the trends on J-V curve parameters of all samples under warm CFL (2700K).

1. Open-circuit Voltage (Voc) per cell behaviour

For a fair comparison, the Voc per cell is being compared as the Si is a single cell and the rest are minimodules with different active areas and number of cells in series.

1. Perovskite (PVK) and OPV minimodules demonstrate relatively high Voc values, with Perovskite maintaining Voc around 0.60-0.67V across the 100lx to 1000lx illumination, while OPV varies between 0.59-0.64V.
2. Silicon (Si) cell show significantly lower Voc values, starting at 0.23V at 100lx and increasing slightly to 0.32V as the illumination intensity increases to 1000lx.
3. CIGS cells also exhibit a significant increase in Voc with illumination, ranging from 0.22V to 0.42V from 100 to 1000lx.

The increasing trend in Voc for all technologies is consistent with the theoretical expectation that Voc is logarithmically dependent on the light intensity as recalled by Equation 4.4.

$$V_{OC} = \frac{nk_BT}{q} \ln\left(\frac{I_L}{I_0} + 1\right) \tag{4.4}$$

Thus, Voc has a logarithmic dependence on the photo-generated current which is ultimately dependent on the light intensity. Thus, as the illumination increases, more electron-hole pairs are generated, resulting in higher charge carrier concentration and a corresponding increase in Voc. This trend has been observed in literature studies on indoor PV behaviour, confirming that Voc increases with increasing illuminance [62] [45].

However, there are high Voc losses observed in silicon technology, from 0.5V under 1 Sun to 0.32V at 1000lx, this is mainly because of high thermalization losses suffered in indoor environments [10]. The silicon sample, with a bandgap of 1.11 eV (approximately 1100 nm in the infrared region), exhibits good absorption near its bandgap due to its thicker absorber layer. However, this results in significant Voc losses since the CFL light spectrum is predominantly in the visible region (360 - 830nm), causing the excess energy from visible light to be wasted as heat.

Similarly, CIGS, with a bandgap of 1.12 eV, also experiences thermalization losses, contributing to Voc losses. In contrast, PVK, with its wider bandgap of 1.6 eV corresponding to 760nm, enables efficient light absorption in the visible region exhibiting higher Voc due to reduced thermalization losses, ranging from 0.98V under 1 Sun and 0.67V at 1000lx.

Although the exact bandgap for OPV is not specified, its relatively high Voc suggests the presence of a wide bandgap, likely above 1.4 eV. Additionally, literature indicates that for producing high Voc under indoor light conditions, the donor material of the OPV solar cell should possess a wide bandgap [14]. Therefore, supporting the assumption that OPV possesses a wide bandgap.

2. Short-Circuit Current Density (Jsc) behaviour:

1. The Si cell demonstrates the highest Jsc values among all the technologies, significantly increasing from 20.96 µA/cm² at 100 lx to 115.78 µA/cm² at 1000 lx, representing a fivefold increase from 100 lx to 1000 lx.
2. The CIGS minimodule also shows a significant rise in Jsc, starting from 17.82 µA/cm² at 100 lx to 97.26 µA/cm² at 1000 lx.
3. PVK exhibits an increase in Jsc, from 24.4 µA/cm² at 100 lx to 102.33 µA/cm² at 1000 lx. It shows the least increase in Jsc, likely due to recombination losses increasing with increasing light intensities.
4. OPV shows an increase from 14.86 µA/cm² at 100 lx to 82.24 µA/cm² at 1000 lx.

Silicon technology shows the highest Jsc at 1000 lx, with close competition from PVK. This is attributed to perovskite's high absorption coefficients, although silicon has a lower absorption coefficient than PVK it is able to extract the highest Jsc because of its thicker absorber layer, allowing for more absorption and its ability to extract current into the external circuit. CIGS shows moderate Jsc values, due to their spectral mismatch with indoor light sources and given that there is some degree of non-uniformity in illuminating the large sample area at 1000lx.

OPV demonstrates the smallest rise in Jsc values from 100lx to 1000lx and overall, the lowest among the tested PV technologies. This reduced Jsc might be attributed to the relatively lower thickness of the metal contacts in the OPV sample which limits current collection to a low microampere range compared to other samples. The choice of thinner metal contacts can be a cost-saving measure, as the product is designed for indoor use, where handling small currents is sufficient.

3. Fill Factor (FF) behaviour:

1. OPV cells maintain a relatively constant FF of around 72% which indicates good internal device properties even under varying light conditions and intensities [45].
2. However, the perovskite (PVK) module shows a slight decline in FF from 68.68% at 100lx to about 65.48% at 1000lx. This decrease in FF at higher illumination levels is often linked to increased recombination rates, particularly due to trap-assisted or non-radiative recombination that becomes more significant as light intensity rises [10].
3. Si and CIGS cells exhibit an increasing trend in FF, starting at 49% and 35%, respectively, at 100 lux, and increasing to 55% and 47% at 1000 lux, respectively. This behaviour can be explained by reduced recombination losses at higher light intensities, likely by an increase in Voc and photon carrier concentration as illumination intensifies from 100lx to 1000lx. These factors enhance the charge extraction efficiency and an overall improvement in FF.

Si and CIGS cells benefit from lower recombination rates, which improve charge extraction as illumination intensity increases, resulting in a higher FF. In contrast, PVK and OPV cells are more prone to recombination losses, particularly bimolecular recombination in OPV and trap-assisted recombination in PVK, which leads to a decrease in FF as light intensity increases [4].

It is interesting to note here, that the FF for OPV under AM 1.5G was only 25.44% but under warm CFL lighting it maintains an FF of 72%. A plausible explanation is that the OPV sample, designed for indoor applications, effectively converts the low photon-carrier concentrations under indoor lighting (in the µA range) into electricity. In contrast, under AM 1.5G illumination, where current extraction is

nearly 1000 times higher (in mA), the OPV sample encounters significant resistive losses, resulting in a lower FF. Additionally, the increased resistive losses can cause heat generation that can further reduce the performance, leading to lower FF.

4. Maximum Power Output (Pmax) behaviour:

1. Perovskite (PVK) module delivers the highest power output, reaching 47.42 $\mu W/cm^2$ at 1000lx. This is followed by OPV cells, which achieve 38.38 $\mu W/cm^2$ at the same illumination level.
2. CIGS and Si display lower power outputs, with CIGS reaching 19.94 $\mu W/cm^2$ and Si reaching 20.71 $\mu W/cm^2$ at 1000lx.

The power output trends reflect the combined effects of Voc, Jsc, and FF. Despite a slight decrease in FF at higher illumination levels, perovskite cells still generate the highest power under indoor conditions due to their relatively high Voc and decent Jsc. OPV cells, with their consistently high FF, maintain competitive power output. Si cells, despite having lower Voc and FF, compensate with a high Jsc, leading to lower power output under indoor lighting.

The observed behaviours of Voc, Jsc, FF, and Pmax in indoor PV technologies align with theoretical expectations and highlight the distinct strengths and weaknesses of each technology. Perovskite and OPV technologies excel in terms of Voc and FF, making them strong candidates for indoor energy harvesting, while Si technology's thick absorber layer contributes to higher Jsc, however because of its low Voc and FF, the maximum power output is also lower. CIGS shows low performance across all parameters, making it less suitable for indoor applications. From the above results, it seems Voc is the most important factor that determines how well the wide bandgap samples (PVK and OPV) perform under indoor conditions. As recalled by Equation 4.4, Voc is logarithmically dependent with light intensity, thus PVK and OPV having reduced Voc losses enhances an overall good performance under indoor lighting conditions.

Indoor performance under Cold LED (4000K) bulb

Table 4.4 lists down the key JV curve parameters under the cold LED bulb (4000K) at 100, 500 and 1000lx illuminance levels. Figure 4.10 illustrates the overview of the JV curve key parameters at the mentioned illumination levels.

Table 4.4: Indoor performance of samples under Cold LED (4000K), in the EnergyVille2, imec, Belgium experimental setup.

Device	Light source	Illumination	JV curve parameters				
		lux	Voc	Voc per cell	Jsc	FF	Pmax
		lx	[V]	[V]	$[\mu A/cm^2]$	[%]	$[\mu W/cm^2]$
monocrystalline Si cell		100	0.22	0.22	22.68	45.75	2.28
(Rigid, opaque),	Cold LED (4000K)	500	0.31	0.31	93.61	53.07	15.89
single cell		1000	0.36	0.36	157.58	54.60	30.97
CIGS minimodule		100	1.30	0.21	14.4	33.92	1.06
(Flexible, opaque),	Cold LED (4000K)	500	1.99	0.33	37.08	38.99	4.82
6 cells connected in series		1000	2.00	0.34	43.2	37.31	5.37
Organic minimodule		100	3.59	0.59	16.54	74.16	7.36
(Flexible, semi-transparent),	Cold LED (4000K)	500	3.87	0.64	59.58	74.33	28.63
6 cells connected in series		1000	3.94	0.65	80.74	77.34	41.11
Perovskite minimodule		100	4.15	0.59	22	66.62	9.62
(Rigid, semi-transparent),	Cold LED (4000K)	500	4.78	0.68	94.06	65.61	44.35
7 cells connected in series		1000	4.86	0.69	164.13	70.13	79.75

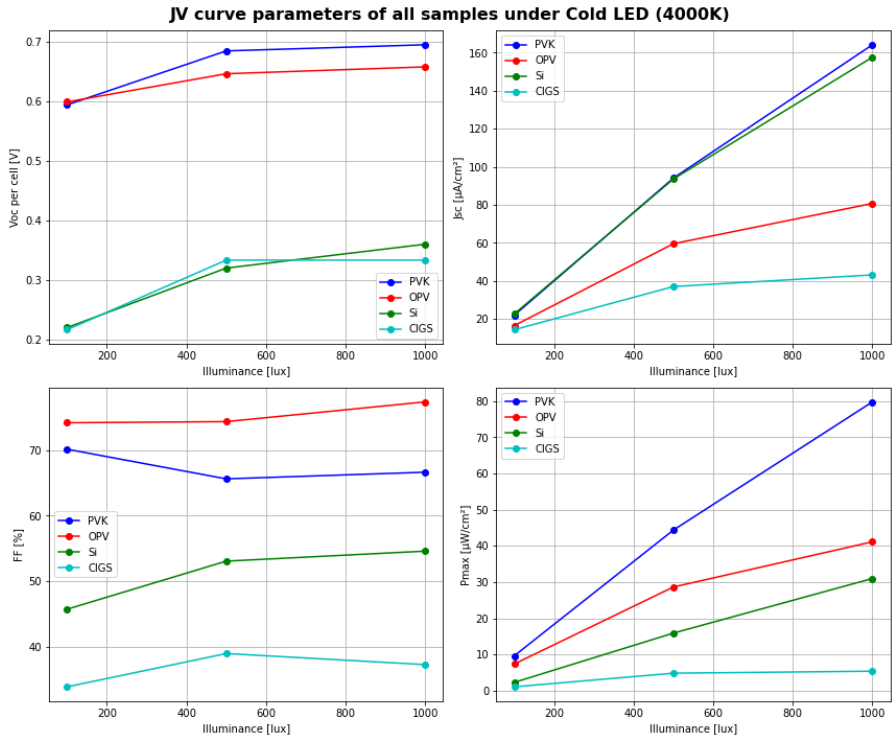

Figure 4.10: JV parameters of all samples under cold LED (4000K) bulb at 100lx, 500lx and 1000lx.

1. Open-Circuit Voltage (Voc) per cell behaviour:
For a fair comparison, the Voc per cell is considered.

1. PVK consistently exhibits the highest Voc per cell values, ranging from 0.59V at 100 lx to 0.69V at 1000 lx. This is followed by OPV with values between 0.59V at 100 lx and 0.65V at 1000 lx.
2. In contrast, silicon shows significantly lower Voc values due to its high thermalization losses having a bandgap of 1.11eV, starting at 0.22V at 100 lx and increasing only to 0.36V at 1000 lx.
3. CIGS demonstrates the least increase in Voc values compared to Si, with Voc ranging from 0.21V at 100 lx to 0.34V at 1000 lx.

2. Short-Circuit Current Density (Jsc) behaviour:

1. Si displays relatively high Jsc values along with perovskite across all illuminance levels, rising sharply from 22.68 µA/cm² at 100 lx to 157.58 µA/cm² at 1000 lx due to its thicker absorber layer contributing to more photon absorption.
2. CIGS minimodule shows the lowest increase, starting from 14.4 µA/cm² at 100 lx to 43.2 µA/cm² at 1000 lx, indicating moderate photon absorption.
3. PVK cells demonstrate high Jsc, from 22 µA/cm² at 100 lx to 164.13 µA/cm² at 1000 lx, surpassing the Si sample at higher illuminance levels. This is due to the perovskite's high absorption coefficient.
4. OPV while exhibiting lower Jsc values overall, shows a gradual increase with illumination. OPV ranges from 16.54 µA/cm² to 80.74 µA/cm² over the same illuminance range.

3. Fill Factor (FF) behaviour:

1. OPV maintains a relatively high FF, ranging from 74.16% at 100 lx to 77.34% at 1000 lx, indicating stable internal device properties and efficient charge extraction under varying light intensities under indoor light.

2. PVK, on the other hand, experiences a slight increase in FF, dropping from 66.62% at 100 lx to 70.13% at 1000 lx, likely due to increased trap-assisted recombination losses as the light intensity increases.

3. Si and CIGS cells exhibit an increasing FF trend. Si's FF rises from 45.75% at 100 lx to 54.60% at 1000 lx, while CIGS increases from 33.92% to 37.31%.

4. Maximum Power output (Pmax) behaviour:

1. Perovskite (PVK) modules deliver the highest power output, reaching 79.75 $\mu W/cm^2$ at 1000 lx, followed by OPV with 41.11 $\mu W/cm^2$. These values are consistent with PVK's higher Voc, competitive Jsc, and FF.

2. Silicon (Si) and CIGS cells display lower Pmax values, with Si reaching 30.97 $\mu W/cm^2$ and CIGS 5.37 $\mu W/cm^2$ at 1000 lx. The lower Pmax in Si is primarily due to its significantly lower Voc, which limits its overall power generation, despite its high Jsc. In contrast, the lower Pmax in CIGS can be attributed to both lower Voc, Jsc and FF compared to PVK and OPV.

Overall, the performance of all the PV technologies was better under Cold LED (4000K) when compared to Warm CFL (2700K). This improvement in performance can be due to more light absorption under LED lighting. This effect is particularly evident in Perovskite (PVK) and Silicon (Si), which both produce relatively high Jsc values. For Si, although lower absorption coefficient than PVK it compensates with a thicker absorber layer facilitating greater absorption. Meanwhile, PVK's high absorption coefficient and wide bandgap (1.6 eV) make it highly effective for photon absorption under indoor conditions, positioning it as a strong candidate in indoor testing.

Power Conversion Efficiency (PCE) is calculated as the ratio of the device's power output to the incident power density, which must be determined separately due to the indoor testing conditions unlike under 1 Sun illuminations. The spectrometer is responsible for measuring the illuminance and calculating the incident power intensity falling on the device. However, the PCE could not be determined accurately because the spectrometer was not properly calibrated, leading to inconsistent results. To verify whether the lack of calibration was the source of the issue, the samples were sent to the Centre for Hybrid and Organic Solar Energy (CHOSE) in Italy, where they have a similar setup to imec and a properly calibrated spectrometer. The results obtained from the CHOSE setup are discussed in Section 4.2.

4.2. Results from the Experimental Setup at CHOSE

In the second phase, further experiments were performed at the Center for Hybrid Organic Solar Energy lab in Italy. This collaboration was crucial for cross-verifying the indoor performance of the PV technologies at the EnergyVille2 setup. The experimental setup, described in Section 3.2.2, involved testing under different illumination intensities using a warm LED (3000K) and a cool LED (6500K). The JV curves obtained have been analyzed to evaluate the indoor performance of the samples. And the correlation between irradiance and illuminance will also be verified.

4.2.1. Correlation between Irradiance and Illuminance

As previously discussed and demonstrated in Section 4.1.2, a linear relationship exists between the irradiance and illuminance of the light source as its intensity decreases or increases. These experiments were conducted at the CHOSE lab, using Cold (6500K) and Warm (3000K) LED lamps. The results of this correlation are illustrated in Figure 4.11 for Cold LED and Figure 4.12 for Warm LED at illuminance levels of 200 lx, 500 lx, and 1000 lx.

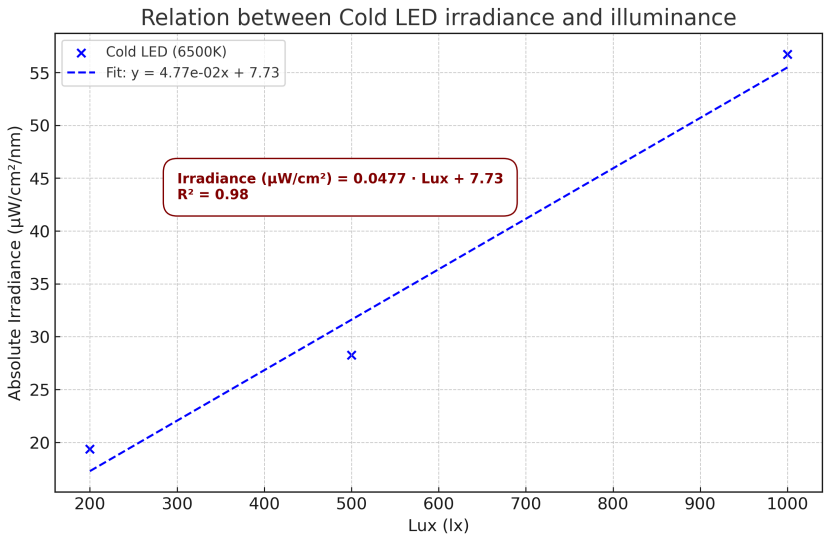

Figure 4.11: Linear relation between Irradiance and Illuminance of Cold LED (6500K).

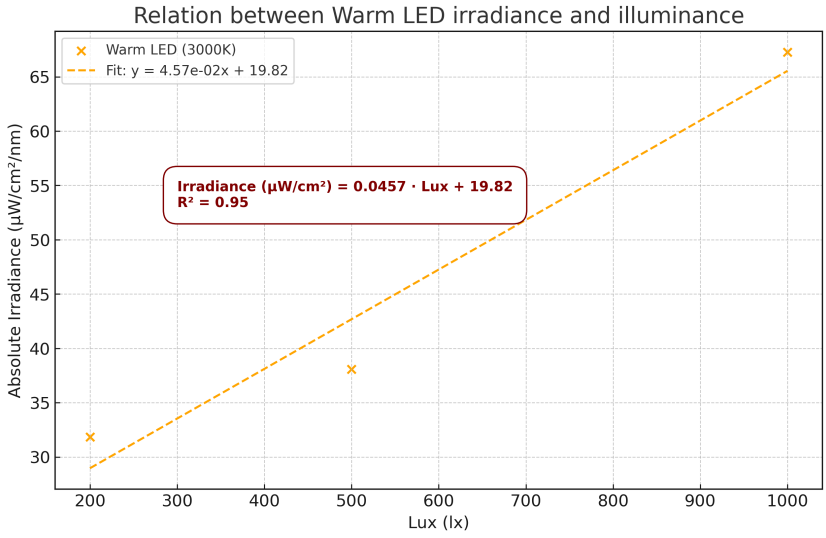

Figure 4.12: Linear relation between Irradiance and Illuminance of Warm LED (3000K).

$$Irradiance(\mu W/cm^2) = 0.0477 \cdot Lux + 7.73 \tag{4.5}$$

$$Irradiance(\mu W/cm^2) = 0.0457 \cdot Lux + 19.82 \tag{4.6}$$

Equation 4.5 is for Cold LED and Equation 4.6 is for Warm LED. The R^2 values are used to verify the percentage of the linear relation between irradiance and illuminance. Furthermore, the difference in slope and intercept for Cold and Warm LED illuminations highlights the variation in energy distribution between the two light sources. Thus proving the linear relation between irradiance and illuminance. These correlations are crucial for analyzing the performance of solar cells under indoor lighting environments.

The linear regression equations conducted in the imec experimental setup, indicated notably higher slopes and intercepts, indicating a much steeper increase in irradiance with illuminance compared to measurements conducted in CHOSE's experimental setup. For instance, imec's LED has a slope of

0.28μW/cm² per lx and an intercept of 157.04 μW/cm², while CHOSE's Cold LED has a much lower slope of 0.0477 μW/cm² per lx and an intercept of 7.73 μW/cm². This discrepancy can be attributed to several potential factors including the difference in experimental setups, the imec spectrometer miscalibration, detector non-linearity, or improper tuning of the spectrometer for specific light sources, particularly LED. The notable differences in intercepts and slopes confirm that these variations in the imec spectrometer are likely due to equipment-related inconsistencies rather than genuine differences in the light sources.

4.2.2. Indoor Performance of samples at the CHOSE setup

This section presents the key results of the indoor performance of the evaluated PV technologies at illuminance levels of 200 lx, 500 lx, and 1000 lx. The 200 lx illuminance level is specifically chosen as it is commonly used in indoor PV research studies [10] [79]. Chakraborty et al. recommend starting measurements at 200 lx, a moderate illumination level that serves as a useful benchmark for comparison [10]. The JV curves of the samples were analyzed under both Cold and Warm LED illumination conditions to assess their performance across different lighting illuminations.

Indoor performance under Cold LED (6500K)

Table 4.5: Indoor Performance of samples under CLED (6500K) in the CHOSE, Italy experimental setup.

Device	Light source	Illuminance	IncidentPower			JV curve parameters			
		lux	Pin	Voc	Voc per cell	Jsc	FF	Pmax	PCE
		lx	$[\mu W/cm^2]$	[V]	[V]	$[\mu A/cm^2]$	[%]	$[\mu W/cm^2]$	[%]
monocrystalline Si		200	75.4	0.24	0.24	25.65	49.35	3.1	4.13
(Rigid, opaque),	CLED (6500K)	500	170	0.29	0.29	57.39	53.03	9.09	5.34
single cell		1000	338	0.34	0.34	117.05	55.33	22.5	6.65
CIGS		200	75.4	1.16	0.26	19.08	37.77	1.93	2.57
(Flexible, opaque),	CLED (6500K)	500	170	2.18	0.36	43.86	44.12	7.03	4.13
6 cells in series		1000	338	2.61	0.43	90.54	50.51	19.89	5.88
Organic		200	75.4	3.47	0.57	17.02	67.94	6.7	8.89
(Flexible, semi-transparent),	CLED (6500K)	500	170	3.64	0.60	37.82	67.32	15.47	9.09
6 cells in series		1000	338	3.79	0.63	78.34	64.92	32.33	9.53
Perovskite		200	75.4	4.09	0.58	24.86	69.45	10.61	14.07
(Rigid, semi-transparent),	CLED (6500K)	500	170	4.42	0.63	57.53	68.11	26.02	15.3
7 cells in series		1000	338	4.57	0.65	116.2	66.76	53.23	15.75

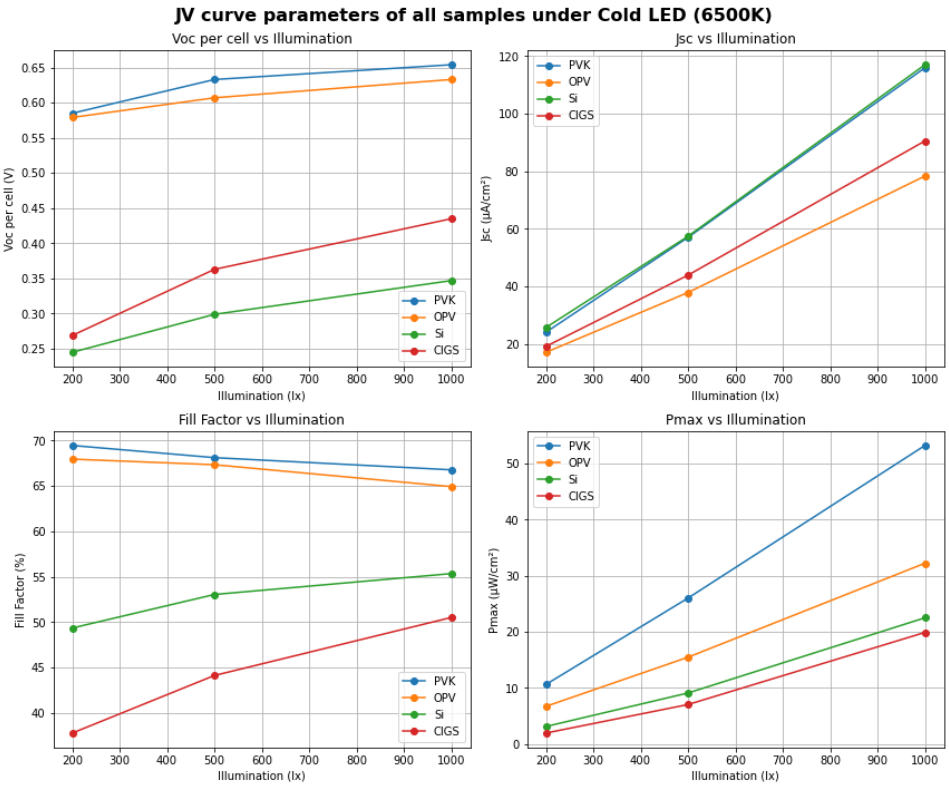

Figure 4.13: JV parameters of all samples under Cold LED (6500K) at 200lx, 500lx and 1000lx, respectively.

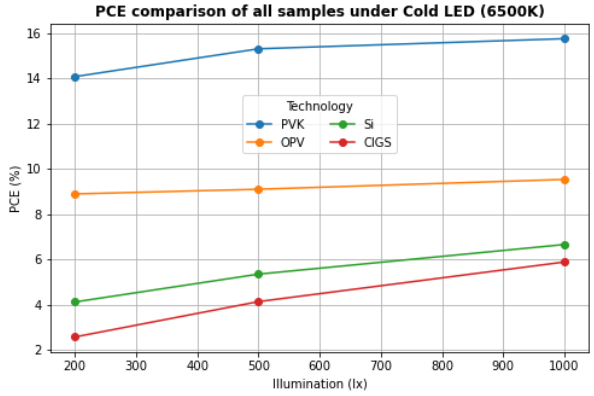

Figure 4.14: PCEs of all samples under Cold LED (6500K) at 200lx, 500lx and 1000lx, respectively.

Voc per cell vs Illumination

Perovskite technology stands out with the highest open circuit voltage (Voc) per cell across the illumination levels, ranging from 0.58V at 200 lx to 0.65V at 1000 lx, showing high performance under cold LED lighting, due to its wide bandgap and superior performance under 1 Sun illumination as well. Next is the OPV technology with Voc per cell values between 0.57V at 200 lx and 0.63V at 1000 lx. Silicon and CIGS show comparatively low values, with Si ranging from 0.24V at 200 lx to 0.34V at 1000 lx, while CIGS varies from 0.26V to 0.43V in the 200-1000lx range.

Jsc vs Illumination

Silicon and perovskite (PVK) devices both exhibit high Jsc, with silicon having the highest values, ranging from 25.65 µA/cm² at 200 lx to 117.05 µA/cm² at 1000 lx, closely followed by PVK, which ranges from 24.86 µA/cm² to 116.2 µA/cm² over the same illumination range. CIGS shows an increase, from

19.08 µA/cm² at 200 lx to 90.54 µA/cm² at 1000 lx. In contrast, organic photovoltaic (OPV) technologies exhibit lower Jsc values, with a maximum of 78.34 µA/cm² at 1000 lx.

FF vs Illumination

OPV cells display a minor decline in fill factor (FF) of approximately 67% to 65%, illustrating effective charge extraction with limited recombination losses across the illumination levels. Similar to OPV, Perovskite shows a slight reduction in FF, from 69.45% at 200 lx to 66.76% at 1000 lx, which is attributed to increased trap-assisted recombination at higher light intensities. In contrast, Silicon and CIGS show improvements in FF, with Si rising from 49.35% at 200 lx to 55.33% at 1000 lx, and CIGS increasing from 37.77% to 50.51%.

Pmax vs Illumination

Perovskite minimodule achieves the highest maximum power output (Pmax), reaching 53.23 µW/cm² at 1000 lx. OPV follows with 32.33 µW/cm² at 1000 lx, while Silicon reaches 22.50 µW/cm² at the same illumination level. CIGS shows the lowest Pmax values, peaking at 19.89 µW/cm² at 1000 lx. The overall trend indicates that Perovskite performs best, attributed to their superior Voc and Pmax.

PCE vs Illumination

The power conversion efficiency (PCE) trends align with the Pmax results. Perovskite achieved the highest PCE of 15.75% at 1000 lx, followed by OPV with a PCE of 9.53%. Silicon records a PCE of 6.65%, while CIGS shows 5.88% at 1000lx. These results confirm the superior performance of Perovskite minimodule under cold LED illuminations, outperforming the other technologies and the expected low performance of Si and CIGS.

The key observations from these experiments reveal that Silicon exhibits significant Voc losses but achieves high Jsc values. The high Jsc is primarily due to the thicker absorber layer, which captures more photons, while the Voc losses are a result of thermalization losses [10]. Perovskite (PVK) and OPV technologies demonstrate superior performance, with both showing high Voc and moderate Jsc values. OPV and PVK both show a slight reduction in fill factor (FF) and overall both show stable performance due to favourable material properties. In contrast, CIGS cells show the lowest overall performance, as confirmed by their lower PCE values, making it the least efficient among the other PV technologies.

Indoor performance under Warm LED (3000K)

The JV characteristics of various photovoltaic technologies—Perovskite (PVK), OPV, Silicon (Si), and CIGS—were analyzed under a Warm LED (3000K) at illumination levels of 200 lx, 500 lx, and 1000 lx. The results are summarized in terms of Voc, Jsc, FF, Pmax, and PCE.

Table 4.6: Indoor performance of samples under WLED (3000K) in the CHOSE, Italy experimental setup.

Device	Light source	Illuminance	Incident Power	JV curve parameters					
		lux	Pin	Voc	Voc per cell	Jsc	FF	Pmax	PCE
		lx	$[\mu W/cm^2]$	[V]	[V]	$[\mu A/cm^2]$	[%]	$[\mu W/cm^2]$	[%]
monocrystalline Si cell (Rigid, opaque), single cell	WLED (3000K)	200	68.62	0.24	0.24	25.25	48.95	3.00	4.39
		500	160	0.29	0.29	58.11	52.74	9.04	5.66
		1000	316	0.34	0.34	117.12	55.05	22.24	7.05
CIGS minimodule (Flexible, opaque), 6 cells connected in series	WLED (3000K)	200	68.62	1.64	0.27	19.8	37.69	2.046	2.98
		500	160	2.20	0.36	43.74	44.04	7.06	4.41
		1000	316	2.59	0.43	86.22	50.56	18.879	5.97
Organic minimodule (Flexible, semi-transparent), 6 cells connected in series	WLED (3000K)	200	68.62	3.48	0.58	17.02	67.8	6.61	9.62
		500	160	3.65	0.60	37.88	67.1	15.5	9.69
		1000	316	3.83	0.63	82.12	65.56	34.46	10.9
Perovskite minimodule (Rigid, semi-transparent), 7 cells connected in series	WLED (3000K)	200	68.62	4.10	0.58	24.26	70.43	10.52	15.34
		500	160	4.44	0.63	55.8	68.66	25.53	15.96
		1000	316	4.61	0.65	115.2	69.49	55.36	17.52

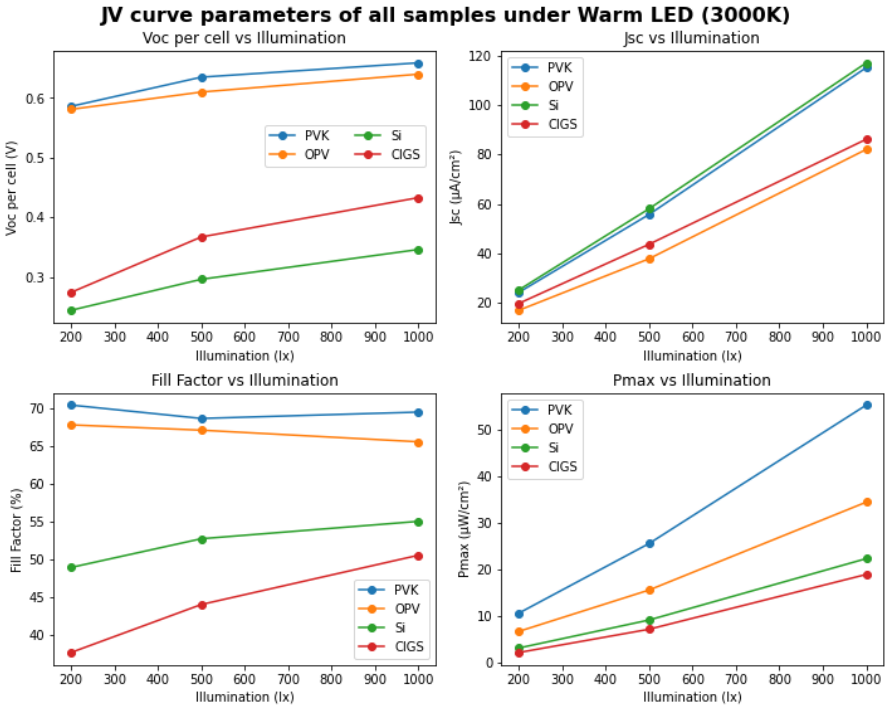

Figure 4.15: JV parameters of all samples under Warm LED (3000K) bulb.

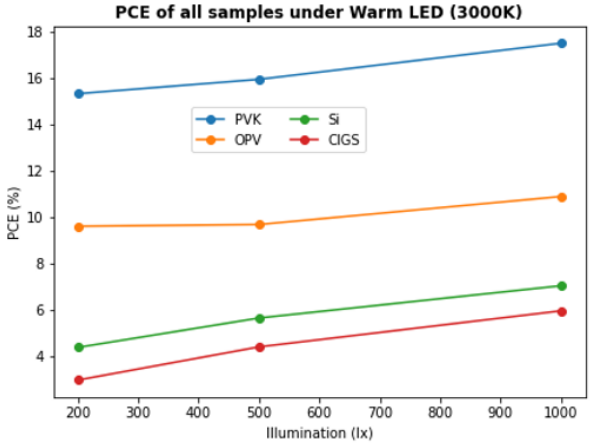

Figure 4.16: PCEs of all samples under Warm LED (3000K) bulb.

Voc per cell vs Illumination

Perovskite shows the highest open-circuit voltage (Voc) values, ranging from 0.58V at 200 lx to 0.65V at 1000 lx, indicating its strong performance under indoor lighting conditions. OPV cells also maintain relatively high Voc values, ranging from 0.58V at 200 lx to 0.65V at 1000 lx. In contrast to that Silicon and CIGS exhibit lower Voc values, with Silicon increasing from 0.24V at 200 lx to 0.34V at 1000 lx, while CIGS exhibits 0.27V at 200 lx and 0.43V at 1000 lx. With both Si and CIGS having a low bandgap around 1.11eV for Si and 1.12eV for CIGS, significant Voc losses are expected.

Jsc vs Illumination

Silicon demonstrates a high Jsc, peaking from 25.25 μA/cm² at 200 lx to 117.12 μA/cm² at 1000 lx because of its thicker absorber layer. Similarly, PVK follows a similar trend, with Jsc values reaching 24.26 μA/cm² at 200 lx to 115.2 μA/cm² at 1000 lx. On the other hand, CIGS and OPV display lower Jsc values, with CIGS peaking at 86.22 μA/cm² and OPV reaching 82.12 μA/cm² at 1000 lx.

FF vs Illumination

OPV minimodule demonstrates a relatively stable fill factor (FF) ranging from 67.8% at 200 lx to 65.56% at 1000 lx. Thus, indicating efficient charge extraction and low recombination losses under varying illumination levels. Perovskite shows a slight decrease in FF as illumination increases, from 70.43% at 200 lx to 69.49% at 1000 lx. In contrast, Silicon and CIGS cells show improvement in FF as the illumination increases, with Si rising from 48.95% at 200 lx to 55.05% at 1000 lx, and CIGS increasing from 37.69% to 50.56%.

Pmax vs Illumination

The maximum power output (Pmax) of the Perovskite minimodule increases significantly with an increase in illumination level, peaking at 55.36 µW/cm² at 1000 lx. This indicates the highest Pmax among the tested PV technologies. OPV follows with 34.46 µW/cm², while Silicon and CIGS show lower Pmax values of 22.24 µW/cm² and 18.88 µW/cm², respectively at 1000lx.

PCE vs Illumination

As mentioned before the power conversion efficiency (PCE) trend mirrors that of Pmax. Perovskite achieves the highest PCE of approximately 17.52% at 1000 lx, followed by OPV at 10.9%. In contrast, Silicon and CIGS show lower PCE values, with Si reaching a maximum of 7.05%, while CIGS achieves 5.97%. Hence, PVK technology showcasing superior performance under warm LED compared to other tested PV technologies.

Comparison of indoor performance in Cold and Warm LED

This section is to understand the difference between the indoor performance of PV technologies under Cold (6500K) and Warm (3000K) LED. Figure 4.17 illustrates the comparison between the PCE values of the PV technologies at 200lx, 500lx and 1000lx, respectively, with the dotted lines representing PCE values under Warm LED (WLED) and the solid line representing the PCE values under Cold LED (CLED).

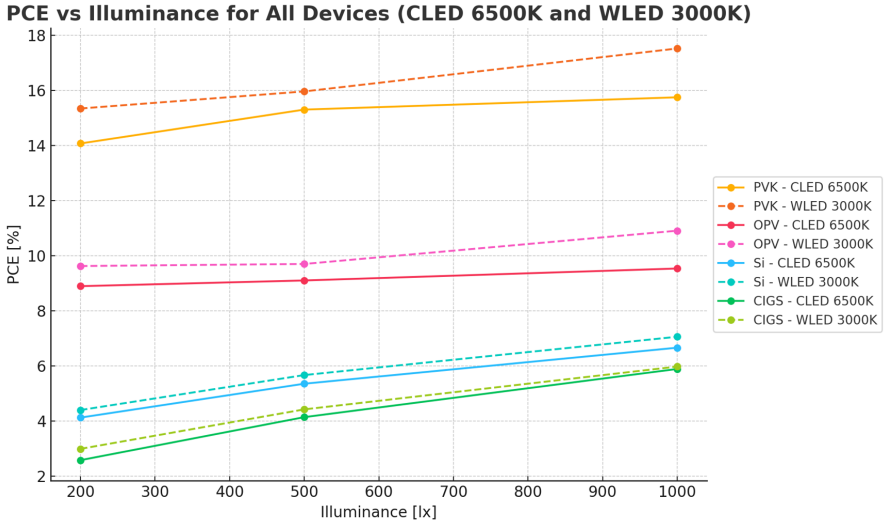

Figure 4.17: Comparison between the indoor performance of all technologies in Warm LED and Cold LED.

Perovskite consistently showed a high PCE, ranging from 14.1% to 16.7% under CLED going from 200lx to 1000lx and the highest values under WLED (15.3% to 17.5%), indicating high performance under warm LED. Organic photovoltaics (OPV) also performed well, with stable PCE values of 9.0% to 10.3% under CLED and better PCEs from 9.6% to 10.9% under WLED, showing minimal sensitivity to the lighting type.

Monocrystalline silicon (Si) displayed moderate PCE, increasing from 4.4% at 200lx to 7.2% at 1000lx under WLED and 4.3% to 7.0% under CLED, suggesting a slight drop in performance under cold LED. CIGS minimodule exhibited the lowest PCE, increasing from 2.7% to 5.6% under CLED and

from 3.0% to 6.0% under WLED. In general, all technologies demonstrated improved PCE with higher illuminance, with slightly better overall performance under WLED, particularly for Perovskite and OPV. This is in line with literature, where the PCE has reduced going from lower colour temperature LED to higher temperature LEDs i.e, from warm LED to cold LED.

This improvement in PCE performance can be better understood by looking at the spectral profile of the Cold (6500K) and Warm (3000K) LED light sources. Figure 4.18, illustrates the spectral profiles of the Cold and Warm LED light source at 200lx, where the blue line is the cold LED (6500K) and the red line is the warm LED (3000K).

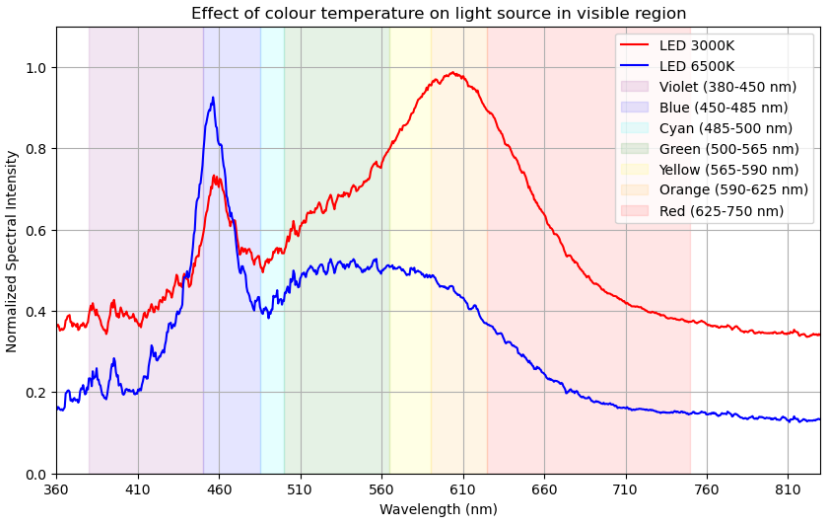

Figure 4.18: Comparison between Cold LED (6500K) and Warm LED (3000K) at 200lx.

In the first experiment analyzing the spectral profiles of the typical artificial lights used indoors, it was observed that common LEDs emit in two spectral regions: a narrow peak in the blue region centered around 450nm and a broader peak centered around 600nm in the orange region of the visible spectrum.

As observed in Figure 4.18, the cold LED spectrum which has a peak in the blue region, has most of its energy concentrated in shorter wavelengths, which correspond to higher photon energies. In contrast, the warm LED displays a stronger peak in the orange region at longer wavelengths, corresponding to lower energy photons. Notably, the photon flux under the warm LED is greater than that of the cold LED, as indicated by the higher peak of warm LED surpassing that of cold LED, resulting in more generation of charge carriers compared to the cold LED.

The efficiency in indoor environments are calculated by the ratio of maximum output power to input power or incident power. Cold LEDs have a higher input power, the input power of the cold LED in this experiment was 75.4 $\mu W/cm^2$, 170 $\mu W/cm^2$ and 338 $\mu W/cm^2$ at 200lx, 500lx and 1000lx, respectively. In contrast, the warm LED had lower input powers of 68.62 $\mu W/cm^2$, 160 $\mu W/cm^2$ and 316 $\mu W/cm^2$ for 200lx, 500lx and 1000lx, respectively. Thus, cold LEDs provide relatively more input power. However, this extra input power is not utilized, resulting in the reduction of PCE under cold LED compared to warm LED. This reduction is mainly because the increase in Jsc is simply not sufficient enough to raise the maximum power output of the solar cells high enough so that it can result in an increase in the PCE [73].

For instance, the Jsc increase in PVK going from 3000K colour temperature to 6500K colour temperature is only 0.87% ($J_{sc,3000K}$ is 115.2 $\mu A/cm^2$ and $J_{sc,6500K}$ is 116.2 $\mu A/cm^2$), which is relatively small. This demonstrates that, even if the input power increases going from LED of 3000K to 6500K, it does not necessarily result in a significant Jsc boost or higher power output, as the device is unable to fully utilize the extra input power for electricity generation. This highlights that higher input power does not always lead to a proportionate increase in electrical output.

Therefore the reduction in PCE is majorly affected by the spectrum of the LED bulb. Thus, the match

between the active layer absorption with respect to the LED emission spectrum needs to be carefully considered so that the Jsc increase is large enough to compensate for higher input power intensities of the cold LED light source [121]. Therefore, the reduction in PCE is observed in going from lower colour temperature LEDs to higher colour temperature LEDs, i.e. from warm LEDs to cold LEDs.

4.3. Discussion

This section presents a discussion of the results obtained from the EnergyVille2 and CHOSE experimental setups, focusing on the performance of various PV technologies under indoor lighting conditions. While the experimental setups are different in dimensions, the measurement methodologies employed were consistent across both labs. Additionally, this section provides insights into which indoor light sources are most favourable for the performance of the tested PV technologies and evaluates the practical implications of the results.

Collaboration between imec and CHOSE was crucial, as the primary goal of this thesis is to compare the indoor performance of different PV technologies, primarily by examining their JV curve parameters, ultimately in the power conversion efficiency (PCE). PCE is calculated as the ratio of the maximum power output of the solar cell to the incident light power, which is typically measured using a spectrometer. However, due to a malfunction with the spectrometer at EnergyVille2, the opportunity arose to collaborate with the CHOSE lab in Italy, allowing for more accurate measurements of incident power and PCE values. This collaboration also provided a means to verify whether the spectrometer at imec was indeed yielding inaccurate readings of incident power intensities and illuminance values.

In reviewing the indoor performance of the PV technologies under both warm CFL and cold LED lighting, PCE values could not be accurately determined at EnergyVille2 due to incorrect incident power measurements. However, maximum power output values were used for comparison. The results indicated that all technologies performed better at 1000lx under LED lighting compared to CFL. This improved performance is likely due to LED lighting emitting more energy in the visible spectrum compared to the CFL spectrum.

While exact input power values are not available since the spectrometer malfunctioned, the spectral profiles of the CFL and LED reveal that the LED, with a sharp peak at 450 nm and a broad spectral distribution from 500 nm to 800 nm, provides more usable energy for PV devices. In contrast, the CFL spectrum displays several distinct peaks around 450 nm, 550 nm, and 620 nm, offering less continuous coverage across the visible spectrum, as between these peaks there is little to no energy emission at certain wavelengths. Notably, this result is particularly interesting given the LED's lower power rating of only 1.6 W compared to the 11 W of the CFL bulb. According to the calculations of Freunek M. et al., the LED spectra align better with the absorption properties of PV materials, especially those with bandgaps near or 1.9 eV (refer Table 3.1 for sample bandgaps), making LED light more efficiently absorbed [62] [60].

Furthermore, considering the widespread adoption of LED bulbs in households over the next 10-15 years due to their energy efficiency and longer lifespans, it became increasingly relevant to investigate the indoor performance of the technologies under warm and cold LED lighting. Consequently, further experiments were conducted at the CHOSE lab to assess the indoor efficiency of the PV technologies under these specific lighting conditions at different illumination levels.

The results under both Warm LED (3000K) and Cold LED (6500K) lighting conditions revealed that the photovoltaic (PV) technologies performed better under Warm LED. The difference in performance can be attributed to the variation in colour temperature of the LED light source, which not only affects whether the light appears warm or cool but also the energy of the photons emitted by the light source. Cold LEDs emit their peak centered at shorter wavelengths in the 300-500nm regime, corresponding to high-energy photons, compared to warm LEDs which have their peak at longer wavelengths higher than the cold LED peak, indicating a high photon flux under warm LED which can be extracted effectively and converted into electrical energy by the PV devices.

Another reason is that the higher input power from the cold LED increases Jsc in PV devices; however, this increase is not sufficient to significantly raise the maximum power output high enough to improve the power conversion efficiency (PCE) under cold LED, as the rise in generated power density is smaller

than the increase in input power [121]. Therefore, the absorber layer absorption needs to be carefully matched with the LED light emission spectra.

This behaviour is also observed in the literature, where Yin et al. reported a PCE reduction in an organic bulk heterojunction (BHJ) going from 3000K colour temperature LED to 6000K colour temperature LED [43]. Zhang et al, reported a decrease in PCE of using an organic PV with a composition of the acceptor:donor material of PM6:IT-4F, having a PCE of 14.0% at 3000 K to 13.2% at 6000 K LED colour temperature [121].

However, from a practical perspective, Cold LEDs are more commonly used in indoor environments such as offices, libraries, and other workspaces, where bright, high-energy light is preferred for visual tasks. Warm LEDs, on the other hand, are typically found in residential areas, providing softer, more comfortable lighting. Despite the higher efficiency observed under Warm LED lighting, Cold LEDs are more practical for indoor environments where functionality is prioritized.

For typical indoor illumination levels of 200 to 1000 lx, increasing the intensity of cold LEDs beyond 1000 lx may yield some performance gains due to the higher number of incoming photons incident on the PV. However, only a portion of the high-energy photons, primarily in the blue region of the visible spectrum, would be absorbed by the bandgap of the material, with excess energy lost as thermalization losses. While high-bandgap materials may be more suitable for capturing these high-energy photons, thermalization losses would still limit the efficiency gains achievable under cold LED lighting. Notably, it meets the minimum power requirement of $100 \mu W/cm^2$ for sensor nodes and other IoT devices, indicating sufficient power output for these applications.

The use of two experimental setups arose from calibration issues with the imec spectrometer. Collaboration with CHOSE was essential to confirm the miscalibration of the spectrometer. While a direct comparison between the imec and CHOSE experiments is not possible due to the different LED bulbs used in each setup with differing colour temperature and power, an analysis of the overall trend in Pmax values showed that the imec spectrometer consistently overestimated incident power intensities, especially at lower illumination levels (100 lx to 500 lx), resulting in incorrect power conversion efficiency values. This overestimation is also reflected in the high intercept values observed in the linear regression equations derived from the imec spectrometer, especially under LED lighting. Despite these discrepancies, the behaviour of the PV devices was consistent with the measurements obtained from the imec experimental setup, confirming similar trends in the J-V curve parameters.

It is evident that Perovskite PV technology demonstrates superior indoor performance compared to other PV technologies, with OPV emerging as a close competitor. This is consistent with the extensive body of literature focused on improving the indoor efficiency of OPV devices, which enables them to perform competitively with Perovskite. Silicon technology, while not the most optimal for indoor applications, remains a competitive choice due to its high Jsc values, which help offset the significant Voc losses. CIGS, on the other hand, exhibited the lowest performance, confirming that it is not well-suited for indoor environments, as expected.

The key findings regarding Silicon (Si) and CIGS technology, when compared to Perovskite and OPV, reveal significant Voc losses in indoor experimental testing conditions. This is mainly due to their bandgaps—1.11 eV for Si and 1.12 eV for CIGS—which correspond to wavelengths around 1100 nm in the infrared region. For Si, the thicker absorber layer facilitates the absorption of energy at these longer wavelengths, while for CIGS, its direct bandgap and higher absorption coefficient than crystalline silicon enables effective absorption just above the bandgap energy, allowing it to efficiently utilize infrared light. Thus, the excess energy from the visible region results in thermalization losses. Low Voc per cell of Si and CIGS significantly lowers the performance under indoor conditions.

OPV sample, as it is a commercial product, the exact polymer used in the absorber layer and the bandgap is not publicly disclosed. However, it is specifically optimized for indoor applications. In both experimental setups, OPV's performance closely competed with Perovskite, delivering although low Jsc values, its high Voc, and a stable fill factor (FF) proving to be competitive with Perovskite. It is likely that the OPV employs fullerene-based acceptors, known for their strong absorption in the visible and near UV regions, as well as their large bandgaps [96].

Literature indicates that under low illumination, OPV devices often exhibit improved FF due to re-

duced recombination effects. The relationship between short-circuit current density (J_{sc}) and light intensity (I) follows the $J_{sc} \propto I^{\alpha}$ relation [14]. Here, α is the proportionality factor that determines how J_{sc} scales with light intensity. Ideally, if $\alpha = 1$, J_{sc} would increase linearly with light intensity, meaning the current generated would double if the light intensity doubled. However, based on experimental observations, α is estimated to be less than 1 for OPV devices. This indicates a sublinear relationship, where J_{sc} increases less than proportionally as light intensity increases.

The fact that $\alpha < 1$ suggests that as the light intensity rises, bimolecular recombination (where two charge carriers recombine directly without defects) becomes more prominent. This recombination limits the number of charge carriers that contribute to the current, preventing J_{sc} from increasing in direct proportion to the light intensity. As a result, J_{sc} grows more slowly at higher illumination levels than it would if recombination were minimized.

The sublinear behaviour of Jsc is also observed in Perovskite, where α is similarly less than 1. Like OPV, perovskite also experiences increased bimolecular recombination as the light intensity rises, which limits the efficiency of current generation. Furthermore, the FF in perovskite tends to decrease as light intensity increases from 100lx to 1000lx, due to the higher recombination processes such as trap-induced recombination [10], preventing efficient charge extraction, resulting in a decline in FF at higher illumination levels.

Despite this sublinear behaviour in J_{sc}, both OPV and Perovskite technologies maintain consistent FF and relatively high Voc at lower light levels, making them well-suited for indoor environments where recombination losses are minimized. This performance highlights their potential for ambient energy harvesting, where stable performance at low light intensities is crucial for practical applications.

In the case of the CIGS sample, it showed certain performance limitations. The narrow and lower light intensity spectrum of artificial light sources does not fully align with the optimal absorption range of CIGS, which is more efficient at absorbing a broader solar spectrum, including infrared. This spectrum mismatch results in reduced Jsc and low PCE under indoor conditions compared to 1 Sun illuminations. Additionally, recombination losses are also more pronounced, leading to lower Voc and FF. Therefore, while CIGS retains the inherent advantages such as flexibility, lightweight and high absorption [10], its effectiveness in indoor environments is limited by its spectral response and recombination dynamics.

In conclusion, the comparative analysis of different PV technologies under indoor lighting conditions revealed that Perovskite and OPV technologies outperform traditional silicon and CIGS technologies.

5

Conclusion

This chapter presents the conclusions of the research, titled "Comparison of Perovskite and Other Photovoltaic (PV) Technologies under Indoor Illuminations." It summarizes the key findings, focusing on how each PV technology behaves in an experimental setup specifically designed to simulate illumination conditions representative of indoor environments. The analysis is based on key J-V curve parameters, namely open-circuit voltage (Voc), short-circuit current density (Jsc), fill factor (FF), maximum power output (Pmax), and power conversion efficiency (PCE). Additionally, the chapter discusses the suitability of various artificial light sources commonly used in indoor environments for these PV technologies.

The first research objective—exploring the differences between outdoor and indoor illumination—was successfully addressed. The investigation analyzed the spectral profiles of common indoor light sources and explored why indoor illumination levels are significantly lower—typically 10 to 1000 times less intense—than outdoor illumination under the AM 1.5G spectrum. To achieve this, an optical fibre spectrometer was used to analyze three light sources: an incandescent lamp, a compact fluorescent lamp (CFL), and a light-emitting diode (LED). The results revealed that CFL emits narrow spectral bands with sharp peaks at specific wavelengths (450nm, 550nm, and 620nm), whereas the LED bulb showed a broader spectral distribution with a sharp peak centered around 450nm. The incandescent bulb, typical of a black-body radiator, exhibited a continuous increase in spectral irradiance across the visible spectrum without distinct peaks. These spectral profiles were consistent with the expected behaviour of these light sources in indoor environments, as reported in the literature.

The correlation between spectral irradiance and illuminance was further examined, revealing a clear linear relationship. Linear regression analysis confirmed this, with variations in the rate of change in irradiance depending on the light source type, power, and colour temperature. Incandescent lamps, for instance, showed a greater change in irradiance for each unit increase in illuminance compared to LED and CFL bulbs, which are more energy-efficient and exhibit smaller changes due to their design.

The second research objective—evaluating and comparing the performance of Perovskite and other PV technologies—was addressed through an experimental setup that simulated indoor illumination conditions ranging from 100 to 1000 lux. The setup included a light chamber, spectrometer, and source meter (Keithley 2400) for J-V curve analysis at different illumination levels (100, 500, and 1000 lux). The experiments at the EnergyVille2 lab were conducted using both a warm CFL bulb (2700K) and a cold LED bulb (4000K), providing valuable insights into the performance of Perovskite, OPV, silicon, and CIGS technologies.

Results under Warm CFL (2700K): Perovskite minimodules consistently achieved the highest Voc per cell (up to 0.67 V) and Pmax (47.42 $\mu W/cm^2$) at 1000lux, making them highly suitable for indoor applications. Silicon cells exhibited the highest Jsc (115.78 $\mu A/cm^2$)in competition with perovskite (102.33 $\mu A/cm^2$). OPV demonstrated a stable FF around 72%, while CIGS cells showed the lowest performance with increasing illumination.

Results under Cold LED (4000K): Perovskite cells again delivered the highest Voc per cell (0.69V) and Pmax (79.75 μW/cm^2) at 1000 lux. Silicon cells exhibited the highest Jsc (157.58 μA/cm^2), proving efficient for current generation under low-light conditions. OPV cells maintained a high and stable FF (74-77%), while CIGS cells showed gradual improvement with increasing illumination.

In summary, Perovskite technology exhibited superior indoor performance, characterized by good Jsc and notably high Voc per cell. OPV was a close competitor, demonstrating competitive performance with a stable FF and high Voc per cell. Silicon technology showed the highest Jsc due to its thicker absorber layer, despite lower absorption efficiency compared to Perovskite and OPV. CIGS, on the other hand, showed the lowest performance, with both low Jsc and Voc leading to relatively lower indoor performance.

The overall performance of the PV technologies improved under Cold LED (4000K), primarily due to enhanced light absorption and better conversion efficiencies. Freunek M. et al. calculated that the maximum achievable conversion efficiency under ideal conditions can reach 58.4% for LED lighting, compared to 46% under fluorescent tube lighting [60]. This finding reinforces that LED lighting, with its targeted spectral output, is more conducive to indoor PV performance. Consequently, further experiments were conducted to compare Cold and Warm LED lighting to assess PCE under different lighting conditions.

Due to inconsistent incident power intensity values obtained by the imec spectrometer, it was not possible to calculate the PCE at EnergyVille2. Thus, a collaboration with the CHOSE lab in Italy was established to obtain reliable measurements and cross-verify if the issue was with the imec spectrometer. The CHOSE experimental setup, based on Rossi et al., maintained the same methodology, differing only in the chamber size [79].

The CHOSE lab experiments compared the performance of Perovskite, OPV, silicon, and CIGS under Cold LED (6500K) and Warm LED (3000K) at illuminance levels of 200 lx, 500 lx, and 1000 lx.

Results under Cold LED (6500K): Perovskite technology demonstrated the highest performance, achieving a PCE of 15.75% at 1000 lux, with superior Voc and Pmax. OPV showed stable performance with a PCE of 9.53%. Silicon cells, despite Voc losses, achieved the highest Jsc, confirming their efficiency for current generation. CIGS exhibited the lowest performance, with limited PCE and Jsc values.

Results under Warm LED (3000K): Perovskite modules achieved the highest PCE (17.52%) and Pmax (55.36 μW/cm^2) at 1000 lux. OPV showed a stable FF and PCE of 10.9%, while silicon cells exhibited high Jsc but a lower PCE (7.05%). CIGS cells showed the lowest performance but improved with increasing illumination.

Overall, the results from Warm and Cold LED experiments revealed that the PCEs improved under warm LED lamp. This improvement is attributed to the spectral profile of the warm LED, which has a higher peak surpassing that of cold LED at longer wavelengths indicating more number of photons incident on the solar samples under warm LED, hence, more generation of charge carrier. Additionally, the Jsc increase under cold LED is not sufficient to raise the maximum output of the solar cells high enough to show improvement in PCE. Thus, the PCE reduces when going from low colour temperature LEDs (warm) to high colour temperature LED (cold).

In practical terms, however, most indoor environments, such as offices and libraries, use high-colour temperature Cold LEDs, with a spectral peak in the blue region. If the intensity of the cold LED is increased beyond 1000lx, the performance gains are limited as PV devices with very high bandgaps would be able to absorb a portion of it as the excess energy would be lost as thermalization losses. Thus, the research should be more focussed on maximising the match between the LED light emission spectra and the absorber layer of PV materials.

As previously mentioned, the imec spectrometer was not calibrated, leading to inconsistent incident power intensity measurements and inaccurate PCE values. Therefore, the PCE values obtained from the CHOSE experiments are discussed in this study. While a direct comparison between the imec and CHOSE experiments is not feasible firstly, due to the differences in the experimental setup and secondly, due to differences in the light sources used—such as varying colour temperature, type and power—an overall analysis of the maximum power outputs revealed that the imec spectrometer overestimated incident power intensity values, particularly at lower illumination levels (100 lx to 500 lx). Thus, it

is very essential to have a calibrated spectrometer, especially for LED light sources, when conducting experiments for indoor conditions. Despite these discrepancies, the J-V parameter trends of the PV devices remain consistent with those observed in the imec experimental setup.

In conclusion, Perovskite technology emerged as the top performer in indoor environments, due to its bandgap tunability, high absorption coefficient, and long carrier diffusion lengths. OPV, while slightly behind Perovskite, demonstrated strong stability and competitive performance. Silicon, although affected by Voc losses, exhibited strong current generation due to its thicker absorber layer, while CIGS showed the lowest performance, proving to be the least suitable candidate for indoor PV as also observed in literature. Thus, the high bandgap materials in indoor testing typically reach lower Jsc and higher Voc than lower bandgap materials.

The highest PCE achieved in this study was 17.52% under warm LED (3000K) lighting at 1000lx, observed for the Perovskite sample. Although this is not the highest PCE reported for perovskite in literature —the highest being 40.1% under warm LED (2700K) at 824lx [102] — this result remains significant, especially considering the baseline composition used. It highlights strong potential for further optimization. Moreover, the achieved performance is comparable to the lead-free PVK efficiencies commonly reported in literature [10] [14], highlighting the competitiveness of the baseline formulation even without advanced compositional modifications. With further modifications, such as compositional engineering, even higher efficiency levels could be achieved.

These findings emphasize the potential of Perovskite and OPV for indoor energy harvesting, particularly under practical indoor lighting conditions and highlight the need for further optimization of silicon and CIGS technologies to improve their performance under indoor lighting conditions.

6

Recommendations

This section provides a series of recommendations based on the findings and analyses presented in this study, aimed at guiding future research and improving the understanding of how various factors impact the performance of PV technologies in indoor environments.

The first recommendation is to explore the effect of incident light angle on the performance of indoor PV devices. In practical indoor applications, PV devices are not always positioned directly beneath the light source. The orientation of IoT devices or other PV-integrated systems may vary, impacting how light interacts with the PV surface. Therefore, conducting experiments where the PV cells are illuminated at different angles would provide valuable insights. It is generally understood that optimal performance is achieved when the PV device is illuminated at a zero-degree angle, where the light source is directly overhead. However, studying the performance at various angles could identify the threshold at which significant degradation occurs and determine the angle that still allows for reasonable efficiency. This is particularly relevant for real-world applications where perfect alignment with the light source is not always feasible.

The second recommendation is to assess the performance of PV technologies under varying temperature and humidity conditions. The experiments in this study were conducted in a controlled laboratory environment with a standard temperature of 25°C and relative humidity levels between 40% and 60%. However, real-world indoor environments are subject to fluctuations in temperature and humidity, which can vary significantly based on geographic location and seasonal changes. These environmental factors can have a direct impact on the efficiency and stability of PV technologies. Future research should investigate how variations in temperature and humidity influence the performance of perovskite, OPV, silicon, and CIGS technologies in indoor settings. Understanding the extent of these effects will provide a more comprehensive picture of the long-term viability of these technologies in diverse indoor environments.

The third recommendation is to assess the performance of PV technologies in mixed indoor lighting environments, where both natural sunlight and artificial light are present. In real-world indoor settings, it is common to have a combination of sunlight filtering in through windows along with artificial lighting. This hybrid lighting condition is likely to affect the overall performance of PV devices, potentially reducing PCE compared to fully indoor, artificial-light conditions. Investigating the performance under these mixed lighting scenarios would provide more practical and comprehensive data, making the analysis more applicable to everyday use cases of indoor PV technologies, such as in homes and offices.

The fourth recommendation is based on the observations during the experiment, that in this research study, the perovskite minimodule was fabricated on a rigid substrate, whereas flexible substrates are generally more suitable for indoor applications, as demonstrated by the OPV commercial sample used. While the PCE may vary depending on the composition of the PVK layer, the use of a flexible substrate is likely to enhance the practicality of the device for indoor applications. Therefore, fabricating and testing flexible PVK devices would be a valuable extension of this research. Furthermore, assessing the long-term stability of PVK under indoor lighting conditions would also be a beneficial addition

to future studies. Additionally, studying materials with varying bandgaps could further support the optimization of PVK for indoor environments.

The final recommendation is to incorporate a broader range of typical indoor PV technologies into future analyses. Based on the literature review, common indoor PV technologies include perovskite, organic photovoltaics (OPV), dye-sensitized solar cells (DSSCs), and amorphous silicon technologies. Expanding the scope to include these widely studied technologies, while ensuring uniform sample sizes and using minimodule configurations, would enable a more comprehensive and practical comparison. This approach would enhance the robustness of the results, providing a more accurate reflection of the performance potential of each technology in real-world indoor environments.

Bibliography

[1] Nicole Glanemann, Sven N Willner, and Anders Levermann. "Paris Climate Agreement passes the cost-benefit test". In: *Nature communications* 11.1 (2020), p. 110.

[2] Irene CL Ng and Susan YL Wakenshaw. "The Internet-of-Things: Review and research directions". In: *International Journal of Research in Marketing* 34.1 (2017), pp. 3–21.

[3] Fang-Chung Chen. "Emerging organic and organic/inorganic hybrid photovoltaic devices for specialty applications: low-level-lighting energy conversion and biomedical treatment". In: *Advanced Optical Materials* 7.1 (2019), p. 1800662.

[4] Lin Xie et al. "Recent progress of organic photovoltaics for indoor energy harvesting". In: *Nano Energy* 82 (2021), p. 105770.

[5] Bin Yan et al. "Indoor photovoltaics awaken the world's first solar cells". In: *Science Advances* 8.49 (2022), eadc9923.

[6] G. Morris. *Amorphous solar panels: What you need to know*. Accessed: 2023-12-06. Dec. 2023. URL: https://www.energysage.com/solar/amorphous-solar-panels/.

[7] Ian Mathews et al. "Technology and market perspective for indoor photovoltaic cells". In: *Joule* 3.6 (2019), pp. 1415–1426.

[8] Myung Hyun Ann et al. "Device design rules and operation principles of high-power perovskite solar cells for indoor applications". In: *Nano Energy* 68 (2020), p. 104321.

[9] S Grady. "Energy harvesting powers wireless sensors". In: *Power Sources Manufacturing, 2nd Quarterly* (2012).

[10] Abhisek Chakraborty et al. "Photovoltaics for Indoor Energy Harvesting". In: *Nano Energy* (2024), p. 109932.

[11] Markus C Scharber. "Efficiency of emerging photovoltaic devices under indoor conditions". In: *Solar RRL* 8.2 (2024), p. 2300811.

[12] Shigehiko Mori et al. "Investigation of the organic solar cell characteristics for indoor LED light applications". In: *Japanese Journal of Applied Physics* 54.7 (2015), p. 071602.

[13] Gayoung Kim, Myunghun Shin, and Jung Wook Lim. "Investigation of transparent electrodes and transparent/opaque a-Si: H solar cells for indoor photovoltaics". In: *2018 IEEE 7th World Conference on Photovoltaic Energy Conversion (WCPEC)(A Joint Conference of 45th IEEE PVSC, 28th PVSEC & 34th EU PVSEC)*. IEEE. 2018, pp. 338–340.

[14] Snehangshu Mishra et al. "Solution-processed next generation thin film solar cells for indoor light applications". In: *Energy Advances* 1.11 (2022), pp. 761–792.

[15] Jihong Min et al. "An autonomous wearable biosensor powered by a perovskite solar cell". In: *Nature electronics* 6.8 (2023), pp. 630–641.

[16] Lethy Krishnan Jagadamma and Shaoyang Wang. "Wide-bandgap halide perovskites for indoor photovoltaics". In: *Frontiers in Chemistry* 9 (2021), p. 632021.

[17] Yitian Du et al. "Surface passivation using pyridinium iodide for highly efficient planar perovskite solar cells". In: *Journal of Energy Chemistry* 52 (2021), pp. 84–91.

[18] Antonio Abate. *Specialty Grand Challenges in Optoelectronics*. 2020.

[19] Kelvian T Mularso et al. "Recent Strategies for High-Performing Indoor Perovskite Photovoltaics". In: *Nanomaterials* 13.2 (2023), p. 259.

[20] F. Restuccia, S. D'Oro, and T. Melodia. "Securing the Internet of Things in the Age of Machine Learning and Software-Defined Networking". In: *IEEE Internet of Things Journal* 5.6 (2018), pp. 4829–4842. DOI: 10.1109/JIOT.2018.2846040.

[21] LED Professional. "The Transition to LED Lighting may Trigger a Cataclysmic Change in the Building Automation Industry". In: *LED Professional - LED Lighting Technology, Application Magazine* (n.d.). URL: https://www.led-professional.com/resources-1/articles/the-transition-to-led-lighting-may-trigger-a-cataclysmic-change-in-the-building-automation-industry.

[22] Takatoshi Tsujimura et al. "Development of flexible organic light-emitting diode on barrier film and roll-to-roll manufacturing". In: *Journal of the Society for Information Display* 22.8 (2014), pp. 412–418.

[23] P. Stearns. "Solar Light from Ikea: Sunnan". In: *Voltaic Systems* (July 2024). URL: https://blog.voltaicsystems.com/solar-light-from-ikea-sunnan/.

[24] Zhe Chuan Feng. *Handbook of Solid-State Lighting and LEDs*. CRC press, 2017.

[25] Moncef Krarti, Paul M Erickson, and Timothy C Hillman. "A simplified method to estimate energy savings of artificial lighting use from daylighting". In: *Building and environment* 40.6 (2005), pp. 747–754.

[26] Dipti Chitnis, HC Swart, SJ Dhoble, et al. "Escalating opportunities in the field of lighting". In: *Renewable and Sustainable Energy Reviews* 64 (2016), pp. 727–748.

[27] E Fred Schubert. *Light-emitting diodes (2018)*. E. Fred Schubert, 2018.

[28] Francisco G Montoya et al. "Indoor lighting techniques: An overview of evolution and new trends for energy saving". In: *Energy and buildings* 140 (2017), pp. 50–60.

[29] P Perlin et al. "LASER DIODES GROWN ON BULK GALLIUM NITRIDE SUBSTRATES". In: *III-Nitride Devices And Nanoengineering*. 2008, pp. 223–252.

[30] Huaxu Liang et al. "Progress in full spectrum solar energy utilization by spectral beam splitting hybrid PV/T system". In: *Renewable and Sustainable Energy Reviews* 141 (2021), p. 110785.

[31] L. Krause. *Color temperature explained*. https://www.lightbulbs.com/blog/color-temperature-explained. Accessed: 2024-07-13. n.d.

[32] Khawla Saeed Salim Al-Khawaldi et al. "Ultraviolet Imaging Techniques for Off-Line Condition Monitoring of Power System Equipment". In: *Journal of Student Research* (2019).

[33] The Editors of Encyclopaedia Britannica. *Steradian | Angle, Solid Angle, Radian*. Accessed: 2024-07-09. July 1998. URL: https://www.britannica.com/science/steradian.

[34] S. Bhuyan. *Luminous Intensity: Definition, Unit, and Applications*. Accessed: 2024-07-09. June 2024. URL: https://www.sciencefacts.net/luminous-intensity.html.

[35] Yoshi Ohno. "OSA Handbook of Optics, Volume III Visual Optics and Vision Chapter for Photometry and Radiometry". In: *Optical Technology Division* 26 (1999).

[36] Contributeurs aux projets Wikimedia. *Efficacité lumineuse spectrale*. Accessed: 2024-07-09. Jan. 2024. URL: https://fr.wikipedia.org/wiki/Efficacit%C3%A9_lumineuse_spectrale.

[37] *File: Radiometry photometry units.svg*. https://commons.wikimedia.org/wiki/File:Radiometry_photometry_units.svg. Accessed: 2024-07-09. n.d.

[38] *Photometers, Radiometers, and Photodetectors*. https://www.elliotscientific.com/Gamma-Scientific-Photometers-Radiometers-and-Photodetectors. Accessed: 2024-07-09. n.d.

[39] Collegedunia. *Luminance: Explanation, Formula and Uses*. Accessed: 2024-07-09. Dec. 2023. URL: https://collegedunia.com/exams/luminance-physics-articleid-1379.

[40] International Commission on Illumination. *International lighting vocabulary*. Vol. 1. CIE Bureau central, 1957.

[41] *Photometers Selection Guide: Types, Features, Applications*. https://www.globalspec.com/learnmore/laboratory_equipment_scientific_instruments/spectrometers_analytical_photometers/photometers. Accessed: 2024-07-09. n.d.

[42] AABTools. *AABTools | PCE Instruments CRM 40 Light Meter/Photometer 150,000Lux*. Accessed: 2024-07-09. Aug. 2021. URL: https://www.aabtools.com/p/pce-instruments/crm-40/light-meter-photometer-150000lux.

[43] Hang Yin et al. "Designing a ternary photovoltaic cell for indoor light harvesting with a power conversion efficiency exceeding 20%". In: *Journal of Materials Chemistry A* 6.18 (2018), pp. 8579–8585.

[44] Domat Control System. *Conversion of Lux to W/m²*. Accessed: 2024-07-04. 2024. URL: https://www.domat-int.com/en/conversion-lux-to-w-m2.

[45] Johnny Ka Wai Ho, Hang Yin, and Shu Kong So. "From 33% to 57%–an elevated potential of efficiency limit for indoor photovoltaics". In: *Journal of Materials Chemistry A* 8.4 (2020), pp. 1717–1723.

[46] Arno Smets et al. *Solar Energy: The physics and engineering of photovoltaic conversion, technologies and systems*. Bloomsbury Publishing, 2016.

[47] ASDN - Energy. *Solar cells*. Accessed: 2024-05-25. 2024. URL: https://asdn.net/asdn/energy/solar.php.

[48] Wikipedia contributors. *Solar simulator*. Accessed: 2024-08-22. June 2024. URL: https://en.wikipedia.org/wiki/Solar_simulator.

[49] J. Herisson. *Solar simulator - Pulse-com*. Accessed: 2024-08-22. Mar. 2021. URL: https://www.pulsecom-h2020.eu/solar-simulator/.

[50] PV Education. *IV Curve*. https://www.pveducation.org/pvcdrom/solar-cell-operation/iv-curve. Accessed: 2024-08-06.

[51] Yong Cui et al. "Wide-gap non-fullerene acceptor enabling high-performance organic photovoltaic cells for indoor applications". In: *Nature Energy* 4.9 (2019), pp. 768–775.

[52] LampTwist. *Lux (lx) | Technical Guide*. Accessed: 2023-08-22. 2023. URL: https://lamptwist.com/pages/lighting-guide-lux-lx.

[53] Li Tianze et al. "Methods and analysis of factors impact on the efficiency of the photovoltaic generation". In: *Journal of Physics: Conference Series*. Vol. 276. 1. IOP Publishing. 2011, p. 012176.

[54] PVEDucation. *Short-Circuit Current*. https://www.pveducation.org/pvcdrom/solar-cell-operation/short-circuit-current. Accessed: 2024-10-15. n.d.

[55] Liyuan Han. *Solar cells boosted by an improved charge-carrying material*. 2019.

[56] PV Education. *Surface Recombination*. https://www.pveducation.org/pvcdrom/design-of-silicon-cells/surface-recombination. Accessed: 2024-09-28.

[57] ScienceTech Inc. *IV Measurement Overview*. https://sciencetech-inc.com/page/i-v-measurement. Accessed: 2024-08-08.

[58] PVEDucation. *Effect of Light Intensity*. https://www.pveducation.org/pvcdrom/solar-cell-operation/effect-of-light-intensity. Accessed: 2024-08-09. n.d.

[59] Gregory Burwell et al. "Scaling considerations for organic photovoltaics for indoor applications". In: *Solar RRL* 6.7 (2022), p. 2200315.

[60] Monika Freunek, Michael Freunek, and Leonhard M Reindl. "Maximum efficiencies of indoor photovoltaic devices". In: *IEEE Journal of Photovoltaics* 3.1 (2012), pp. 59–64.

[61] Ossila. *Analyzing and Improving Low Device Metrics: FF, Voc, and Jsc*. https://www.ossila.com/pages/analyzing-and-improving-low-device-metrics. Accessed: 2024-08-08.

[62] Antonio Ricardo Zanatta. "The Shockley–Queisser limit and the conversion efficiency of silicon-based solar cells". In: *Results in Optics* 9 (2022), p. 100320.

[63] Swarup Biswas and Hyeok Kim. "Solar cells for indoor applications: progress and development". In: *Polymers* 12.6 (2020), p. 1338.

[64] Fraunhofer Institute for Solar Energy Systems, ISE. *Photovoltaics Report*. Tech. rep. With the support of PSE Projects GmbH. Freiburg, Germany: Fraunhofer Institute for Solar Energy Systems, ISE, July 2024. URL: https://www.ise.fraunhofer.de.

[65] Dheeraj Devadiga et al. "Dye-sensitized solar cell for indoor applications: a mini-review". In: *Journal of Electronic Materials* 50 (2021), pp. 3187–3206.

[66] Muhammad Jahandar, Soyeon Kim, and Dong Chan Lim. "Indoor Organic Photovoltaics for Self-Sustaining IoT Devices: Progress, Challenges and Practicalization". In: *ChemSusChem* 14.17 (2021), pp. 3449–3474.

[67] LONGI. *LONGI Sets New World-Record for Silicon Solar Cell Efficiency, Launching 2nd Generation Ultra-Efficient BC-Based Module*. https://www.longi.com/en/news/longi-hi-mo9-bc-world-record/. Accessed: 2024-10-15. n.d.

[68] National Renewable Energy Laboratory (NREL). *Best Research-Cell Efficiency Chart*. https://www.nrel.gov/pv/cell-efficiency.html. Accessed: [24-06-2024]. n.d.

[69] R. Krishnamurthy, S. Yadav, and P. Singh. "Performance analysis of crystalline silicon solar cells under indoor and low-light conditions". In: *Solar Energy Materials and Solar Cells* 193 (2019), pp. 21–27. DOI: 10.1016/j.solmat.2018.12.023.

[70] NH Reich et al. "Weak light performance and spectral response of different solar cell types". In: *Proc. of the 20th EU PVSEC*. 2005, pp. 2120–2123.

[71] Martin A Green. "Crystalline and thin-film silicon solar cells: state of the art and future potential". In: *Solar energy* 74.3 (2003), pp. 181–192.

[72] Hidenori Saito et al. "Performance evaluation method of organic photovoltaics under indoor light condition". In: *Electrochemistry* 86.6 (2018), pp. 363–370.

[73] Behrang H Hamadani and Mark B Campanelli. "Photovoltaic characterization under artificial low irradiance conditions using reference solar cells". In: *IEEE journal of photovoltaics* 10.4 (2020), pp. 1119–1125.

[74] Andrew Shore et al. "Indoor light energy harvesting for battery-powered sensors using small photovoltaic modules". In: *Energy science & engineering* 9.11 (2021), pp. 2036–2043.

[75] Chien-Hung Chiang and Chun-Guey Wu. "Large-Area Perovskite Film Prepared by New FFASE Method for Stable Solar Modules Having High Efficiency under Both Outdoor and Indoor Light Harvesting". In: *Advanced Science* 10.7 (2023), p. 2205967.

[76] Gayoung Kim et al. "Transparent thin-film silicon solar cells for indoor light harvesting with conversion efficiencies of 36% without photodegradation". In: *ACS applied materials & interfaces* 12.24 (2020), pp. 27122–27130.

[77] Ian Mathews et al. "Performance of III–V solar cells as indoor light energy harvesters". In: *IEEE Journal of Photovoltaics* 6.1 (2015), pp. 230–235.

[78] M Foti et al. "Efficient flexible thin film silicon module on plastics for indoor energy harvesting". In: *Solar energy materials and solar cells* 130 (2014), pp. 490–494.

[79] Francesca De Rossi, Tadeo Pontecorvo, and Thomas M Brown. "Characterization of photovoltaic devices for indoor light harvesting and customization of flexible dye solar cells to deliver superior efficiency under artificial lighting". In: *Applied Energy* 156 (2015), pp. 413–422.

[80] Yeon Hyang Sim et al. "Application of ac-Si Solar Cell with a Three-Dimensional Structure to Indoor Photovoltaics". In: *Advanced Materials Technologies* 7.7 (2022), p. 2101392.

[81] Motoshi Nakamura et al. "Cd-free Cu (In, Ga)(Se, S) 2 thin-film solar cell with record efficiency of 23.35%". In: *IEEE journal of photovoltaics* 9.6 (2019), pp. 1863–1867.

[82] Leqi Lin and NM Ravindra. "Temperature dependence of CIGS and perovskite solar cell performance: an overview". In: *SN Applied Sciences* 2.8 (2020), p. 1361.

[83] Ian Mathews et al. "Analysis of CdTe photovoltaic cells for ambient light energy harvesting". In: *Journal of Physics D: Applied Physics* 53.40 (2020), p. 405501.

[84] Yoichi Aoki. "Polymer Solar Cells for Indoor Energy Harvesting". In: *MRS Advances* 1.14 (2016), pp. 931–936.

[85] Adriano Sacco et al. "Characterization of photovoltaic modules for low-power indoor application". In: *Applied energy* 102 (2013), pp. 1295–1302.

[86] Francesca De Rossi, Thomas M Brown, and Tadeo Pontecorvo. "Flexible photovoltaics for light harvesting under LED lighting". In: *2015 IEEE 15th International Conference on Environment and Electrical Engineering (EEEIC)*. IEEE. 2015, pp. 2100–2103.

[87] Chen Yang et al. "Power performance of solar energy harvesting system under typical indoor light sources". In: *Renewable Energy* 161 (2020), pp. 836–845.

[88] Manish Kumar and Sandeep Kumar. "Liquid crystals in photovoltaics: a new generation of organic photovoltaics". In: *Polymer Journal* 49.1 (2017), pp. 85–111.

[89] S Matthew Menke, Wade A Luhman, and Russell J Holmes. "Tailored exciton diffusion in organic photovoltaic cells for enhanced power conversion efficiency". In: *Nature materials* 12.2 (2013), pp. 152–157.

[90] Shun-Shing Yang et al. "Toward High-Performance Polymer Photovoltaic Devices for Low-Power Indoor Applications". In: *Solar RRL* 1.12 (2017), p. 1700174.

[91] Soyeon Kim et al. "Recent progress in solar cell technology for low-light indoor applications". In: *Curr. Altern. Energy* 3.1 (2019), pp. 3–17.

[92] Harrison KH Lee et al. "Is organic photovoltaics promising for indoor applications?" In: *Applied Physics Letters* 108.25 (2016).

[93] Ranbir Singh et al. "Ternary Blend Strategy for Achieving High-Efficiency Organic Photovoltaic Devices for Indoor Applications". In: *Chemistry–A European Journal* 25.24 (2019), pp. 6154–6161.

[94] Hwan-Il Je et al. "Understanding the performance of organic photovoltaics under indoor and outdoor conditions: Effects of chlorination of donor polymers". In: *ACS applied materials & interfaces* 12.20 (2020), pp. 23181–23189.

[95] Bernard Kippelen and Jean-Luc Brédas. "Organic photovoltaics". In: *Energy & Environmental Science* 2.3 (2009), pp. 251–261.

[96] Harold W Kroto et al. "C60: Buckminsterfullerene". In: *nature* 318.6042 (1985), pp. 162–163.

[97] Jie Xu et al. "30% efficient triple-cation perovskite solar cells under indoor illumination enabled by rare earth EuCl 3 doping". In: *Sustainable Energy & Fuels* 7.14 (2023), pp. 3404–3411.

[98] Y Lin and JZ Wang. "G. Zhang, H. Bai, Y. Li, D. Zhu, X. Zhan". In: *Adv. Mater* 27 (2015), p. 1170.

[99] Rahim Munir. "Hybrid perovskite thin film formation: From lab scale spin coating to large area blade coating". PhD thesis. 2017.

[100] EnergyVille. *Verbetering van de efficiëntie en stabiliteit van perovskietzonnecellen door moleculaire interface-engineering*. Accessed: 2024-07-04. 2023. URL: https://energyville.be/en/blogs/verbetering-van-de-efficientie-en-stabiliteit-van-perovskietzonnecellen-door-moleculaire-interface-engineering-2/.

[101] Akihiro Kojima et al. "Organometal halide perovskites as visible-light sensitizers for photovoltaic cells". In: *Journal of the american chemical society* 131.17 (2009), pp. 6050–6051.

[102] Xilai He et al. "40.1% record low-light solar-cell efficiency by holistic trap-passivation using micrometer-thick perovskite film". In: *Advanced Materials* 33.27 (2021), p. 2100770.

[103] Giulia Lucarelli et al. "Efficient light harvesting from flexible perovskite solar cells under indoor white light-emitting diode illumination". In: *Nano Research* 10 (2017), pp. 2130–2145.

[104] C.-Y. Chen et al. "High-performance mesoscopic perovskite solar cells based on CH3NH3PbI3–xClx perovskite". In: *Advanced Functional Materials* 25 (2015), pp. 7064–7070. DOI: 10.1002/adfm.201503320.

[105] F Di Giacomo et al. "Mesoporous perovskite solar cells and the role of nanoscale compact layers for remarkable all-round high efficiency under both indoor and outdoor illumination". In: *Nano Energy* 30 (2016), pp. 460–469.

[106] Janardan Dagar et al. "Efficient fully laser-patterned flexible perovskite modules and solar cells based on low-temperature solution-processed SnO 2/mesoporous-TiO 2 electron transport layers". In: *Nano Research* 11 (2018), pp. 2669–2681.

[107] Ming-Ju Wu et al. "Bandgap engineering enhances the performance of mixed-cation perovskite materials for indoor photovoltaic applications". In: *Advanced Energy Materials* 9.37 (2019), p. 1901863.

[108] Jun-Jie Cao et al. "Multifunctional potassium thiocyanate interlayer for eco-friendly tin perovskite indoor and outdoor photovoltaics". In: *Chemical Engineering Journal* 433 (2022), p. 133832.

[109] Yueheng Peng et al. "Lead-free perovskite-inspired absorbers for indoor photovoltaics". In: *Advanced Energy Materials* 11.1 (2021), p. 2002761.

[110] Rui Cheng et al. "Tailoring triple-anion perovskite material for indoor light harvesting with restrained halide segregation and record high efficiency beyond 36%". In: *Advanced Energy Materials* 9.38 (2019), p. 1901980.

[111] Haoxuan Sun et al. "Realizing stable artificial photon energy harvesting based on perovskite solar cells for diverse applications". In: *Small* 16.10 (2020), p. 1906681.

[112] Himanshu Dixit et al. "Assessment of lead-free tin halide perovskite solar cells using J–V hysteresis". In: *Physica status solidi (a)* 219.11 (2022), p. 2100823.

[113] Soumyo Chatterjee and Amlan J Pal. "Influence of metal substitution on hybrid halide perovskites: towards lead-free perovskite solar cells". In: *Journal of Materials Chemistry A* 6.9 (2018), pp. 3793–3823.

[114] Trilok Singh et al. "Effect of electron transporting layer on bismuth-based lead-free perovskite (CH3NH3) 3 Bi2I9 for photovoltaic applications". In: *ACS applied materials & interfaces* 8.23 (2016), pp. 14542–14547.

[115] Epishine. *Epishine is the leading developer and manufacturer of printed organic solar cells*. https://www.epishine.com/. Accessed: 2024-09-06. n.d.

[116] B Strahm et al. "The Swiss Inno-HJT project: fully integrated R&D to boost Si-HJT module performance". In: *29th European Photovoltaic Solar Energy Conference and Exhibition*. 2014, pp. 467–471.

[117] O. Identity. *Yparex, Extrudable Adhesives, Tie-Layer Resins*. https://www.thecompoundcompany.com/products/yparex. Accessed: insert-date-here.

[118] StellarNet, Inc. *BLACK Comet SR*. Accessed: 2024-09-04. Oct. 2023. URL: https://www.stellarnet.us/spectrometers/black-comet-sr/.

[119] Offerprice [by Hamradioshop]. *Lafayette LM-1 - Mini luxmeter*. Accessed: 2024-09-04. n.d. URL: https://offerprice.it/gb/lafayette-lm-1-mini-luxmeter-p-1443.html.

[120] Nikolaos Voudoukis and Sarantos Oikonomidis. "Inverse square law for light and radiation: A unifying educational approach". In: *European Journal of Engineering and Technology Research* 2.11 (2017), pp. 23–27.

[121] Boya Zhang et al. "Color-temperature dependence of indoor organic photovoltaic performance". In: *Organic Electronics* 104 (2022), p. 106477.

[122] Xiang Xu et al. "An Overview of High-Performance Indoor Organic Photovoltaics". In: *ChemSusChem* 14.17 (2021), pp. 3428–3448.

[123] M. Wolosz. *Perovskite Electronic Shelf Labels as a New Tool for the FMCG/Retail Sector*. Saule Technologies. Nov. 2021. URL: https://sauletech.com/perovskite-electronic-shelf-labels-as-a-new-tool-for-the-fmcg-retail-sector/.

[124] GianiNavette. *The Dracula Technologies Market Scope | Various sectors*. Accessed: 2024-02-20. 2024. URL: https://dracula-technologies.com/markets/.

[125] RICOH Co., Ltd. *Solid-State Dye-Sensitized Solar Cells | Industrial Products*. Accessed: 2024-09-16. n.d. URL: https://industry.ricoh.com/en/dye-sensitized-solar-cell.

A

Additional Experiments

A.1. Conversion of Illuminance to Incident Power Density

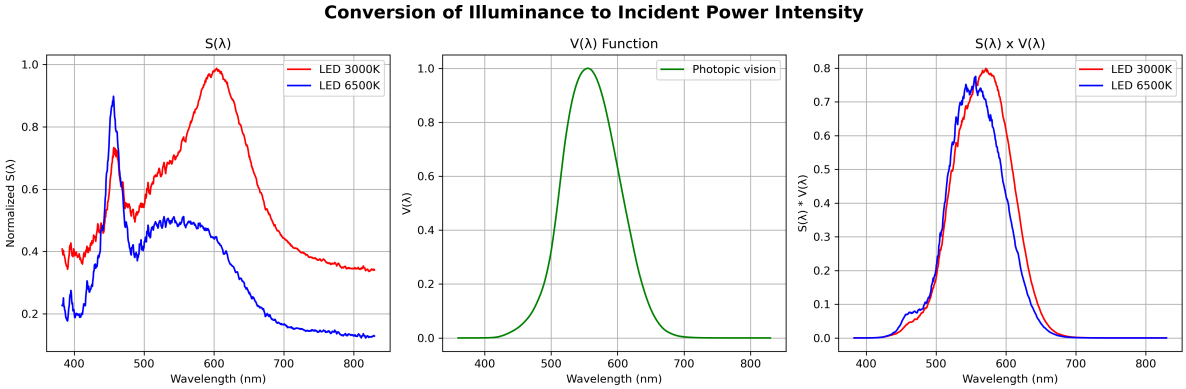

Figure A.1: Conversion of Illuminance to Incident Power Density

The incident power instenisty P_{in} can be derived from illuminance $L(\lambda)$ using Equation A.1.

$$L(\lambda) = K_m \cdot P_{\text{in}} \cdot V(\lambda) \tag{A.1}$$

where, K_m is the luminous efficacy and $V(\lambda)$ is the spectral efficiency function. To normalize the spectral distribution Equation A.2 is used.

$$S_{\text{norm}} = \frac{S(\lambda)}{\int_{\text{visible}} S(\lambda)\, d\lambda} \tag{A.2}$$

The total illuminance for multiple light sources becomes through Equation A.3.

$$P_{\text{in}} = \frac{L}{K_m} \cdot \frac{\int_{\text{visible}} S(\lambda) \cdot V(\lambda), d\lambda}{\int_{\text{visible}} S(\lambda), d\lambda} \tag{A.3}$$

The calculated Pin values are 82.61 $\mu W/cm^2$ for LED 3000K and 75.16 $\mu W/cm^2$ for LED 6500K, compared to the spectrometer's 68.62 $\mu W/cm^2$ and 75.4 $\mu W/cm^2$, respectively. Discrepancies arise from smoothing and interpolation applied during calculations, whereas spectrometer measurements are more accurate due to direct calibration and real-world precision.

A.2. Calculation of Photon flux under Cold LED and warm LED at 200lx

Figure A.2 represents the proportion of high energy and low energy photons under cold LED (6500K) and warm LED (3000K) at 200lx. Clearly, the proportion of high-energy photons to low-energy photons is always low, however, under cold LED the proportion is relatively higher than under warm LED.

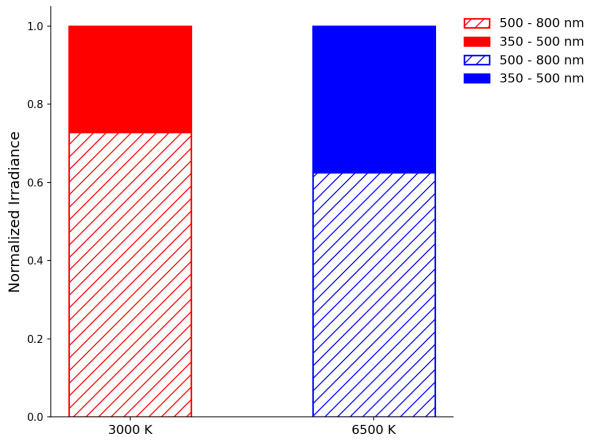

Figure A.2: Proportion of high energy photons and low energy photons in Cold LED and warm LED at 200lx.

As the irradiance is normalized, the ratios can be considered to calculate the intensity of high-energy photons and low-energy photons under both cold LED and warm LED. The total input energy under warm LED at 200lx was 68.62 muW/cm^2 and under cold LED was 75.4 muW/cm^2, respectively. Thus, we can calculate the photon flux under warm LED and cold LED at 200lx. Figure A.3 shows the photon flux under a cold LED of 6500K colour temperature and a warm LED (3000K).

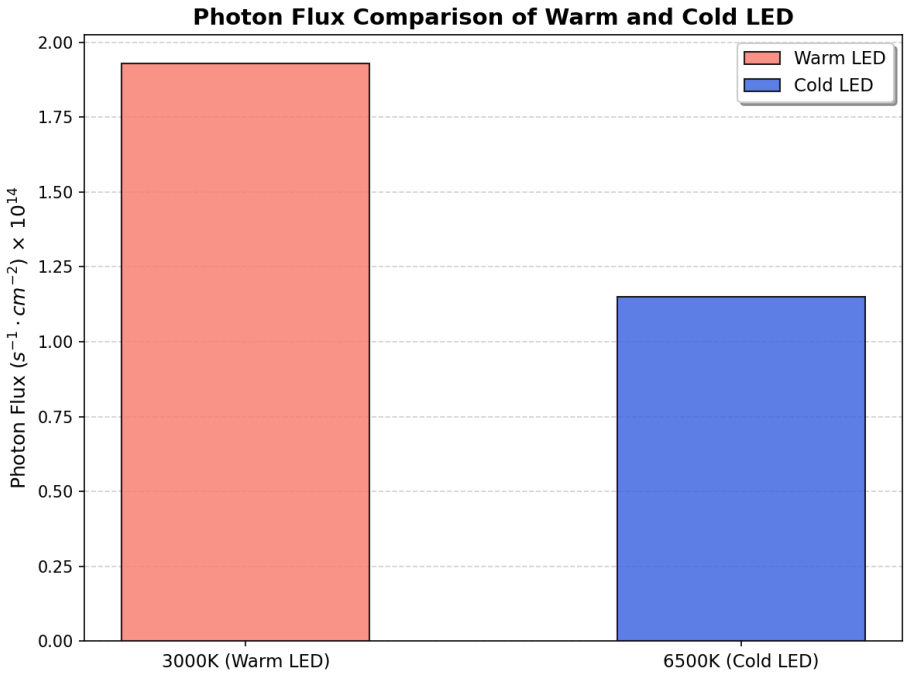

Figure A.3: Photon flux of Cold LED and warm LED at 200lx

B

Appendix

B.1. Figures

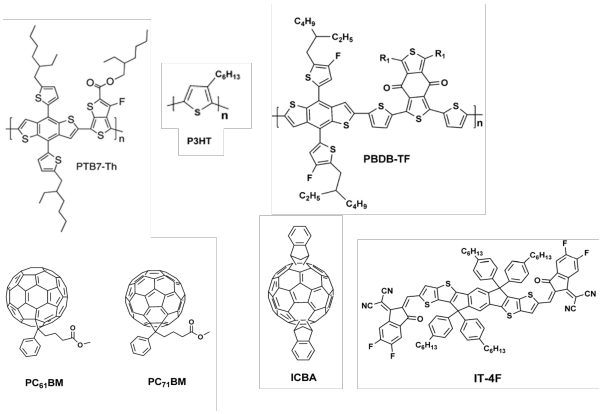

Figure B.1: Typical OPV active layer's chemical structure [122].

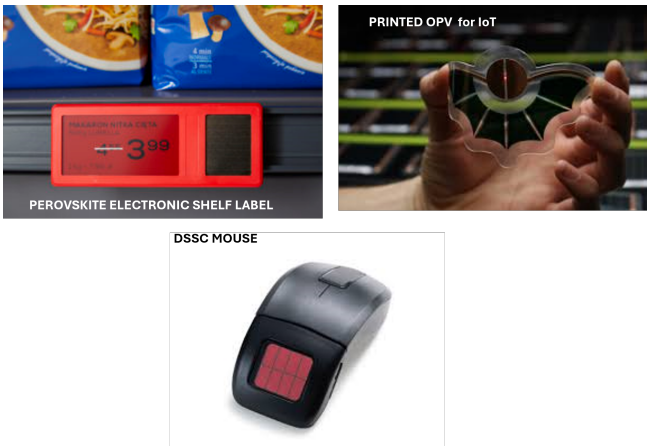

Figure B.2: IoT applications of Perovskite, OPV and DSSC [123] [124] [125]